Metabolic rewiring promotes bacterial survival under oxidative and reductive stress

Thesis by
Richard Davis Horak

In Partial Fulfillment of the Requirements for
the degree of
Doctor of Philosophy in Microbiology

CALIFORNIA INSTITUTE OF TECHNOLOGY
Pasadena, California

2026
(Defended May 18th 2026)

© 2026

Richard Davis Horak
ORCID: 0000-0003-0630-5481

ACKNOWLEDGEMENTS

In writing this thesis, I left this acknowledgements section for last. It feels like an impossible task to adequately acknowledge this experience with words alone. The PhD was harder than I ever could have imagined. From beginning at Caltech during the COVID pandemic, to receiving several enlightening mental health diagnoses, to helping organize a successful unionization campaign, this journey challenged me far beyond the scope of scientific research. Therefore, as I reminisce about the last five to six years, my intellectual accomplishments entombed within this thesis are only one product of this PhD. I would not have crossed this finish line without the support of so many people whom I have had the pleasure of calling friends, family, and mentors. While words alone feel insufficient to express my gratitude to you all, I will try. If you find yourself missing below, know that your impact has not gone unnoticed; my brain tends to forget much of what my soul remembers.

Mom, Dad, Kiki, and Jojo: I love you all more than words can say and more than I sometimes express. I still have some work to do on vulnerability… I couldn't have asked for a better support network. I miss Sunday night family nights. Mom and Dad, you both have provided me with nothing short of a wonderful life. You both have made a Herculean effort to support me financially, emotionally, and professionally. I could not have wished for better role models for how to be a good human and pursue your dreams. Mom, you showed me the importance of an open mind and a caring heart. As I begin my own journey as an educator, I have you to thank for showing me the importance of teaching. I hope one day to have reviews on Rate My Professor as good as yours. Dad, your adventurous spirit and discipline have been guiding lights for me. I cherish our trips together, and I am constantly amazed by the fervor with which you pursue your goals. Thank you for instilling in me a childlike sense of wonder possible only through a mixture of camping and 50's sci-fi.

To Kiki: the best older sibling one could ask for. You made growing up so much easier. Following you from El Paso to Austin to Los Angeles helped life feel a bit less scary. I look forward to more dancing and laughing with you. Your capacity for creative expression is always inspiring. I know I sometimes get annoyed by how often you want to hug, but I want you to know that your constant love and support have helped me feel safe throughout my life. I always know my big sister has my back.

To Jojo: life would be so much duller without you. From sneaking downstairs to play Wizard101 at 2 a.m., to impassioned debates with Dad, to hours spent cackling over internet content, you never cease to impress me with your wit, intellectual curiosity, and willingness to connect. It has been such a blast to watch you mature while still maintaining the playfulness that led to such an incredible childhood together. Even though our differing sleep schedules get in the way, you always make me feel loved and appreciated.

To Willow: what can I say other than I love you. You have been so supportive in helping me through this process and surviving its ups and downs. You remind me why

I became a biologist in the first place: finding wonder and excitement in every critter we come across on our many adventures. I am inspired daily by your determination and passion. I can't wait to see what we get up to in the years to come.

To my Mundo Unidos educators: I know I wasn't always the best student, and my ADHD diagnoses likely came as no surprise, but thank you all for being so compassionate and patient with me. To Ms. Hunt: thank you for your incredible work as an educator. You were not only a teacher but also a mentor to us all. I hope to model my educational practices after your teaching excellence.

To my El Paso friends and found family: you all have supported me since I began forming memories. From long summer days in Fighting Frogs, to making Spanish verb conjugation music videos, to GM road trips, to graduations and reunions, to Lorak ski trips, to watching several of you get married, I love you all dearly and am so happy to have you in my life.

To the Moran Lab: Nancy, thank you for providing me the opportunity and resources to develop into a scientist. Kim and Eli, y'all showed me what it meant to be professional lab superstars while also being great friends and colleagues. Sean, I cannot express how pivotal your mentorship was in getting me to where I am. Your kindness, patience, and support paid dividends, and I hope to mirror these qualities in my own mentorship of undergraduate scientists.

To my friends from UT Austin: I miss you all and am so proud of what you have accomplished. Whether I knew you through Plan II, the Beekeeping Society, the Costa Rica trip, summer crew, exploring the greenbelt, playing DND as COVID descended, absurd national park road trips, late nights grinding away on physics, dance parties, or raucous movie nights, I think about our time together often. I love you all and thank you for the love and support you gave me all those years.

To my friends in graduate school: Hannah and Grace, you both helped make COVID-era grad school feel welcoming. I cherish the many hours we spent screaming at each other to focus up and kill Spooky Richard. Korbi and Amanda – or should I say, "the duel!" – we have shared so many laughs, adventures, and hijinks. I'm so excited to see where life takes us and am sure we will get up to more ridiculous adventures soon. Thank you for supporting me at every turn. To all those in the physical biology bootcamp and our early Zoom happy hours, y'all helped make Caltech feel like home. To the original DND group, I miss our long days spent around a table developing a world together. To the current DND group, I am excited to see what adventures await us. James, thank you for sharing your world with us. Ana, my first rotation mentor, thank you for welcoming me to Caltech and helping make grad school less scary. Abby, Ruth, Tina, Noel, Jarek, Aubrey, and Satchel, we have gone on some truly amazing trips together. You all taught me so much about the outdoors and fueled some ridiculous adventures. Mac, Claire, and Brenna, you have all been radiant lights of joy and optimism. Kara, thank you for always keeping me curious about the world. To all my friends too numerous to name, thank you for the fantastic memories and incredible times spent together.

To all my roommates and the many iterations of Satan's Lair: Grace, Aubrey, and Trista; Mac and Jasmine; Jasmine and Willow. The PhD is hard. You all provided a safe and welcoming home through the darkest days. You also introduced me to fantastic cats: Ranger, Fitzgerald, Archibald, Montgomery, Milo, and Jasper. Thank you for the support.

To all the members of the Newman Lab, past and present: being part of this group has been a true pleasure. Elena, Lucas, Steven, and Renee: thank you for guiding me in the ways of bacterial physiology. Darcy and Avi, thank you for teaching me to focus on the question at hand and do the right experiment. Lev, your compassion for others is inspiring. Georgia and Rei, your guidance and mentorship in my science, personal life, and professional development have been invaluable. To my lab neighbors Zach, Sarah, and Lydia: I cherish the time spent laughing with you all on the best side of the lab. You kept the days fun. Jarek, you were always down to pull open a map and discuss a dumb idea; thank you for the good times. Elin, thank you for making COVID grad school so much better than it would have been and for being by my side during the chaos of rotations. Xiaoyu, Ines, Hannah, and Jinyang: you have all been amazing postdoctoral mentors. Roxy, I miss our hikes and nights out on the town; you always knew how to lift our spirits. Chelsey, you were the best bay-mate someone could ask for. You taught me so much about microbiology and acted as a second mentor both at the bench and in life. I miss bouncing between long existential conversations, therapy trauma dumps, constructive scientific feedback, and gossiping. John, your passion for microbial metabolism and research helped me develop my own love for this field. I hope I have made you and Kluyver proud. Korbi, your companionship in the lab helped the long days fly by and made coming into work enjoyable. To the younger generation: enjoy your time in the lab. It is a good one.

To my collaborators beyond the Newman Lab: I am incredibly grateful to you, particularly Nathan Delleska, Ludmilla Aristilde, and Nanqing Zhou.

To my committee: thank you for guiding me through this process. You always made time to share our passion for microbes and played instrumental roles in developing me as a scientist and future educator.

To UAW 2478, formerly CGPU: playing a role in unionizing the graduate students and postdocs at Caltech was one of the most fulfilling experiences of my life. I am deeply indebted to everyone involved in this movement. I truly believe we enacted meaningful and lasting change at Caltech by giving graduate students and postdocs a voice to advocate for a more equitable workplace.

And of course, to Dianne: I couldn't have asked for a better mentor. I remember our first meeting so clearly during my Caltech interview. Your enthusiasm for microbiology and mentorship is the primary reason I came to Caltech. This passion carried me through the PhD, and for that I am eternally grateful. Thank you for being a fantastic educator, mentor, friend, colleague, and bossita. I promise I will one day remember to use "that" instead of "which".

To my grandparents, to whom this thesis is dedicated: I know life was not always easy, but even in the hard times, you all found the energy to show your love and support. I wish you all were here to see what I accomplished, but I know there was never any doubt in your hearts that I would make it. Thank you.

ABSTRACT

Across the tree of life, all cells must follow unifying metabolic rules. Namely, organisms must balance electron flow to couple energy conservation with energy expenditure. Historically, studies in bacterial metabolism focused on exponential growth where cells are awash in nutrients and electron acceptors, exhibiting high bioenergetic levels. Therefore, from the perspective of both human biology and these fast-growing microbes, loss of redox balance is purely detrimental, leading to suppressed energetic states, growth arrest, and even death. Yet bacteria are commonly found under such conditions across diverse environments from industrial bioreactors to chronic infections to agricultural fields. This thesis was motivated by the remaining mystery behind how and why bacteria exist in such low energy survival states. Specifically, I focus on metabolic shifts during non-growth survival in the opportunistic pathogen *Pseudomonas aeruginosa* due to redox imbalance, as well as the potential benefits to such transitions. In the first section, I focus on oxidative stress, exploring bacterial survival during oxic nutrient starvation. I find that phenazines and toxoflavin – endogenous redox-active metabolites produced by *P. aeruginosa* and *Burkholderia* species respectively – lower the bioenergetic state of *P. aeruginosa*. Such bioenergetic self-poisoning would be traditionally deemed detrimental. Yet I find this phenomenon provides cells with increased tolerance to a variety of clinical antibiotics, suggesting cells might have agency over lowering their energetic state and that there is a benefit to doing so. In the following chapters, I turn my attention to reductive stress, examining the metabolic strategies *P. aeruginosa* uses to support anaerobic survival in the absence of terminal electron-acceptors. I discover that *P. aeruginosa* uses a phosphoketolase-mediated alternative glucose catabolic pathway under reductive stress, reminiscent of fermentative growth metabolisms in many obligate anaerobes. Moreover, this phosphoketolase plays a key role in mediating ribonucleotide homeostasis during survival-triggered macromolecule turnover. I find that many bacteria unable to grow in the absence of respiration contain phosphoketolases and show that at least two of these species, *Dyella japonica* and *Paraburkholderia graminis*, similarly rely on these enzymes for anaerobic survival. Finally, I speculate a generalizable role for phosphoketolases in supporting ribonucleotide turnover across bacterial taxa. These studies expose the large gaps remaining in our understanding of growth arrest metabolisms, even in well-studied model organisms. I hope this thesis motivates further exploration of these enigmatic yet important bacterial lifestyles.

PUBLISHED CONTENT AND CONTRIBUTIONS

Horak, R. D., Ciemniecki, J. A., & Newman, D. K. (2024). Bioenergetic suppression by redox-active metabolites promotes antibiotic tolerance in Pseudomonas aeruginosa. *Proceedings of the National Academy of Sciences*, *121*(46), e2406555121. https://doi.org/10.1073/pnas.2406555121

J.A.C. performed proton pumping measurements. R.D.H conceived and performed all other experiments under the guidance of D.K.N. R.D.H. wrote the initial manuscript and edited it according to co-author's feedback. This work is adapted in Chapter 2.

Horak, R. D., Zhou, N., Thalhammer, K. O., Dalleska, N. F., Aristilde, L., & Newman, D. K. (2026). Pseudomonas aeruginosa Relies on a Phosphoketolase to Support Anaerobic Survival Under Reductive Stress. *Molecular Microbiology*, *125*(5), 361–374. https://doi.org/10.1111/mmi.70059

Metabolomic profiles were measured by N.Z. under the guidance of L.A. Acetate measurements were performed by K.O.T. under the guidance of N.F.D. All other experiments were performed and conceived by R.D.H. under the guidance of D.K.N, L.A., and N.Z. R.D.H. wrote the initial manuscript and edited it according to co-author's feedback. This work is adapted in Chapter 3.

TABLE OF CONTENTS

Acknowledgements iii
Abstract vii
Published Content and Contributions viii
Table of Contents ix
Nomenclature xi
Chapter I: Introduction 1
1.1 Thesis Chapter Overviews 4
Chapter II: Bioenergetic suppression by redox-active metabolites promotes antibiotic tolerance in *Pseudomonas aeruginosa* 5
2.1 Introduction 6
2.2 Redox-active metabolites lower the membrane potential, proton pumping efficiency, and ATP levels of *P. aeruginosa* 9
2.3 RAMs lower the membrane potential at different rates and produce unique subpopulations conferring stress tolerance 13
2.4 RAM-mediated bioenergetic suppression is tunable, does not rely on efflux pumps, and affects tolerance to diverse antibiotics 16
2.5 RAM-mediated bioenergetic suppression and antibiotic tolerance extends to biofilms 19
2.6 Discussion 21
2.7 Methods 26
2.8 References 32
2.9 Supplemental Figures 41
Chapter III: *Pseudomonas aeruginosa* relies on a phosphoketolase to support anaerobic survival under reductive stress 49
3.1 Introduction 50
3.2 *P. aeruginosa* relies on a phosphoketolase during anaerobic survival on glucose under reductive stress 55
3.3 *P. aeruginosa* utilizes a phosphoketolase-mediated pathway for catabolism of glucose to acetate during anaerobic survival 59
3.4 *P. aeruginosa* relies on Xfp for metabolic homeostasis of endogenous metabolites during anaerobic survival on glucose 62
3.5 *P. aeruginosa*'s Xfp maintains metabolic homeostasis and viability during anaerobic survival on diverse carbon sources and in the absence of exogenous carbon 66
3.6 Anaerobic survival triggers purine degradation and Xfp is essential for maintaining ribonucleotide homeostasis 68
3.7 Discussion 73
3.8 Methods 80
3.9 References 86
3.10 Supplemental Figures 96
Chapter IV: Phosphoketolases support ribonucleotide homeostasis and

survival under anaerobic growth arrest in diverse bacteria.....106
4.1 Introduction 107
4.2 Degradation and salvage of ribonucleotide derivatives during anaerobic survival necessitates Xfp to support metabolic homeostasis and viability 111
4.3 Ribose addition complements anaerobic survival and metabolic dysregulation in the PA14 *xfp* mutant 115
4.4 Phosphoketolases support anaerobic survival in *Parabukholderia graminis* and *Dyella japonica* as well as glucose catabolism in *P. graminis*....121
4.5 Use of phosphoketolases for ribonucleotide processing may be isolated to specific phosphoketolase homologs or the presence of flanking genes 126
4.6 Discussion.....129
4.7 Methods 135
4.8 References.....141
4.9 Supplemental Figures 150
Chapter V: Conclusions and future directions.....156
5.1 Summary 156
5.2 Key Findings 157
5.3 Future Directions 158
5.4 Concluding Perspective 165

NOMENCLATURE

Oxidation/reduction: Oxidation = loss of electrons, reduction = gain of electrons.

Reducing equivalents: A chemical species that acts as an electron donor (reductant) and transfers electrons to an electron acceptor (oxidant). The most discussed reducing equivalents are NADH, NADPH, and $FADH_2$.

Oxidative stress: An imbalance in the electron flow typically caused by the presence of too many "oxidants" or electron acceptors, particularly reactive chemical species that cause "unwanted" oxidation reactions.

Reductive stress: An imbalance caused by a lack of oxidants – electron acceptors – leading to an increase in reducing equivalents.

Redox-active metabolite (RAM): Small molecules produced by cells that can act as both electron acceptors and donors based on their chemical properties.

***Pseudomonas aeruginosa*:** A gram-negative model-bacterium primarily discussed for its metabolic versatility and role as an opportunistic pathogen. Notorious for its ability to cause chronic infections that are hard to clear with current methods.

***Δphz*:** A mutant of *Pseudomonas aeruginosa* strain UCBPP-PA14 that is lacking the genes involved in biosynthesis of phenazines – redox-active metabolites.

Bioenergetic state: regarding the balance of energy conservation and consumption. Due to the link between electron flow, energy budgets, and carbon metabolism, this term can be synonymous with metabolic or energetic state.

Membrane potential $\Delta\Psi$: While this term has many definitions based on the model used, we use it to mean the charge difference across the cell inner membrane. The membrane potential is one component of the proton-motive force which powers ATP generation via the ATP synthase, flagella, nutrient uptake, and other processes.

Oxic/hypoxic/anoxic: These terms refer to the presence, limitation, or absence of molecular oxygen (O_2) from the environment, respectively.

Aerobic: A cellular or physiological process done in either the presence of oxygen or requiring it. Commonly used to refer to growth requiring oxygen.

Anaerobic: A cellular or physiological process done in the absence of oxygen or requiring its absence. Commonly used to refer to growth occurring in the absence of oxygen or requiring oxygen's absence.

Respiration: An energy-conserving metabolism where electrons are donated to a membrane-bound electron transport chain and finally a terminal electron acceptor. This transfer powers formation of a motive force and membrane potential to drive ATP generation via oxidative phosphorylation.

Fermentation: Entire papers are written discussing the appropriate definition of this term. We generally define it as an energy-conserving metabolic pathway where metabolites are used as both electron donors and acceptors for reducing equivalents, with ATP formation via substrate-level phosphorylation.

Central carbon metabolism: An organism's core network of metabolic reactions which fuel energy conservation and makes precursors for biosynthesis.

Embden-Meyerhof-Parnas pathway (EMPP): Typically referred to as "glycolysis". From 1 glucose the EMPP generates ATP and reducing equivalents as well as 2 pyruvate molecules. This pathway can run in reverse for "gluconeogenesis". *Pseudomonas aeruginosa* lacks a functional EMPP for glycolysis but can use the reverse gluconeogenic pathway.

Entner-Duodoroff pathway (EDP): An alternative glucose catabolic pathway found in certain bacteria. Also generates 2 pyruvate from 1 glucose with less required enzymatic steps but at the cost of a lower ATP yield. During aerobic growth, *Pseudomonas aeruginosa* uses this pathway for glucose catabolism.

Pentose-phosphate pathway (PPP): A central carbon metabolism pathway conserved across most organisms, containing the "oxidative" pathway which generates NADPH and the "non-oxidative" pathway which generates no reducing equivalents. The PPP is used primarily known for generating biosynthetic precursors and reducing equivalents but can also be used as an alternative glucose catabolism pathway. *Pseudomonas aeruginosa* does not contain an oxidative PPP.

Phosphoketolase: Proteins which cleave two carbon atoms from PPP metabolites such as fructose-6-phosphate and xylulose-5-phosphate, releasing acetyl-phosphate and erythrose-5-phosphate or glyceraldehyde-3-phosphate, respectively.

Ribonucleotides: Essential molecules composed of a ribose sugar, a phosphate group, and a nitrogenous base (typically adenine, cytosine, guanine, or uracil). Are used in the biosynthesis of energy-carriers, RNA, NAD+, the cell wall, or various macromolecule modifications. Deoxyribonucleotides differ in the use of a deoxyribose sugar and are used to produce DNA.

Colony-forming-units (CFUs): A technique for identifying the number of culturable cells from a sample by growing serial-dilutions of the cell population.

Chapter 1

INTRODUCTION

It is astounding to me that I would find myself writing a thesis revolving around bacterial metabolism. If the reader is anything like me, there was a time where the subject of metabolism was simultaneously terrifying and quite boring. Cellular metabolism networks looked like a tangled mess of Christmas lights. Meanwhile, memorizing the TCA cycle in biochemistry classes felt horribly dull. So, what changed? One transformative experience came from a class taught by my advisor entitled "Microbial Metabolic Diversity". Through this course it became clear that underlying these complex metabolic webs there were unifying rules which one could build an intuition for. Namely, that all metabolism is based on the movement of electrons from source to sink, with each metabolic node simply representing a way to regulate, balance, or use these redox reactions for cellular processes. The second transition in my appreciation for metabolism occurred over the course of the entire PhD. This being the slow realization of how insane it is that all life relies on such redox balancing.

In biology classes we are taught the "central dogma of biology" which corresponds to the transcription of DNA to RNA and its subsequent translation to protein. Yet to even carry out such a feat, cells must already have on hand the DNA, enzymes, and energy to power this process. A blueprint of a house is essential, but it is no replacement for the tools and supplies to build it. So, if a cell needs these supplies before it can even build another cell, how do you begin? Thankfully, this was handled by our parents, with the essential enzymes, energy, and blueprints provided for us as an

embryo. Yet where did our parents receive their IKEA set to build their own cells? Well from their parents of course. If this line of reasoning is followed to its completion, it leads to what I find is an insane conclusion. That we owe our existence to a gift from a single cell which found a way to balance the flow of electrons to power the construction of entire organisms with the capability to replicate *ad infinitum*.

In this framing, life is a self-sustaining redox reaction. This is why humans eat – electron and biomass source – and breathe – electron sink. Meanwhile, for microbes, the continuation of this directive across changing environments has led to a vast diversity of metabolic strategies, the consequence of this diversity leading these invisible organisms to terraform our entire planet. While this framing of life lacks a responsible amount of the nuance and emotion behind the nature of existence, I hope by now in the thesis the reader shares my excitement for metabolism.

Throughout the history of microbiology, the study of metabolism has focused primarily on exponential growth, where cells are awash in nutrients and electron acceptors, dividing rapidly at sub-hour generation times. Such an emphasis on growth metabolism made sense, for a time, as replication is essential for evolutionary success and growth rate is a fantastic quantitative output that is highly descriptive of cellular physiology. Additionally, this research focus on growth has paid off, helping us to maximize bacterial culture yields and metabolism of novel substrates for use in bio-production of alternative fuels or medicine. However, such redox balance and rapid growth is rarely seen in nature, with bacteria commonly found under nutrient limitation (the focus of Chapter 2) or electron-acceptor limitation (the focus of Chapters 3 and 4).

The resulting redox imbalance caused by such conditions leads to cessation of growth. For a bacterium in this state, the goal is now to survive.

Therefore, this historic focus on growth metabolism has left us fairly in the dark concerning the unity and diversity of metabolic strategies bacteria use to support non-growth survival. Furthermore, it has led to assumptions of what a "good metabolism" entails and classifications that fail to capture the tools bacteria use to support survival. Research into bacterial survival frequently challenges these assumptions. Yet further work is desperately needed. In clinical settings we fail to eradicate growth-arrested pathogenic bacteria, many of our antibiotics relying on a steady metabolic rate for their lethality. Within synthetic biology we struggle to engineer bacteria to achieve certain functions when metabolism slows. Across our biosphere we lack an understanding of the rate of bacterial metabolism and therefore their contribute to biogeochemical cycles.

Throughout this thesis, I hope to play my part in bridging this gap. The opportunistic pathogen *Pseudomonas aeruginosa* is a highly studied organism known for its metabolic versatility and ability to survive long-periods of nutrient or redox stress. *P. aeruginosa* can colonize a diversity of environments from the ocean, to soil, to the keyboard being used to type this thesis. Sadly, this metabolic personality allows it to excel at forming chronic infections within immunocompromised individuals. Unlike some bacteria, *P. aeruginosa* is unable to grow in the absence of terminal electron acceptors such as molecular oxygen or nitrogen-oxides. Historically, this inability to grow fermentatively would be deemed as a "failing" on *P. aeruginosa*'s part. Yet its ability to persist and not grow during redox imbalance is at the heart of its sinister nature, being incredibly hard to clear with clinical antibiotics. In the following chapters I investigate strategies

employed by *P. aeruginosa* to tolerate stress under growth arrest, with an emphasis on survival during redox imbalance. Later, I show that some of these strategies are generalizable across bacterial taxa.

Chapter overviews

More specifically, in the second chapter I dive into a study I conducted finding that *P. aeruginosa* can suppress its bioenergetic state under carbon starvation via phenazines – endogenous redox-active metabolites that act as electrons donors or acceptors. While historically such a lowering of the cellular energy state would be deemed detrimental, I show that this phenomenon provides protection against various clinical antibiotics. This matches previous studies linking antibiotic lethality to the metabolic rate of the cell and calls for further work to investigate how to target these low energy populations or avoid their formation.

In the preceding chapter I show how bacterial metabolic strategies can challenge our assumptions of what a "good metabolism" means under oxidative stress, aka the lack of electron source in presence of a sink. Within the third chapter I transition to the metabolic strategies of *P. aeruginosa* under reductive stress, aka the lack of electron sinks in the presence of an electron donor, specifically a lack of oxygen. I find that during anaerobic survival, *P. aeruginosa* uses a previously undiscovered glucose catabolic pathway relying on the pentose-phosphate pathway and a phosphoketolase. The similarity between this pathway used by this "non-fermentative" organism for survival and that used by many obligate anaerobes to grow fermentatively highlights how survival metabolism can challenge our previous classifications. Further discovery of what cells

are actually doing during survival will help us understand what processes to target or manipulate in these organisms.

Bridging the third and fourth chapter I find that under anaerobic survival cells undergo dramatic ribonucleotide degradation, with any re-synthesis being via the salvage pathway. Such molecular turnover in the context of continued catabolism leads to accumulation of metabolite pools, requiring *P. aeruginosa*'s phosphoketolase to regain balance. These experiments highlight shared metabolic patterns during survival under oxidant-limitation between *P. aeruginosa* and cancer cells while exposing continued mysteries concerning the role of ribonucleotide homeostasis in these systems. Finally, through bioinformatics and classical genetics, we show that phosphoketolases broadly support anaerobic survival for bacteria as well as propose a new function for phosphoketolases in promoting ribonucleotide homeostasis.

In the fifth and final chapter, I attempt to briefly summarize my conclusions and discuss future directions for other scientists. There were a vast number of observations and hypotheses generated throughout my PhD, and while I have tried to note and explain what I have deemed the most fruitful of these directions, I encourage readers to reach out and fuel my hobby of discussing bacterial metabolism.

C h a p t e r 2

BIOENERGETIC SUPPRESSION BY REDOX-ACTIVE METABOLITES PROMOTES ANTIBIOTIC TOLERANCE IN *PSEUDOMONAS AERUGINOSA*

Abstract

The proton-motive force (PMF), consisting of a pH gradient and a membrane potential ($\Delta\Psi$) underpins many processes essential to bacterial growth and/or survival. Yet bacteria often enter a bioenergetically diminished state characterized by a low PMF. Consequently, they have increased tolerance for diverse stressors, including clinical antibiotics. Despite the ubiquity of low metabolic rates in the environment, the extent to which bacteria have agency over entry into such a low-bioenergetic state has received relatively little attention. Here, we tested the hypothesis that production of redox-active metabolites (RAMs) could drive such a physiological transition. *Pseudomonas aeruginosa* is an opportunistic pathogen that produces phenazines, model RAMs that are highly toxic in the presence of molecular oxygen (O_2). Under oxic conditions, the phenazines pyocyanin and phenazine-1-carboximide, as well as toxoflavin—a RAM produced by *Burkholderia* species—suppress the $\Delta\Psi$ in distinct ways across distributions of single cells, reduce the efficiency of proton pumping, and lower cellular ATP levels. In planktonic culture, the degree and rate by which each RAM lowers the $\Delta\Psi$ correlates with the protection it confers against antibiotics that strongly impact cellular energy flux. This bioenergetic suppression requires the RAM's presence and corresponds to its cellular reduction rate and abiotic oxidation rate by O_2; it can be reversed by increasing

the ΔΨ with nigericin. RAMs similarly impact the bioenergetic state of cells in (hyp)oxic biofilm aggregates. Collectively, these findings demonstrate that bacteria can suppress their bioenergetic state by the production of endogenous toxins in a manner that bolsters stress resilience.

Significance Statement

All life relies on redox reactions to conserve energy, typically via the generation and dissipation of an electrochemical gradient across the cell membrane. Attenuation of this gradient leads to a lowered cellular energetic state, promoting survival to various stressors, including clinical antibiotics. *Pseudomonas aeruginosa* is an opportunistic pathogen that is highly antibiotic tolerant and persists at low metabolic rates. Here we test the hypothesis that redox-active secondary metabolites made by *P. aeruginosa* and other bacteria can result in bioenergetic suppression under oxic conditions, promoting tolerance to select antibiotics in planktonic culture and biofilms. Our results exemplify the adage "what doesn't kill you makes you stronger," and reinforce emerging efforts to combat pathogens by modulating their bioenergetic state.

Introduction

One of the most effective bioenergetic strategies employed by all forms of life to conserve energy is the production of an electrochemical gradient across the cell membrane. The most classically studied example of this is the proton-motive force (PMF), made up of both a proton gradient (ΔpH) and an electrical gradient, the membrane potential (ΔΨ). The PMF is vital for energy conservation, being used to drive ATP synthesis via proton influx through ATP synthase during oxidative

phosphorylation (1). At circumneutral pH, the PMF is dominated by ΔΨ. Beyond energy conservation, under these conditions, a sufficient ΔΨ is required for cell division (2, 3), membrane transport (4), and motility (5). Additionally, changes in ΔΨ have been shown to facilitate cell-to-cell communication (6) and mechanosensation (7). Yet even though ΔΨ is a core pillar of cellular physiology, its physiological modulation in bacteria is poorly understood.

Under nutrient-rich conditions during exponential phase, a lowering of ΔΨ and metabolic rates is detrimental to a bacterium's fitness. However, it is now well-appreciated that many bacteria live under nutrient-limited conditions where their metabolic rates are attenuated (8). This physiological state can be beneficial, such as in the case of "dormant" or "persister" cells that can withstand many stressors, including clinical antibiotics (9–11). The bioenergetic strategies bacteria use to regulate entry into these attenuated metabolic states are not well understood, though recent studies have begun to shed light on them (12–15). For example, when bacteria experience nutrient limitation, the stringent response can result in persister formation via the induction of Type 1 toxin-antitoxin systems that lead to PMF collapse and ATP release (16, 17).

Though diverse exogenous perturbations can trigger bioenergetic suppression, the potential for cells to lower their own bioenergetic state via the production of endogenous metabolites has received less attention. Previously, it was shown that salicylic acid, an endogenous metabolite, can inhibit the respiration of mitochondria, alter the redox-state of cells, cause reactive-oxygen species (ROS) bursts, and collapse the ΔΨ of *E. coli*, generating persister cells. (18–20). While the mechanisms behind these effects of salicylic acid are unknown, these effects are comparable to those of

endogenous redox-active metabolites (RAMs) that directly alter the redox state of the cell and produce ROS (21). Given the conserved chemical properties of RAMs and ecological diversity of RAM producers (22) we hypothesized that these metabolites could lower a bacterium's bioenergetic state.

RAMs are small diffusible compounds produced by many different bacteria and can alter bacterial physiology in different ways depending on the chemical microenvironment (22, 23). Phenazines are a class of RAMs produced by many actinomycetes and proteobacteria, including *Pseudomonas aeruginosa*—an organism in which the physiological effects of phenazines have been well studied (23, 24). For example, phenazines can be beneficial or detrimental to the cell depending on how much O_2 is present. Under anoxia, *P. aeruginosa* can utilize phenazines as an alternative electron acceptor to aid in redox balancing and facilitate pyruvate fermentation (25, 26). However, under oxic conditions, phenazines can kill various cell types, including their producers, by stimulating the production of reactive oxygen species or diverting reducing equivalents away from cellular metabolism (27–29). Phenazines are regulated by quorum sensing (30), and their production in batch culture begins at the end of exponential growth—a period when nutrients are becoming limited, reaching concentrations upwards of 100 μM in biofilms or during late stationary phase *in vitro* (31, 32), and similar concentrations in human infections (33). Phenazines have the potential to affect the electron transport chain in multiple ways: (i) by consuming cellular reducing power (25, 34) (ii) by donating electrons to the quinone pool (25, 35) and (iii) by depleting O_2 via reduction to superoxide (28). Additionally, phenazines can indiscriminately oxidize Fe-S clusters, flavoproteins, and thiols (34, 36, 37). In the

presence of phenazines, *P. aeruginosa* induces various defense pathways, including efflux pumps, oxidative stress genes, and protein repair pathways--many of which further consume reducing power and ATP (27). While these bioenergetic consequences might seem detrimental, we wondered whether—paradoxically—the bioenergetic toll phenazines exact might promote cellular fitness in the presence of exogenous stressors.

To answer this question we investigated the bioenergetic response of *P. aeruginosa* to its own phenazines as well as to toxoflavin, a different RAM produced by members of the *Burkholderia* genus (38). Because *P. aeruginosa* is a notorious opportunistic pathogen that tolerates frontline antibiotics such as tobramycin and ciprofloxacin, we asked if the increased tolerance RAMs confer to these drugs under oxic conditions—both in the planktonic (39, 40) and biofilm state (41, 42)—might be linked to bioenergetic suppression. Given that the lethality of bactericidal antibiotics in general is positively correlated with metabolic rates (10, 11, 43), we hypothesized that under oxic conditions, RAM-mediated lowering of the PMF would provide a fitness advantage in the presence of these antibiotics.

Results

Redox-active metabolites lower the membrane potential, proton pumping efficiency, and ATP levels of *P. aeruginosa*

While phenazines have been shown to be reduced directly by NADH and cellular reductases (25, 34), to react with O_2 and generate superoxide (28), and to be lethal when energy is limited (27), whether they lower the PMF under these conditions has not been studied. Therefore, we sought to measure the effects of three primary phenazines made by *P. aeruginosa* (pyocyanin—PYO, phenazine-1-carboxylic acid—

PCA, and phenazine-1-carboxyamide—PCN) and another RAM (toxoflavin) on both components of the PMF, ΔΨ and ΔpH, under oxic nutrient-limited conditions. RAM structures shown in Figure S1. To control RAM exposure, we utilized a *P. aeruginosa* UCBPP-PA14 Δ*phz* strain unable to make phenazines (39).

We began our comparative studies of RAMs with PYO. Stationary-phase LB cultures were washed into PBS to remove nutrients, then treated with physiologically-relevant concentrations of PYO (33), CCCP, or nigericin. CCCP is a protonophore that lowers ΔΨ while nigericin is an ionophore that has been empirically shown to increase the ΔΨ (44, 45). We used stationary-phase cells as phenazines are not produced until late exponential phase, and we were interested in the bioenergetics of non-growing, nutrient-limited populations. To measure ΔΨ, we utilized the dye 3,3'-diethyloxacarbocyanine iodide ($DiOC_2(3)$), that is imported in a ΔΨ-dependent manner. $DiOC_2(3)$ fluoresces green, but aggregates when concentrated within cells, causing a fluorescence shift to red. Therefore, a ratio of red/green fluorescence serves as a proxy for ΔΨ: the higher the ratio, the higher the ΔΨ (46). As expected, nigericin increased the red/green ratio, while CCCP dramatically lowered it (Figure 1A). As hypothesized, PYO caused a pronounced lowering of ΔΨ (Figure 1A). Untreated cell suspensions had two subpopulations, one more highly polarized, and the other as lowly polarized as PYO-treated cells, while PYO-treated cells were homogenously depolarized (Figure 1A). Nigericin-treated suspensions also contained several subpopulations (Figure 1A). These data support our hypothesis that RAMs can lower ΔΨ under conditions that promote their toxicity and suggests that PYO primarily affects the more polarized subpopulation.

Cells generate a ΔΨ via respiration-dependent proton pumping, simultaneously producing a ΔpH; other ions also contribute to the ΔΨ (47). We hypothesized that PYO's lowering of the ΔΨ could be caused by upstream effects upon the coupling of respiration to ΔpH generation. To test this, we measured proton pumping during O_2 respiration using a classic oxidant-pulse assay (48). Anaerobic, weakly-buffered suspensions of *Δphz* cells were given known concentrations of O_2 via air-equilibrated H_2O, and proton translocation was measured as a change in the extracellular pH via a sensitive pH electrode. As expected, the addition of air-equilibrated H_2O led to sudden drops in the pH, consistent with respiration-dependent proton pumping (Figure 1B). At the end of each experiment, different volumes of anoxic 1 mM HCl (i.e. known amounts of protons) were added to create a proton vs. ΔpH standard curve (Figure 1B). We measured the protons pumped per atom of oxygen respired (H^+/O) to be about 5, similar to a measurement of about 4 previously made in *P. aeruginosa* strain PAO1 (49). In the presence of PYO, H^+/O was suppressed in a dose-dependent manner (Figure 1C). These data show that PYO lowers its producer's ability to conserve energy during respiration, presumably contributing to its reduction of the ΔΨ under these conditions. Similar suppressive effects on the ΔΨ and the H^+/O ratio were also observed in the presence of PCN, PCA and TOX, though to different extents (Figures 1D, 1E). We confirmed that our $DiOC_2(3)$ findings were not affected by changes to cell dimensions following RAM pre-treatment (Figure S2A and S2B).

The PMF drives oxidative phosphorylation, the primary ATP generating mechanism used by *P. aeruginosa* under oxic conditions (1). ATP can also be broken down into ADP + P_i, driving proton translocation across the membrane to aid in PMF

formation. Therefore, we wondered if a drop in ΔΨ was also associated with a loss of ATP. All RAMs tested lowered the cellular ATP concentration in the same order in which they suppressed the ΔΨ (Figure 1F). We also found that the addition of PYO to cells suspended in PBS prevented reductive divisions commonly observed upon nutrient starvation (Figure S3), consistent with the need for a strong PMF to support cell division (2, 3, 50).

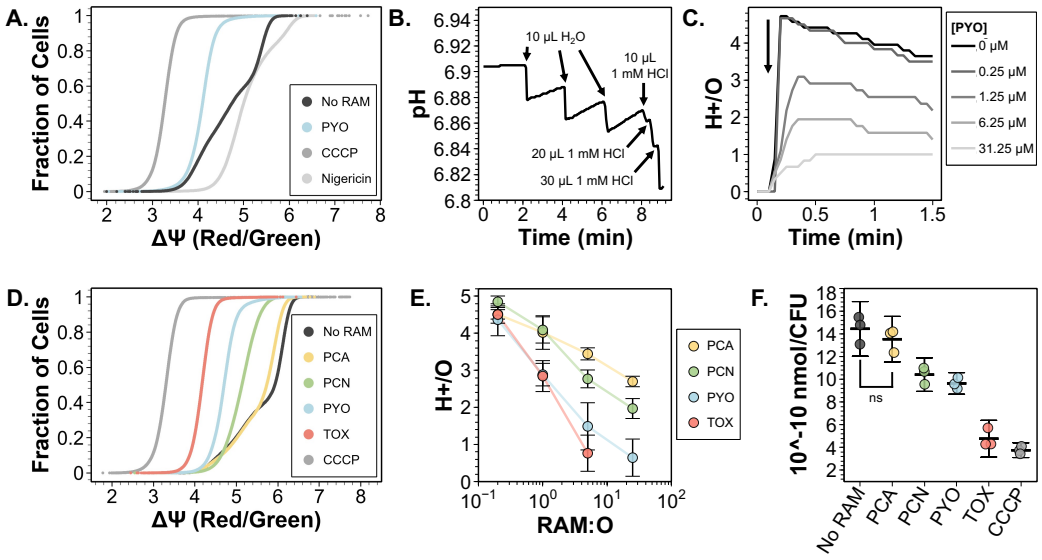

Figure 1. RAMs lower the ΔΨ, proton-pumping, and cellular ATP levels of *Δphz* cell suspensions. (A, D) ECDFs showing $DiOC_2(3)$ Red/Green fluorescence ratios of representative cell suspensions treated for 1 hour. Nigericin raises the ΔΨ while PYO, PCN, PCA, TOX, and CCCP lower it. PCA has a minimal effect. Each condition contains 50,000 events. (B) Representative single replicate of respiratory proton translocation measured from whole cells in response to pulses of oxygen added as air-equilibrated water. See Methods for conditions. (C) Representative replicate showing proton translocation inhibition in response to increasing concentrations of PYO. Cells were incubated with the added PYO for 1.5 min before oxygen pulses began. (E) Proton

translocation inhibition of various RAMs. RAM:O is the molar ratio of the RAM present to the O atoms added in a single oxygen pulse. Each data point is an average of two biological replicates and error bars represent the standard deviation. Proton translocation at the highest concentration of toxoflavin was not detectable. (F) Cellular ATP concentrations (10^-10 nmoles/CFU) measured from cell lysates show that a 1 hour incubation with PCA causes no change to cellular ATP levels, while PCN, PYO, TOX, and CCCP all lower it. Errors bars represent 95% confidence intervals. Each data point represents a biological replicates.

RAMs lower the membrane potential at different rates and produce unique subpopulations conferring stress tolerance

To determine whether bioenergetic suppression by RAMs would increase survival of cells to an exogenous stressor, we examined their effects on tolerance to tobramycin – an aminoglycoside antibiotic that disrupts protein synthesis, and whose import is dependent on the ΔΨ (51, 52). Planktonic *Δphz* cells were incubated with a RAM for up to an hour, and either stained to measure the ΔΨ, or treated with tobramycin for 2 hours and plated for colony forming units (CFUs). Cells incubated in PBS alone slowly lost ΔΨ over the hour incubation, while CCCP significantly lowered ΔΨ to a plateau within 15 minutes (Figure 2A). Each RAM other than PCA increased the rate of ΔΨ loss, with ΔΨ plateauing between 45 to 60 minutes of RAM treatment, and none lowering it to the same degree as CCCP (Figure 2A). Notably, PYO, PCN, and TOX lowered the ΔΨ within 15 minutes, but not to a steady state like CCCP. The degree of ΔΨ suppression correlated with tobramycin survival in each treatment, with PCA having no significant effect on ΔΨ or survival, PCN, PYO, and TOX decreasing

ΔΨ and increasing survival as a function of RAM exposure time, and CCCP causing an immediate and large drop in ΔΨ and increase in survival that remained constant (Figure 2A, 2B). To confirm that starvation and RAM-mediated tobramycin tolerance was not specific to *Δphz* cells, we repeated these experiments with washed WT PA14 cells, observing similar trends (Figure S4A). Incubation in PBS alone led to a decrease in ΔΨ and slight increase in tobramycin tolerance (Figure 2A, 2B), as would be expected due to a loss of energy sources (8, 9). Consistent with this interpretation, cells harvested from oxic stationary-phase cultures that were moved into PBS under anoxic conditions survived better than suspensions kept under oxic conditions (Figure S4B). In the absence of tobramycin, none of the pre-treatments significantly affected survival (Figure S4C). Additionally, the solvents used in RAM pre-treatments did not significantly alter the ΔΨ or tobramycin lethality (Figure S5A, S5B).

While the mean ΔΨ of a population of cells was predictive of their survival to tobramycin, RAMs generated unique ΔΨ population distributions. *Δphz* cells incubated solely in PBS had a more polarized and a less polarized subpopulation (Figure 2C). Following incubation in PBS, cells became increasingly depolarized (Figure 2C). PYO-treated cells had a singular population, whose distribution narrowed during the experiment, centering around the most depolarized subpopulation of untreated cells (Figure 2C). This suggests that PYO is buffering ΔΨ, leaving a lowly polarized population relatively unaltered, while preventing cells from generating a more highly polarized population. Like PYO, both TOX and CCCP generate single populations with depolarized membranes within 15 minutes (Figure 2D). While PCN-treated cells yield a single depolarized population within 15 minutes compared to the no-RAM condition,

their heterogeneity increases over time, shifting to increasingly lower polarization states (Figure 2D). Finally, PCA-treated and no-RAM conditions had similar mean ΔΨ levels and similar 15-minute population distributions (Figure 2D). However, PCA-treated cells maintained their initial distribution shape. This suggests that while PCA does not alter the bulk ΔΨ, it is inhibiting formation of a highly depolarized subpopulation. Population distributions at additional time points are shown in Figure S6.

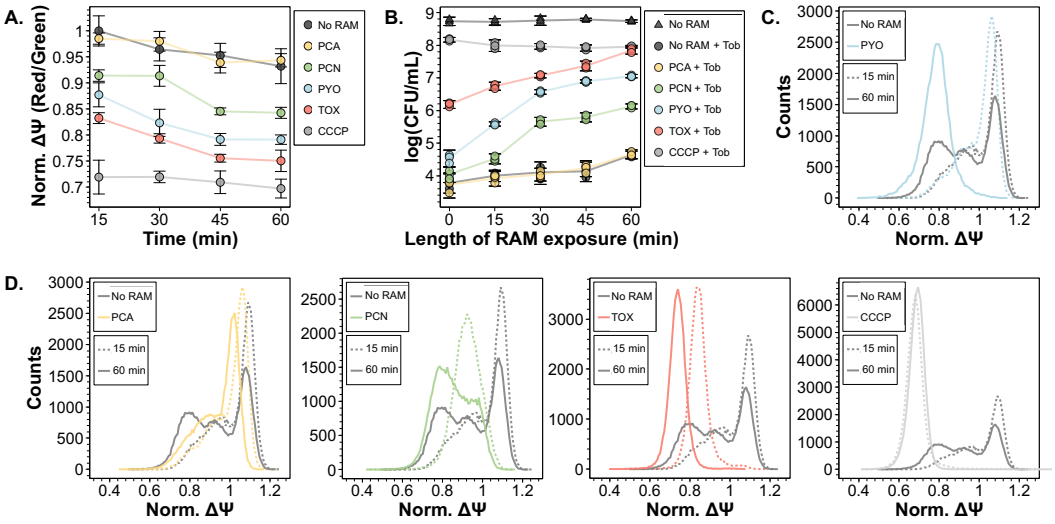

Figure 2. RAMs lower the ΔΨ to different degrees and generate unique population distributions over an hour of incubation, predictive of how well they protect cell suspensions against tobramycin. (A) RAMs lower the ΔΨ at different rates and to different magnitudes over an hour of incubation in PBS. Data points are the average of the mean of $DiOC_2(3)$ values from 3 biological replicates, normalized to the 15-minute No RAM condition. Error bars represent the standard deviation. Each data point represents 150,000 events. (B) RAMs differentially increase survival to tobramycin over an hour of incubation in PBS +/- RAM followed by an addition of 100 μg/mL of

tobramycin for 2 hours. Data points are log-transformed CFU/mL values from 3 biological replicates. Error bars represent 95% confidence intervals. (C, D) RAMs produce unique ΔΨ subpopulations. Incubation in PBS leads to depolarized subpopulations while PYO may buffer the ΔΨ at a level like the most depolarized No RAM subpopulation. Histograms of $DiOC_2(3)$ values from representative replicates from specific incubations and time points. Values are normalized to the No RAM 15-minute time point. Each line represents 50,000 events.

RAM-mediated bioenergetic suppression is tunable, does not rely on efflux pumps, and affects tolerance to diverse antibiotics

Because RAM-mediated tobramycin tolerance strongly correlated with lowering the ΔΨ, we predicted that this phenotype could be manipulated by tuning the ΔΨ. To test this prediction, we exposed cells to PYO in addition to CCCP (to lower ΔΨ) or nigericin (to raise ΔΨ). Treatment with both PYO and CCCP provided no additional benefit (Figure 3A). Pre-treatment with nigericin alone lowered survival to tobramycin, and co-treatment with nigericin and PYO prevented the PYO protective effect (Figure 3B). Utilizing $DiOC_2(3)$, co-treatment with nigericin and PYO led to ΔΨ levels similar to cells given no-treatment, consistent with the logic that if lowering the ΔΨ begets tobramycin tolerance, raising the ΔΨ should abolish PYO's protective effect (Figure 3B, 3C). As another test of this idea, the addition of succinate increased tobramycin killing, whereas the addition of glyoxylate decreased it (Figure S7A), consistent with previous studies demonstrating that these carbon sources increase or decrease the metabolic rate of cells, respectively, with corresponding consequences for antibiotic lethality (53, 54). Interestingly, PYO's presence was required to impact tobramycin survival (Figure 3D),

yet inhibition of efflux pumps (including those known to be induced by PYO) (27), did not appreciably impact the phenotype (Figure 3E). Finally, PYO-mediated protection was dose dependent, with concentrations as low as 12.5 μM increasing survival to tobramycin by around a log (Figure 3F). Within cystic fibrosis sputum, PYO has been measured at concentrations up to 130 μM (33).

To determine whether the protective effect of RAM-mediated bioenergetic suppression extended to other antibiotics, we tested representatives of different antibiotic classes: gentamicin (like tobramycin, an aminoglycoside), ciprofloxacin (a fluoroquinolone) and colistin (a polymyxin). Because sensitivity to aminoglycosides and fluoroquinolones is maximal when cells are metabolically active (10, 11, 43, 55), we anticipated that the ability of RAMs to confer tolerance to gentamicin and ciprofloxacin would resemble their effects on tobramycin tolerance. As expected, CCCP and all RAMs, except for PCA, protected cells from gentamicin whereas nigericin increased their susceptibility (Figure 3G). Likewise, all RAMs, except for PCA, protected cells from ciprofloxacin (Figure 3G). While CCCP confers ciprofloxacin tolerance, nigericin does as well (Figure 3G). Because the lethality of DNA-damaging agents, like ciprofloxacin, can depend upon DNA-replication, nigericin's known toxicity (56) could inhibit DNA replication – as seen in cancer cells (57) – or overall metabolic rates despite increasing the $\Delta\Psi$ (58). As previously observed in biofilm systems (42, 59), PYO slightly synergizes with colistin, a polymyxin that mechanically disrupts the outer membrane (Figure S7B). RAM-mediated antibiotic tolerance thus appears most relevant to antibiotics that are strongly dependent on metabolism (55) that disrupt processes

impacting the cellular energy budget (i.e. balance of energy usage and conservation) (11, 60).

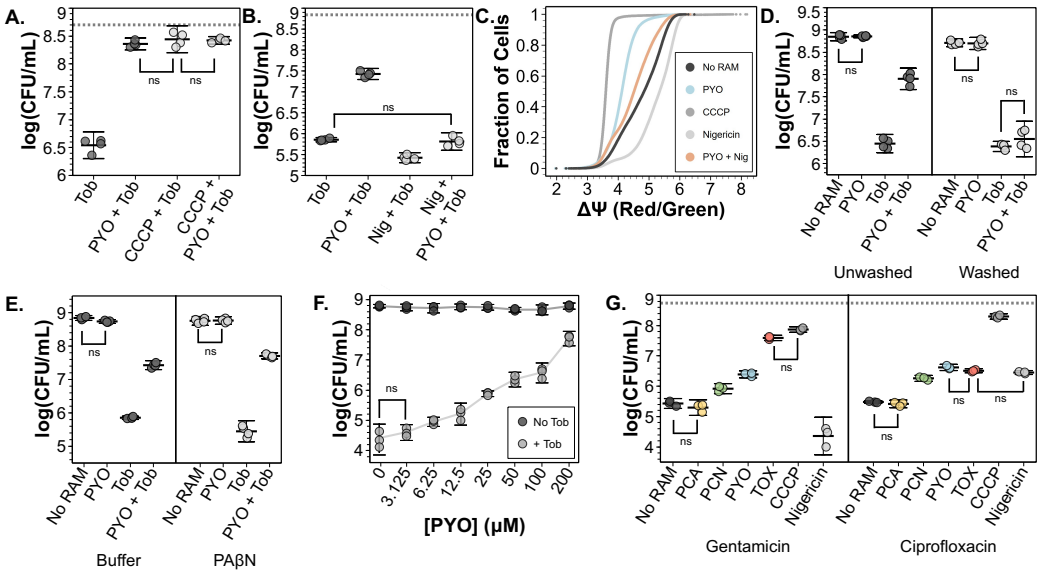

Figure 3. PYO-mediated tobramycin tolerance can be abolished with increases to the ΔΨ or removal of PYO, efflux pumps are not vital to this phenotype, and RAMs protect against gentamicin and ciprofloxacin similarly to tobramycin. (A, B) CCCP and PYO protect PBS cell suspensions from tobramycin while nigericin abolishes PYO-mediated tobramycin protection during PYO and nigericin co-treatment. (C) ECDFs of $DiOC_2)3$_ values from PBS cell suspensions treated with PYO, CCCP, nigericin, or a co-treatment of PYO + nigericin (PYO + Nig). Nigericin increases the ΔΨ of PYO-treated cells. (D) Washing PYO away after a 1-hour treatment abolishes PYO-mediated tobramycin tolerance. (E) Treatment with an efflux pump inhibitor does not dramatically alter PYO-mediated tobramycin tolerance. (F) Pre-treatment of cell suspensions with increasing concentrations of PYO leads to higher tobramycin tolerance. (G) RAMs protect against gentamicin and ciprofloxacin similarly to

tobramycin. (A, B, D, E, F, G) Log-transformed CFU/mL values. Each data point represents a biological replicate, 3 or 4 replicates per experiment. Error bars represent 95% confidence intervals. Where present, dotted lines represent mean survival of No RAM, non-antibiotic treated cells. (A, B, D, E, F, G) Antibiotics were added to PBS cell suspensions after a 1-hour pre-treatment (ex. PYO) and incubated 2 hours before CFU plating. Concentrations used were 100 μg/mL tobramycin, 10 μg/mL ciprofloxacin, or 200 μg/mL gentamicin.

RAM-mediated bioenergetic suppression and antibiotic tolerance extends to biofilms

Because the primary mode of bacterial life is within biofilms (61) – aggregates of cells in close proximity to each other enmeshed within an extracellular matrix – we sought to determine whether the RAM-mediated bioenergetic suppression we observed in planktonic culture translated to this lifestyle. For this purpose, we focused on PYO as a representative RAM. Specifically, we aimed to test if: (i) PYO increases biofilm survival against tobramycin, (ii) suppression of ΔΨ leads to biofilm protection, and (iii) tobramycin is lethal within the oxic exteriors of biofilms where PYO could be lowering ΔΨ. As we have done before (41, 62), we used the Agar Block Biofilm Assay (ABBA) to mimic how biofilm aggregates exist in chronic infections, where steep O_2 gradients develop over millimeter scales across the aggregate population and also within large individual aggregates in the hypoxic zone (Figure S8, 4A).

ABBAs were grown with WT PA14, ⊿*phz*, or ⊿*phz* + 100 μM PYO, before being exposed to tobramycin or ciprofloxacin. WT ABBAs and ⊿*phz* ABBAs chemically complemented with PYO survived tobramycin and ciprofloxacin more than ⊿*phz*

ABBAs (Figure 4B). Additionally, CCCP protected ABBAs from tobramycin, more so in ⊿*phz* ABBAs than in WT biofilms, suggesting bioenergetic suppression promotes tobramycin tolerance (Figure 4C). This effect operates in the (hyp)oxic zone, as seen by staining WT aggregates with SYTO-9 and propidium iodide (PI) following tobramycin treatment: cellular damage was restricted to aggregates occupying the top half of the ABBA block, coinciding with the region where O_2 is detectable (Figure 4D, 4E, S7).

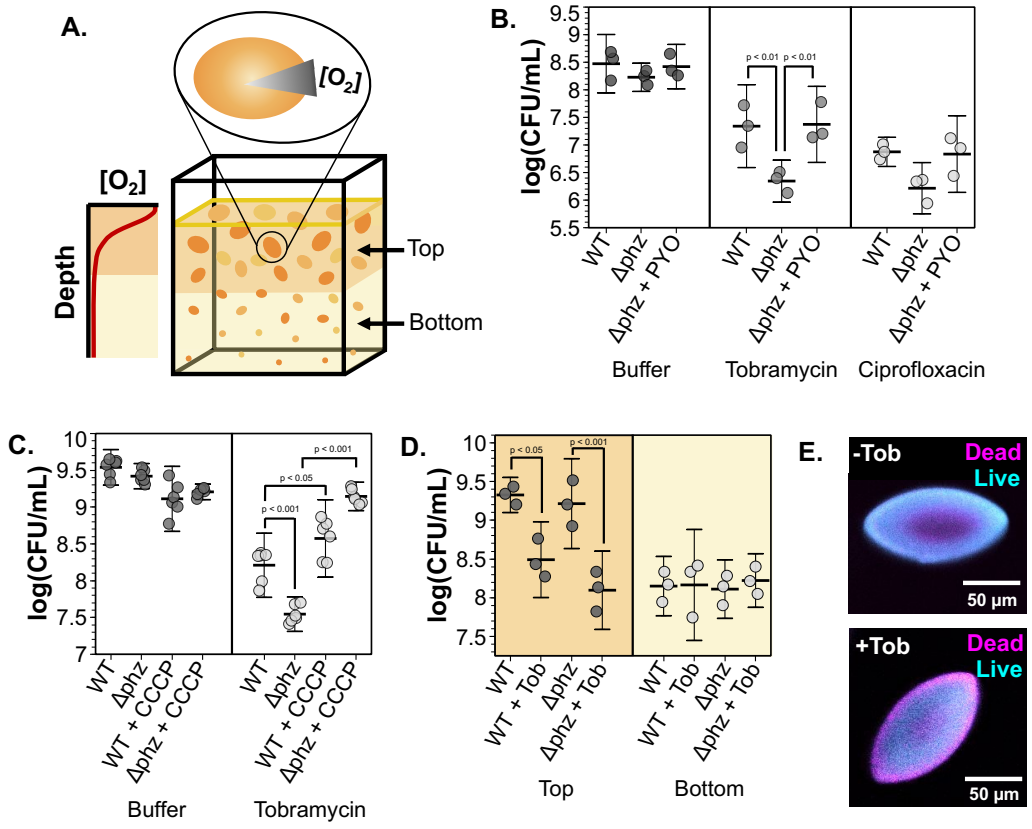

Figure 4. RAM bioenergetic suppression extends to aggregate biofilms, protecting cells in (hyp)oxic zones. (A) Graphical illustration of an Agar Block Biofilm Assay (ABBA) (B) PYO significantly protects ABBAs from tobramycin, and minorly from ciprofloxacin. (C) CCCP protects ⊿*phz* ABBAs from tobramycin more so than WT ABBAs. (D) Tobramycin lethality occurs in the top half of ABBAs. (E) Tobramycin

lethality occurs in the exterior of individual oxic/hypoxic ABBA aggregates. (B, C, D) Log-transformed CFU/mL values. Each data point represents a biological replicate, 3 or 6 per experiment. Error bars represent 95% confidence intervals. (E) Representative image of a slice of an individual ABBA aggregate stained with PI (magenta) and SYTO-9 (cyan). Scale bar = 50 μm. Antibiotic treatments were done for 4 hours using either 100 μg/mL tobramycin or 10 μg/mL of ciprofloxacin.

Discussion

The importance of bioenergetic suppression –typically represented by low $\Delta\Psi$ or ATP levels – in promoting bacterial stress tolerance is well documented (8–11), but the idea that cells themselves can drive entry into a state of metabolic attenuation has been less explored. In this work, we tested the hypothesis that "self-poisoning" induced by physiologically-relevant concentrations of redox-active secondary metabolites (31–33) can protect cells against killing by certain antibiotics. Using *P. aeruginosa* and four different RAMs, including three phenazines and toxoflavin, we found that RAMs exact a bioenergetic penalty to different extents (both on average and across a cellular population) and at different rates, in a manner that correlates with each RAM's reactivity. Because RAM-mediated bioenergetic suppression extends to biofilms and can be reversed by physiological interventions, such as treatment with nigericin, succinate, or removal of PYO, our results reinforce emerging observations (53, 54, 59, 63, 64) that modulating the bioenergetic state of pathogens holds promise for infection control.

Under oxic conditions, we find that RAMs directly suppress the bioenergetic state of cells over short time scales (minutes), enabling cells to resist killing by commonly used antibiotics. Interestingly, such protection appears to apply to antibiotics that are

strongly metabolism-dependent and inhibit energy-intensive processes such as translation (aminoglycosides) or DNA replication (fluoroquinolones) (11, 55). In contrast, PYO synergizes with colistin—a polymyxin antibiotic that disrupts the outer membrane and whose lethality is less dependent on cellular metabolic rates (55). This pattern of RAM-induced energy-depletion being broadly beneficial is consistent with studies showing that metabolic suppression can confer protection by 1) attenuating the physiological processes that antibiotics target and/or 2) preventing downstream lethal futile metabolic cycles (11, 65–67). Additionally, aminoglycosides, such as tobramycin, are imported in a ΔΨ-dependent manner (51). The ability of RAMs to increase tobramycin tolerance within 15 minutes, but not to its maximum extent, suggests they may act through any of these mechanisms. Moreover, our observation that RAM-mediated bioenergetic protection can be reversed by nigericin is consistent with previous studies showing that treatment of *P. aeruginosa* with promethazine (a drug that also increases the ΔΨ) or provision of TCA cycle-stimulating carbon metabolites increase respiration and tobramycin killing (53, 54, 63). That salicylic acid, a metabolite that also alters the cellular redox state and O_2 consumption, can induce similar bioenergetic protection against ciprofloxacin and ampicillin in *E. coli*, albeit requiring longer time scales of exposure (18, 68), leads us to speculate that bioenergetic suppression by endogenous metabolites may be more widespread than previously appreciated. While it is possible that RAMs function as ionophores, as has been suggested for indole – a non-redox cyclable metabolite that may act as a protonophore in *E. coli*, lowering the ΔΨ and arresting cell division (2, 13) – our observation that RAMs lower the ΔΨ more slowly than CCCP suggests additional mechanisms are at play.

The simplest explanation for RAM-mediated bioenergetic suppression under the condition of our experiments is direct RAM impact on ETC flux and consumption of O_2 (25, 28, 34, 69). This conclusion is supported by our data showing that the order in which each phenazine alters ΔΨ, proton pumping, ATP levels, and antibiotic survival (PYO > PCN > PCA) positively correlates with its cellular reduction rate (25), oxidation rate by O_2 (70), and its toxicity to *P. aeruginosa* (27). Yet RAMs may also impact the cellular energy budget in other ways, such as by inducing energy-consuming oxidative stress response machinery, protein repair systems, RAM efflux pumps, or increasing energy demand via direct or ROS-mediated cellular damage (27). Therefore, over longer timescales (hours), we expect RAMs to tune the bioenergetic state of the cell in multiple ways. However, it is significant that under the short-term conditions of our experiments, bioenergetic suppression required RAM presence. For instance, our observation that washing PYO away after an hour of pre-treatment provided no protection from subsequent tobramycin exposure, suggests that RAM induction of defense systems played a limited role in the observed tolerance or was rapidly reversed, in contrast to studies using indole, salicylic acid, or previous studies of PYO-mediated ciprofloxacin tolerance (14, 20, 39). This conclusion is reinforced by the fact that addition of an efflux pump inhibitor did not impact PYO-mediated tobramycin tolerance.

The increase in heterogeneity of single cell ΔΨ values observed during carbon starvation was striking, as was the rapid "buffering" of the ΔΨ in the presence of PYO and to a lesser extent in the presence of PCN and PCA (*i.e.* PYO treatment rapidly induced uniform bioenergetic suppression across the population, whereas PCN and PCA-treated cultures retained a broader ΔΨ distribution). Several studies have shown

the ΔΨ of *E. coli* and the metabolism of *P. aeruginosa* is heterogenous in stationary-phase populations (17, 71), therefore, we speculate that ΔΨ heterogeneity in non-RAM treated cells is due to previously described stochasticity in metabolic pathway usage under stress conditions, with consequences for antibiotic tolerance (72–75). In the presence of RAMs that are rapidly reduced (e.g. PYO and TOX), the transition from a more polarizing metabolic strategy to a more depolarized one is hastened. How might this work? Beyond lowering flux through the ETC by diverting electrons from NADH dehydrogenases or reducing NADH production by substituting for NAD^+ in Krebs cycle enzymes such as pyruvate or alpha-ketoglutarate dehydrogenase (25, 34), the ability of reduced RAMs to reduce O_2 could potentially "short-circuit" the ETC (28, 29), leading to less efficient ATP formation. For this later scenario to be plausible, the abiotic rate of RAM oxidation by O_2 would need to exceed the rate of electron transfer to O_2 through the ETC, motivating future studies of both abiotic and respiratory reaction rates under different levels of O_2. Lastly, ATP may also be lost to maintain a PMF in the presence of RAMs, as cells treated with DCCD – an ATPase inhibitor – die in the presence of PYO even when given abundant nutrients, or via induction of ATP-dependent stress responses (27). All together, we speculate these effects would force the entire population into a more homogenous metabolic state.

While RAMs are known to generate superoxide in the presence of O_2, they may attenuate antibiotic-mediated oxidative radical generation or generate ROS at less-lethal sites. For instance, aminoglycoside-induced ribosome inhibition is proposed to cause backpressure in the electron transport chain, leading to build up of reduced enzyme redox-centers (43, 60, 76, 77). ROS generation by these redox-centers directly damages

enzymes and catalyzes further radical generation, such as hydroxyl radicals (77). These highly reactive radicals react with any adjacent biomolecule, leading to lipid, protein, and DNA damage (60, 77, 78). RAM reduction by flavins and Fe-S clusters could relieve this backpressure, preventing ROS generation at these sensitive sites, and instead generating superoxide at a distance. In a similar vein, multiple studies have shown transient hyperpolarization to lead to cell death upon antibiotic exposure (45, 76, 79), thought to be caused by use of ATPase during metabolic dysregulation, driving proton translocation and furthering ETC backpressure. Therefore, RAM relief of this backpressure, or burning of ATP via a similar mechanism would prevent such spiking (76). Usage of recently-developed voltage gated fluorescent reporters (45) to observe single-cell responses to RAM addition under different nutrient conditions would allow this hypothesis to be tested.

In conclusion, a growing number of studies have documented that lowering the bioenergetic state confers increased antibiotic tolerance to diverse pathogens (11, 12, 15, 17). Our contribution to this literature is to add RAMs as a general class of causative agents by which such metabolic attenuation is achieved. Though our study demonstrates a proof-of-concept using three different phenazines and toxoflavin as model RAMs, we believe it points to a broader phenomenon. Awareness of RAMs' ability to tune the PMF up or down as a function of the cellular microenvironment motivates consideration of how secreted secondary metabolites may influence the bioenergetic state of microbial communities.

Materials and Methods

Strains, culture conditions, and reagents

Strains were derived from *P. aeruginosa* UCBPP-PA14 (DKN263, laboratory strain). The ⊿*phz* mutant for proton pumping assays lacked the *phzA1-G1* and *phzA2-G2* operons (80) while the ⊿*phz* mutant for all other assays additionally lacked the *phzH*, *phzS*, and *phzM* genes (39).. Cells were streaked from 20% glycerol -80 °C freezer stocks onto Difco LB 1.5% agar plates (BD Biosciences) and grown overnight at 37 °C. Planktonic cultures were made with 5 mL of Difco LB and grown for 20 hours at 37 °C at 250 RPM to reach late stationary phase, OD_{500nm} ~ 5. Exponential-phase cells were made by diluting overnight cultures 1:1000 in fresh 5 mL of LB and grown for 4 hours at 37 °C at 250 RPM to an OD_{500nm} ~0.6. Cell suspensions for ΔΨ, ATP, and antibiotic-survival experiments were made by diluting stationary-phase cells to an OD_{500nm} of 0.5 in 2 mL Eppendorf tubes and washing 3x at 10,000xg for 3 minutes in PBS (137 mM NaCl, 2.7 mM KCl, 10 mM Na2HPO4, 1.8 mM KH2PO4, adjusted to pH 7.2 with 6M HCl and autoclaved) and resuspended to an OD_{500nm} of 0.5. 300 μL of cells were aliquoted into 2 mL Eppendorf tubes with holes poked in the lids with a 20 G needle to ensure O_2 exposure and incubated at 37 °C at 250 RPM. In Figure S7, cell suspensions were made as described above, except cells were washed and resuspended in a MOPS MM lacking a carbon source (100 mM anhydrous MOPS, 50 mM NH_4Cl, 3.7 mM KH_2PO_4,1 mM $MgSO_4$, 3.6 μM $FeSO_4$, adjusted to pH 7.2 with NaOH and filter sterilized). For all cell-suspension assays, the starting CFU/mL was around 10^8.5 to 10^9 CFU/mL and did not change dramatically in control experiments such as shown in Figure S4C.

PYO was synthesized and purified using a modified protocol presented in (41). Stocks of 6.89 mM PYO, 10 mM PCN (Chemscene), 10 mM PCA (Princeton Bio), 10 mM TOX (MedChemExpress), 10 mg/mL tobramycin (TCI), 50 mg/mL gentamicin (Gibco), 1 mg/mL ciprofloxacin (Fluka), 1 mg/mL colistin (Sigma), 20 mM $DiOC_2(3)$ (Invitrogen), 20 mM CCCP (MedChemExpress), 10 mM nigericin (MedChemExpress), 20 mM PI (Invitrogen), 5 mM Syto-9 (Invitrogen), 20 mM Cy5-Carboxylic acid, and 20 mM Cy5-Tobramycin were all stored at -20 °C. PYO and ciprofloxacin stocks were made using 20 mM HCl. PCA stocks were made using 20 mM NaOH. Tobramycin and gentamicin stocks were made using deionized H_2O. All others were solubilized in DMSO. Unless otherwise stated, final concentrations of CCCP, PYO, PCN, PCA, and TOX were 100 μM; nigericin was 50 μM, tobramycin was 100 μg/mL, gentamicin was 200 μg/mL, ciprofloxacin was 10 μg/mL, and colistin was 10 μg/mL.

ΔΨ measurements

ΔΨ was measured with $DiOC_2(3)$ via a method adapted from the ThermoFisher BacLight Bacterial Membrane Potential Kit protocol. Cell suspensions were given 1 mM EDTA pH 8 and 75 uM $DiOC_2(3)$ and incubated at 37 °C at 250 RPM for 15-20 minutes. Staining occurred in the presence of RAM, CCCP, or nigericin treatments. Cells were washed once at 8000 xg for 2 minutes and resuspended in 500 μL of PBS. Samples were analyzed on an Accuri C6 flow cytometer (BD Biosciences). Cell fluorescence was measured at 488 nm excitation and 530 nm (green, FL1) and 610 nm emission (red, FL3). Thresholds of FSC-H of 10,000 and FL1 of 1,000 were used during sample capture and data with FL3 levels below 1,000 was removed to ensure only dyed bacteria were captured. FL3 fluorescence was divided by FL1 fluorescence, multiplied by an

arbitrary value of 385 – adapted from the BacLight protocol – to obtain values above 0, and log transformed to obtain red/green ratios. For figure 2A, the mean fluorescence ratio for each biological replicate was normalized to the average mean ratio of the first No RAM timepoint. For Figure 1A, 1D, and 3B, cell suspensions were incubated in PBS +/- treatment (ex. PYO) for 40 minutes before a 20-minute $DiOC_2(3)$ stain within the same solution. For Figure 2A, 2C, and 2D, cells were given treatments for 0, 15, 30, or 45 minutes before a 15-minute $DiOC_2(3)$ stain.

Measurement of proton-pumping

Overnight cultures of *Δphz* cells were washed twice at 6800xg for 5 min into 0.5 mM HEPES pH 7.0, and 125 mM KCl. Pellets were brought into an anaerobic chamber (Coy) and resuspended in N_2-sparged 0.5 mM HEPES pH 7.0, 75 mM KCl, and 100 mM KSCN. Cell suspensions were diluted to a total volume of 4 mL and an OD_{500nm} of 4.0 and placed in small glass vials (Fisher Cat. No. 03-339-26C0) with a magnetic stirbar (Fisher) and left to rest for 30 min. A pH electrode (Thermo Orion 8103BNUWP) was calibrated at the beginning of each day. The pH electrode was submerged in the suspension while stirring and left to equilibrate for 4 min. The pH was adjusted with 10 mM KOH to an initial pH between 6.9 and 7.1. A 2 min baseline was recorded with a Thermo Orion STAR COM software, followed by three additions of 10 μL of air-equilibrated H_2O (250 μM O_2). When applicable, RAM was added after the 2 min baseline, followed by 10 μL of water every 1.5 min after. At the end of this series, 10, 20, and 30 μL of 1 mM HCl were added (i.e., 10, 20, and 30 nmoles H+ respectively) to generate a standard curve using linear regression. This was then used to convert ΔpH values to nmoles protons extruded. Dividing the nmoles of protons extruded by the 5

nmoles of oxygen atoms added per pulse gave the final H+/O values reported. The largest ΔpH caused by the three O_2 pulses was used for averaging. All experiments were conducted at 25 °C.

ATP measurements

ATP was measured after 1 hour incubation in PBS. 40 μL of cell suspension was added to 160 μL of DMSO to dissolve cells, then diluted with 800 μL of 0.1 M HEPES pH 7.2. 25 μL of each sample was mixed with 25 μL of Promega BacTiter-Glo reagent in a 96-well opaque microtiter plate and incubated at 25 °C in the dark for 10 minutes. Luminescence was measured at 25 °C in a Spark 10M plate reader (Tecan). A standard curve of ATP was made in the same mixture used to prepare cells. The resulting slope was used to determine the ATP concentrations within samples and normalized to the CFU/mL values from the same suspensions.

Cell suspension antibiotic survival assays and imaging

Cells were incubated in PBS +/-treatment for 1 hour at 37 °C at 250 RPM then given ciprofloxacin, gentamicin, tobramycin, or colistin for 2 hours. 200 μL of each suspension was used for 10-fold serial dilutions by mixing 20 μL of cells into 180 μL of LB. 10 μL of each dilution was spotted onto LB agar and incubated overnight at 37 °C. When possible, dilutions with 20 to 200 colonies were counted. For time-course experiments, cells were given tobramycin immediately post PBS washing or after 15, 30, 45, or 60 minutes of incubation in PBS +/- RAMs or CCCP.

For images of PYO-treated cells, PBS cells suspensions were loaded into a Millipore CellASIC microfluidic chamber bacteria plate and transferred into a OKOLabs incubation cage set to 37 °C around a Nikon Ti2 Eclipse microscope stage. PBS +/-

PYO was flowed over cells at a rate of 10 μL per hour. Phase-contrast images taken with a 40x objective every 5 minutes for 100 minutes.

ABBA antibiotic survival assays, imaging, and O_2 probe measurements

ABBAs were made as previously described (41) using LB and a final starting OD_{500nm} of 0.0005 and incubated at 37 °C for 20 hours. Before staining or treatment, cells on top of the agar were washed away using 400 μL of 25 mM HEPES pH 7.

For antibiotic survival assays, tobramycin was added to Eppendorf tube ABBAs for a final concentration of 100 μg/mL in 100 μL 25 mM HEPES pH 7 and treated for 4 hours at 37 °C at 250 RPM. For ciprofloxacin a concentration of 10 μg/mL was used. Treatment solutions were then removed and 500 μL of 25 mM HEPES (pH 7) was added. Each ABBA was then homogenized on speed 3 of a PRO Scientific Bio-Gen PRO200 Homogenizer. Samples were briefly spun and CFUs carried out as described above. For figure 4D, ABBAs were made by allowing 100 μL of inoculated agar to first solidify before pipetting another 100 μL on top. Before homogenization, the top and bottom half of ABBAs were separated with a palette knife and moved into separate 2 mL Eppendorf tubes.

For microscopy, ABBAs were stained for 30 minutes with PI (final concentration 490 μM) and SYTO-9 (final concentration 16 μM) in 100 μL of 25 mM HEPES pH 7 for live dead staining. Staining solutions and ABBAs were removed from microscopy dishes using a palette knife. The center of each ABBA was isolated using a razor, inverted, and returned to the microscopy dish to closely image large aggregates at the top. Imaging was done using a Leica TCS SPE confocal microscope with a 40x objective. PI and Syto-9 were excited with a 488-nm solid-state laser, using 610-650 nm emission for PI and

510-550 nm for Syto-9. Images were collected from the widest x,y portion each aggregate. Representative images were chosen from 3 independent experiments.

O_2 probe measurements of LB ABBAs were done as previously described in (41) at the exception of collecting data from a total depth of 1050 μm.

Data analysis and plotting

Data was analyzed and processed in Python 3.8.17 using Pandas 2.0.3, NumPy 1.24.3, and SciPy 1.9.3. Image processing was done in ImageJ 1.52. Plotting done using bokeh 2.4.3.

Acknowledgments

This work was supported by the NIH Grant (2R01AI127850-01A1). We thank Chelsey M. VanDrisse, Georgia R. Squyres and Nate Glasser for help with experimental design, and the rest of the Newman Lab for support and mentorship.

References

1. P. C. Maloney, E. R. Kashket, T. H. Wilson, A Protonmotive Force Drives ATP Synthesis in Bacteria. *Proc Natl Acad Sci U S A* **71**, 3896–3900 (1974).

2. C. Chimerel, C. M. Field, S. Piñero-Fernandez, U. F. Keyser, D. K. Summers, Indole prevents *Escherichia coli* cell division by modulating membrane potential. *Biochimica et Biophysica Acta (BBA) - Biomembranes* **1818**, 1590–1594 (2012).

3. H. Strahl, L. W. Hamoen, Membrane potential is important for bacterial cell division. *Proceedings of the National Academy of Sciences* **107**, 12281–12286 (2010).

4. R. J. Poole, Energy Coupling for Membrane Transport. *Annual Review of Plant Biology* **29**, 437–460 (1978).

5. J. B. Miller, D. E. Koshland, Sensory electrophysiology of bacteria: relationship of the membrane potential to motility and chemotaxis in Bacillus subtilis. *Proceedings of the National Academy of Sciences* **74**, 4752–4756 (1977).

6. A. Prindle, *et al.*, Ion channels enable electrical communication in bacterial communities. *Nature* **527**, 59–63 (2015).

7. G. N. Bruni, R. A. Weekley, B. J. T. Dodd, J. M. Kralj, Voltage-gated calcium flux mediates Escherichia coli mechanosensation. *Proceedings of the National Academy of Sciences* **114**, 9445–9450 (2017).

8. M. Bergkessel, L. Delavaine, Diversity in Starvation Survival Strategies and Outcomes among Heterotrophic Proteobacteria. *Microbial Physiology* **31**, 146–162 (2021).

9. D. A. Gray, *et al.*, Extreme slow growth as alternative strategy to survive deep starvation in bacteria. *Nat Commun* **10**, 890 (2019).

10. A. J. Lopatkin, *et al.*, Bacterial metabolic state more accurately predicts antibiotic lethality than growth rate. *Nat Microbiol* **4**, 2109–2117 (2019).

11. J. M. Stokes, A. J. Lopatkin, M. A. Lobritz, J. J. Collins, Bacterial Metabolism and Antibiotic Efficacy. *Cell Metabolism* **30**, 251–259 (2019).

12. Y. Pu, *et al.*, ATP-Dependent Dynamic Protein Aggregation Regulates Bacterial Dormancy Depth Critical for Antibiotic Tolerance. *Mol Cell* **73**, 143-156.e4 (2019).

13. A. Zarkan, *et al.*, Indole Pulse Signalling Regulates the Cytoplasmic pH of E. coli in a Memory-Like Manner. *Sci Rep* **9**, 3868 (2019).

14. N. M. Vega, K. R. Allison, A. S. Khalil, J. J. Collins, Signaling-mediated bacterial persister formation. *Nat Chem Biol* **8**, 431–433 (2012).

15. D. Nguyen, *et al.*, Active Starvation Responses Mediate Antibiotic Tolerance in Biofilms and Nutrient-Limited Bacteria. *Science* **334**, 982–986 (2011).

16. D. Wilmaerts, *et al.*, HokB Monomerization and Membrane Repolarization Control Persister Awakening. *Molecular Cell* **75**, 1031-1042.e4 (2019).

17. N. Verstraeten, *et al.*, Obg and Membrane Depolarization Are Part of a Microbial Bet-Hedging Strategy that Leads to Antibiotic Tolerance. *Molecular Cell* **59**, 9–21 (2015).

18. T. Wang, I. El Meouche, M. J. Dunlop, Bacterial persistence induced by salicylate via reactive oxygen species. *Sci Rep* **7**, 43839 (2017).

19. C. Norman, K. A. Howell, A. H. Millar, J. M. Whelan, D. A. Day, Salicylic Acid Is an Uncoupler and Inhibitor of Mitochondrial Electron Transport. *Plant Physiology* **134**, 492–501 (2004).

20. E. M. E. Sykes, D. White, S. McLaughlin, A. Kumar, Salicylic acids and pathogenic bacteria: new perspectives on an old compound. *Can. J. Microbiol.* **70**, 1–14 (2024).

21. E. K. Perry, L. A. Meirelles, D. K. Newman, From the soil to the clinic: the impact of microbial secondary metabolites on antibiotic tolerance and resistance. *Nat Rev Microbiol* **20**, 129–142 (2022).

22. N. R. Glasser, S. H. Saunders, D. K. Newman, The Colorful World of Extracellular Electron Shuttles. *Annu. Rev. Microbiol.* **71**, 731–751 (2017).

23. K. O. Thalhammer, D. K. Newman, A phenazine-inspired framework for identifying biological functions of microbial redox-active metabolites. *Current Opinion in Chemical Biology* **75**, 102320 (2023).

24. D. V. Mavrodi, *et al.*, Diversity and Evolution of the Phenazine Biosynthesis Pathway. *Applied and Environmental Microbiology* **76**, 866–879 (2010).

25. J. A. Ciemniecki, D. K. Newman, NADH dehydrogenases are the predominant phenazine reductases in the electron transport chain of Pseudomonas aeruginosa. *Molecular Microbiology* **119**, 560–573 (2023).

26. N. R. Glasser, S. E. Kern, D. K. Newman, Phenazine redox cycling enhances anaerobic survival in Pseudomonas aeruginosa by facilitating generation of ATP and a proton-motive force. *Mol Microbiol* **92**, 399–412 (2014).

27. L. A. Meirelles, D. K. Newman, Both toxic and beneficial effects of pyocyanin contribute to the lifecycle of *Pseudomonas aeruginosa*. *Mol Microbiol* **110**, 995–1010 (2018).

28. H. M. Hassan, I. Fridovich, Intracellular production of superoxide radical and of hydrogen peroxide by redox active compounds. *Archives of Biochemistry and Biophysics* **196**, 385–395 (1979).

29. B. Rada, T. L. Leto, Pyocyanin effects on respiratory epithelium: relevance in *Pseudomonas aeruginosa* airway infections. *Trends in Microbiology* **21**, 73–81 (2013).

30. H. Sakhtah, A. Price-Whelan, L. E. P. Dietrich, "Regulation of Phenazine Biosynthesis" in *Microbial Phenazines: Biosynthesis, Agriculture and Health*, S. Chincholkar, L. Thomashow, Eds. (Springer, 2013), pp. 19–42.

31. S. H. Saunders, *et al.*, Extracellular DNA Promotes Efficient Extracellular Electron Transfer by Pyocyanin in Pseudomonas aeruginosa Biofilms. *Cell* **182**, 919-932.e19 (2020).

32. A. Price-Whelan, L. E. P. Dietrich, D. K. Newman, Pyocyanin Alters Redox Homeostasis and Carbon Flux through Central Metabolic Pathways in Pseudomonas aeruginosa PA14. *J Bacteriol* **189**, 6372–6381 (2007).

33. R. Wilson, *et al.*, Measurement of Pseudomonas aeruginosa phenazine pigments in sputum and assessment of their contribution to sputum sol toxicity for respiratory epithelium. *Infection and Immunity* **56**, 2515–2517 (1988).

34. N. R. Glasser, B. X. Wang, J. A. Hoy, D. K. Newman, The Pyruvate and α-Ketoglutarate Dehydrogenase Complexes of Pseudomonas aeruginosa Catalyze Pyocyanin and Phenazine-1-carboxylic Acid Reduction via the Subunit Dihydrolipoamide Dehydrogenase *. *Journal of Biological Chemistry* **292**, 5593–5607 (2017).

35. L. M. Tsypin, D. K. Newman, Nitrate Reduction Stimulates and Is Stimulated by Phenazine-1-Carboxylic Acid Oxidation by Citrobacter portucalensis MBL. *mBio* **12**, 10.1128/mbio.02265-21 (2021).

36. D. Heine, S. Sundaram, M. Beudert, K. Martin, C. Hertweck, A widespread bacterial phenazine forms S-conjugates with biogenic thiols and crosslinks proteins. *Chemical Science* **7**, 4848–4855 (2016).

37. M. Gu, J. A. Imlay, The SoxRS response of Escherichia coli is directly activated by redox-cycling drugs rather than by superoxide. *Molecular Microbiology* **79**, 1136–1150 (2011).

38. J. Lee, J. Park, S. Kim, I. Park, Y.-S. Seo, Differential regulation of toxoflavin production and its role in the enhanced virulence of Burkholderia gladioli. *Molecular Plant Pathology* **17**, 65–76 (2016).

39. L. A. Meirelles, E. K. Perry, M. Bergkessel, D. K. Newman, Bacterial defenses against a natural antibiotic promote collateral resilience to clinical antibiotics. *PLoS Biol* **19**, e3001093 (2021).

40. L. A. Meirelles, D. K. Newman, Phenazines and toxoflavin act as interspecies modulators of resilience to diverse antibiotics. *Molecular Microbiology* **117**, 1384–1404 (2022).

41. C. M. VanDrisse, R. Lipsh-Sokolik, O. Khersonsky, S. J. Fleishman, D. K. Newman, Computationally designed pyocyanin demethylase acts synergistically with tobramycin to kill recalcitrant *Pseudomonas aeruginosa* biofilms. *Proc. Natl. Acad. Sci. U.S.A.* **118**, e2022012118 (2021).

42. K. T. Schiessl, *et al.*, Phenazine production promotes antibiotic tolerance and metabolic heterogeneity in Pseudomonas aeruginosa biofilms. *Nat Commun* **10**, 762 (2019).

43. M. A. Lobritz, *et al.*, Antibiotic efficacy is linked to bacterial cellular respiration. *Proceedings of the National Academy of Sciences* **112**, 8173–8180 (2015).

44. M. A. Alonso, L. Carrasco, Molecular Basis of the Permeabilization of Mammalian Cells by Ionophores. *European Journal of Biochemistry* **127**, 567–569 (1982).

45. X. Jin, *et al.*, Sensitive bacterial Vm sensors revealed the excitability of bacterial Vm and its role in antibiotic tolerance. *Proceedings of the National Academy of Sciences* **120**, e2208348120 (2023).

46. D. Novo, N. G. Perlmutter, R. H. Hunt, H. M. Shapiro, Accurate flow cytometric membrane potential measurement in bacteria using diethyloxacarbocyanine and a ratiometric technique. *Cytometry* **35**, 55–63 (1999).

47. F. M. Harold, ION CURRENTS AND PHYSIOLOGICAL FUNCTIONS IN MICROORGANISMS. *Annual Review of Microbiology* **31**, 181–203 (1977).

48. P. Scholes, P. Mitchell, Respiration-driven proton translocation in micrococcus denitrificans. *J Bioenerg Biomembr* **1**, 309–323 (1970).

49. J. Jo, A. Price-Whelan, L. E. P. Dietrich, An aerobic exercise: defining the roles of Pseudomonas aeruginosa terminal oxidases. *J Bacteriol* **196**, 4203–4205 (2014).

50. T. Nyström, Stationary-Phase Physiology. *Annual Review of Microbiology* **58**, 161–181 (2004).

51. L. E. Bryan, S. Kwan, Roles of ribosomal binding, membrane potential, and electron transport in bacterial uptake of streptomycin and gentamicin. *Antimicrobial Agents and Chemotherapy* **23**, 835–845 (1983).

52. M. Lang, A. Carvalho, Z. Baharoglu, D. Mazel, Aminoglycoside uptake, stress, and potentiation in Gram-negative bacteria: new therapies with old molecules. *Microbiology and Molecular Biology Reviews* **87**, e00036-22 (2023).

53. S. Meylan, *et al.*, Carbon Sources Tune Antibiotic Susceptibility in Pseudomonas aeruginosa via Tricarboxylic Acid Cycle Control. *Cell Chem Biol* **24**, 195–206 (2017).

54. A. Crabbé, *et al.*, Host metabolites stimulate the bacterial proton motive force to enhance the activity of aminoglycoside antibiotics. *PLoS Pathog* **15**, e1007697 (2019).

55. E. J. Zheng, J. M. Stokes, J. J. Collins, Eradicating Bacterial Persisters with Combinations of Strongly and Weakly Metabolism-Dependent Antibiotics. *Cell Chemical Biology* **27**, 1544-1552.e3 (2020).

56. X. Zhu, *et al.*, Nigericin is effective against multidrug resistant gram-positive bacteria, persisters, and biofilms. *Front. Cell. Infect. Microbiol.* **12** (2022).

57. L. B. Margolis, Y. u Novikova I, I. A. Rozovskaya, V. P. Skulachev, K+/H+-antiporter nigericin arrests DNA synthesis in Ehrlich ascites carcinoma cells. *Proceedings of the National Academy of Sciences* **86**, 6626–6629 (1989).

58. N. G. Bush, I. Diez-Santos, L. R. Abbott, A. Maxwell, Quinolones: Mechanism, Lethality and Their Contributions to Antibiotic Resistance. *Molecules* **25**, 5662 (2020).

59. F. Jiménez Otero, D. K. Newman, L. M. Tender, Pyocyanin-dependent electrochemical inhibition of Pseudomonas aeruginosa biofilms is synergistic with antibiotic treatment. *mBio* **14**, e00702-23.

60. P. Belenky, *et al.*, Bactericidal Antibiotics Induce Toxic Metabolic Perturbations that Lead to Cellular Damage. *Cell Reports* **13**, 968–980 (2015).

61. H.-C. Flemming, *et al.*, Biofilms: an emergent form of bacterial life. *Nat Rev Microbiol* **14**, 563–575 (2016).

62. M. A. Spero, D. K. Newman, Chlorate Specifically Targets Oxidant-Starved, Antibiotic-Tolerant Populations of Pseudomonas aeruginosa Biofilms. *mBio* **9**, e01400-18 (2018).

63. M. Donnert, *et al.*, Targeting bioenergetics is key to counteracting the drug-tolerant state of biofilm-grown bacteria. *PLoS Pathog* **16**, e1009126 (2020).

64. D. Lebeaux, *et al.*, pH-Mediated Potentiation of Aminoglycosides Kills Bacterial Persisters and Eradicates In Vivo Biofilms. *The Journal of Infectious Diseases* **210**, 1357–1366 (2014).

65. B. W. Kwan, J. A. Valenta, M. J. Benedik, T. K. Wood, Arrested Protein Synthesis Increases Persister-Like Cell Formation. *Antimicrobial Agents and Chemotherapy* **57**, 1468–1473 (2013).

66. M. A. Lobritz, *et al.*, Increased energy demand from anabolic-catabolic processes drives β-lactam antibiotic lethality. *Cell Chemical Biology* **29**, 276-286.e4 (2022).

67. J. Ling, *et al.*, Protein Aggregation Caused by Aminoglycoside Action Is Prevented by a Hydrogen Peroxide Scavenger. *Molecular Cell* **48**, 713–722 (2012).

68. P. Poór, Effects of Salicylic Acid on the Metabolism of Mitochondrial Reactive Oxygen Species in Plants. *Biomolecules* **10**, 341 (2020).

69. A. Franco, A. Chukwubuikem, C. Meiners, M. A. Rosenbaum, Exploring phenazine electron transfer interaction with elements of the respiratory pathways of *Pseudomonas putida* and *Pseudomonas aeruginosa*. *Bioelectrochemistry* **157**, 108636 (2024).

70. Y. Wang, D. K. Newman, Redox Reactions of Phenazine Antibiotics with Ferric (Hydr)oxides and Molecular Oxygen. *Environ. Sci. Technol.* **42**, 2380–2386 (2008).

71. D. Dar, N. Dar, L. Cai, D. K. Newman, Spatial transcriptomics of planktonic and sessile bacterial populations at single-cell resolution. *Science* **373**, eabi4882 (2021).

72. E. Şimşek, M. Kim, The emergence of metabolic heterogeneity and diverse growth responses in isogenic bacterial cells. *ISME J* **12**, 1199–1209 (2018).

73. S. M. Amato, M. P. Brynildsen, Persister Heterogeneity Arising from a Single Metabolic Stress. *Current Biology* **25**, 2090–2098 (2015).

74. S. Rezaeinejad, V. Ivanov, Heterogeneity of *Escherichia coli* population by respiratory activity and membrane potential of cells during growth and long-term starvation. *Microbiological Research* **166**, 129–135 (2011).

75. S. Ahn, J. Jung, I.-A. Jang, E. L. Madsen, W. Park, Role of Glyoxylate Shunt in Oxidative Stress Response. *Journal of Biological Chemistry* **291**, 11928–11938 (2016).

76. G. N. Bruni, J. M. Kralj, Membrane voltage dysregulation driven by metabolic dysfunction underlies bactericidal activity of aminoglycosides. *eLife* **9**, e58706 (2020).

77. J. A. Imlay, The molecular mechanisms and physiological consequences of oxidative stress: lessons from a model bacterium. *Nat Rev Microbiol* **11**, 443–454 (2013).

78. J. J. Foti, B. Devadoss, J. A. Winkler, J. J. Collins, G. C. Walker, Oxidation of the Guanine Nucleotide Pool Underlies Cell Death by Bactericidal Antibiotics. *Science* **336**, 315–319 (2012).

79. D. D. Lee, *et al.*, Magnesium flux modulates ribosomes to increase bacterial survival. *Cell* **177**, 352-360.e13 (2019).

80. L. E. P. Dietrich, A. Price-Whelan, A. Petersen, M. Whiteley, D. K. Newman, The phenazine pyocyanin is a terminal signalling factor in the quorum sensing network of Pseudomonas aeruginosa. *Mol Microbiol* **61**, 1308–1321 (2006).

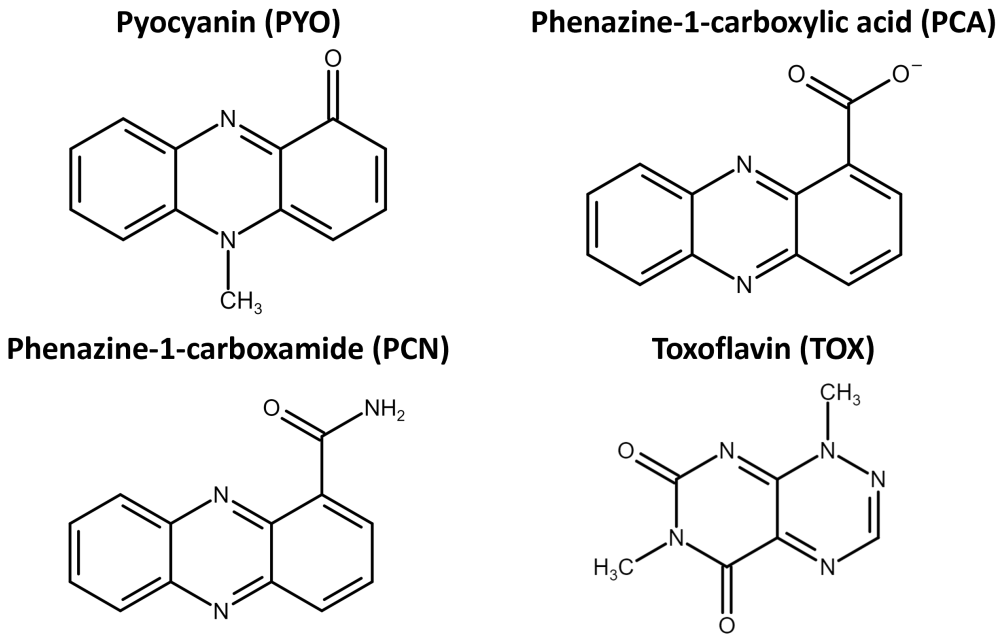

Figure S1. Chemical structures of endogenous RAMs tested.

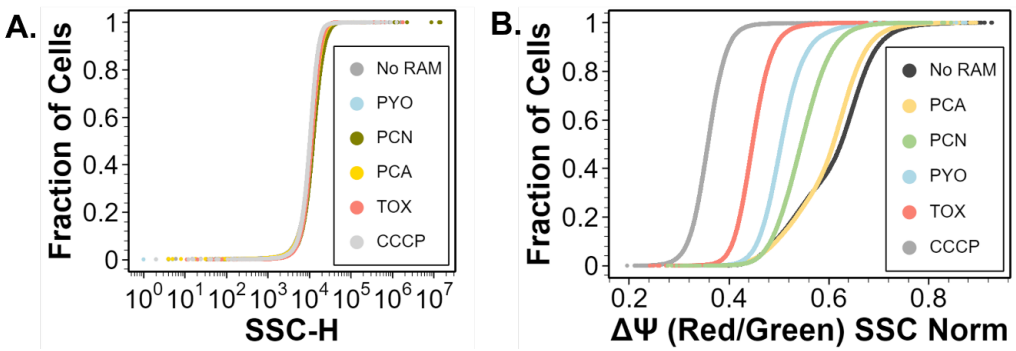

Figure S2. 1 hour RAM treatments in PBS do not dramatically alter the dimensions of cells or conflate the $DiOC_2(3)$ results of Figure 1D. (A) ECDFs of side-scatter-channel values of events used to plot Figure 1A. Cell suspensions treated with RAMs for 1 hour in PBS before $DiOC_2(3)$ staining do not dramatically differ in size. (B) ECDFs of $DiOC_2(3)$ Red/Green fluorescence values used to plot Figure 1D normalized by their side-scatter-channel values. Each condition contains ~50,000 events. Differences in cell dimensions does not account for the changes in $\Delta\Psi$ observed following RAM treatments.

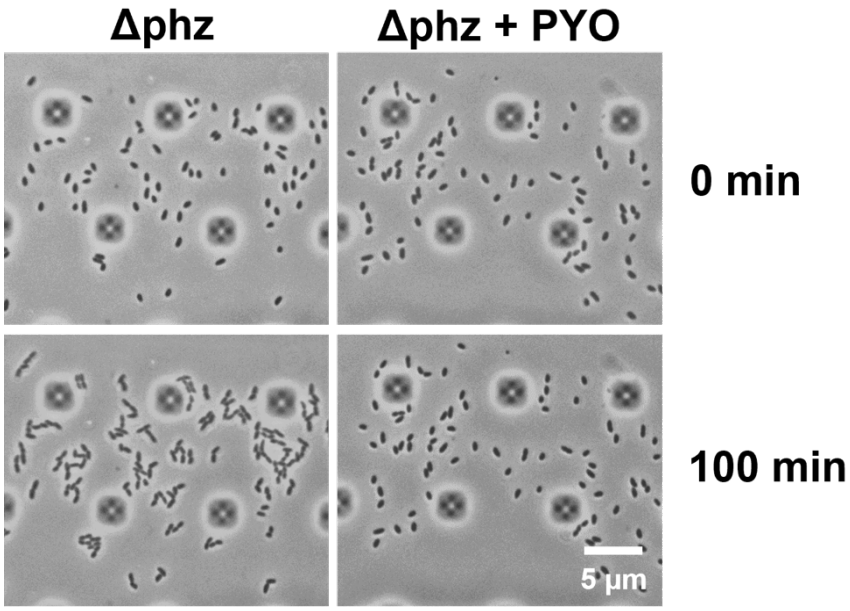

Figure S3. Treatment of cell suspensions with PYO arrests cell doubling. Representative phase-contrast images of cells within a Cell ASICS chamber with or without PYO treatment at 0 minutes and 100 minutes post PYO treatment. Scale bar = 5 μm.

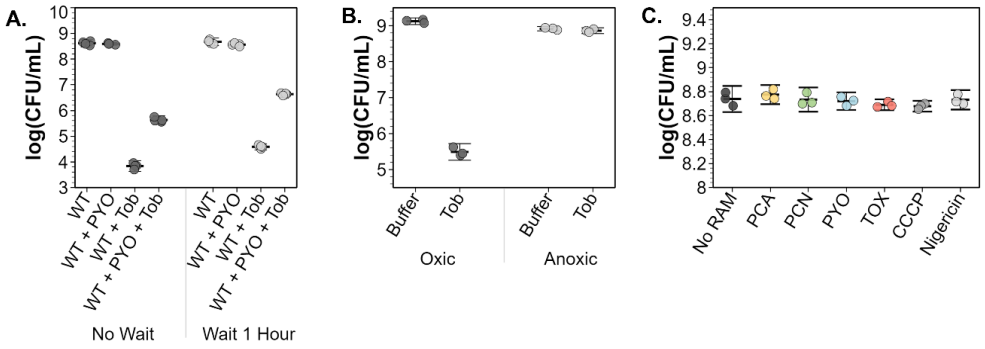

Figure S4. PYO protects WT cell suspensions like Δ*phz* suspensions, moving cells into anoxia lower tobramycin killing, and RAMs, CCCP, or nigericin do not affect cell survival in the absence of antibiotics. (A) PYO and PBS incubation affects the tobramycin tolerance of WT PBS cell suspensions like Δ*phz* suspensions. "No Wait" suspensions were pre-treated in PBS with 100 μM PYO for 1 hour then given 100 μg/mL tobramycin for 2 hours. "Wait 1 Hour" suspensions were incubated in PBS for 1 hour, then treated with 100 μM PYO for 1 hour, then given 100 μg/mL tobramycin for 2 hours. (B) Cell suspensions moved into anoxic conditions survive 2 hour tobramycin treatments more than those left in oxic conditions during treatment. (C) PCA, PCN, PYO, TOX, CCCP, and nigericin do not affect the survival of cells in the absence of antibiotics. (A, B, C) Log-transformed CFU/mL values of biological replicates. Error bars represent 95% confidence intervals. (A) Shows 4 biological replicates per condition. (B, C) Shows 3 biological replicates per condition.

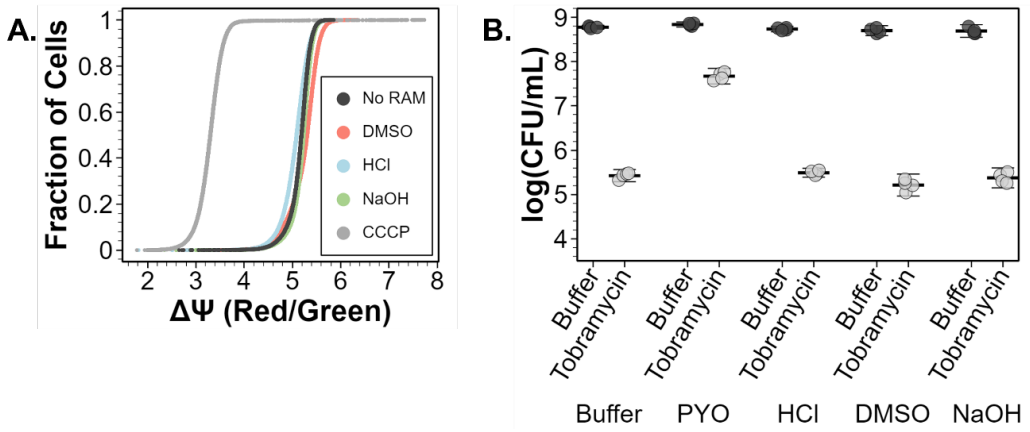

Figure S5. Solvents used in RAM stocks did not dramatically alter $DiOC_2(3)$ Red/Green fluorescence ratios or survival to tobramycin. (A) ECDFs of $DiOC_2(3)$ red/green fluorescence ratios following 1 hour treatment with PBS (No RAM), DMSO, HCl, NaOH, or CCCP. Equimolar amounts of solvents used in RAM treatments did not dramatically change the observed ΔΨ values. Each conditions contains ~50,000 events. (B) Log transformed CFU/mL values of cell suspensions pre-treated in PBS for 1 hour with, PYO, HCl, DMSO, NaOH, or no treatment, before addition of tobramycin for 2 hours. While PYO – solubilized in 20 mM HCl – increases survival to tobramycin, equimolar amounts of solvents used in RAM treatments do not protect cells against tobramycin.

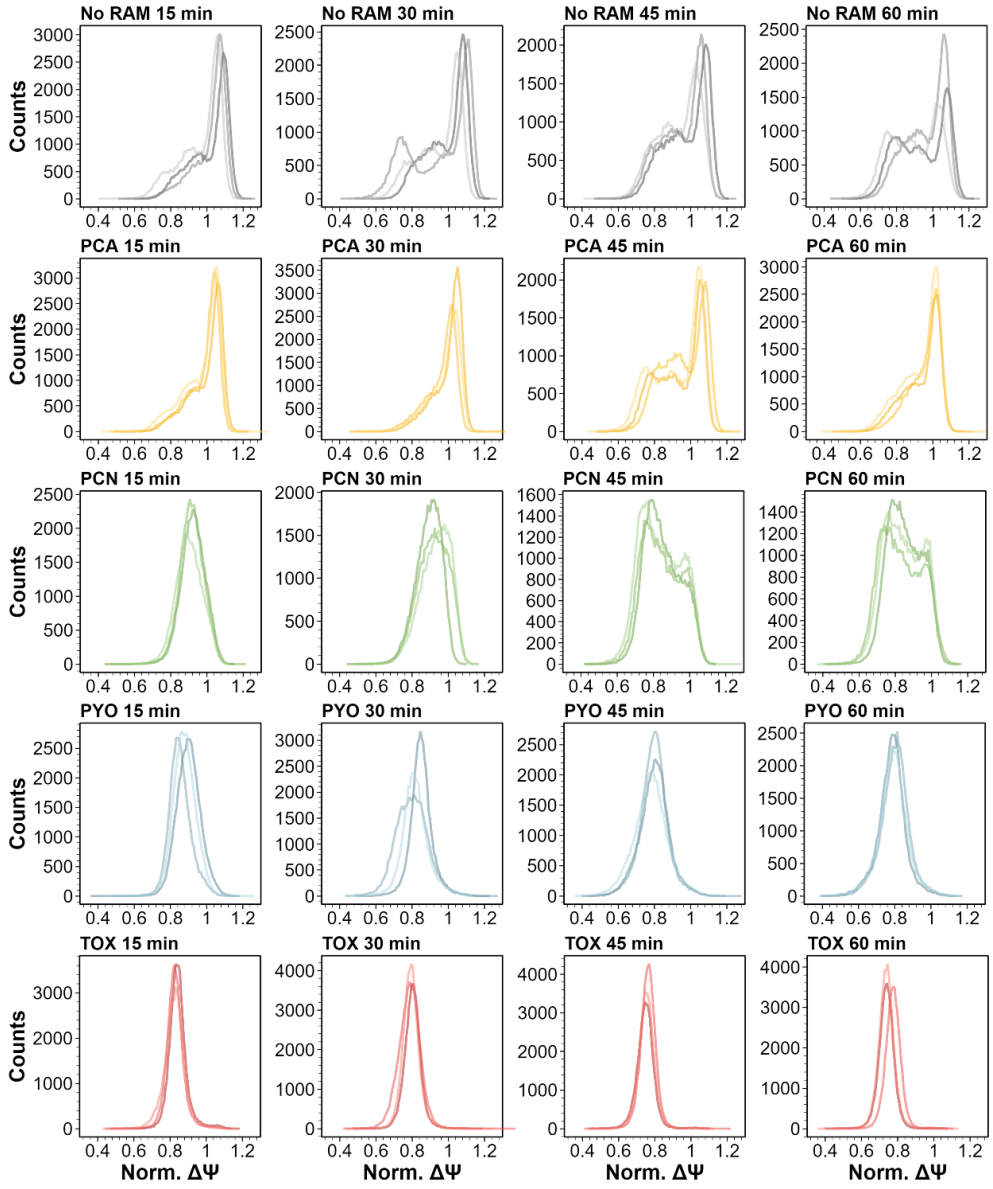

Figure S6. RAMs produce unique ΔΨ subpopulations over time. Histograms of 3 biological replicates of $DiOC_2(3)$ Red/Green fluorescence ratios of PCA, PCN, PYO, TOX, or CCCP treated cells at 15-, 30-, 45-, or 60-minutes post treatment. Values normalized to the mean fluorescence ratio of the 15-minute No RAM condition. Each histogram line contains 50,000 events.

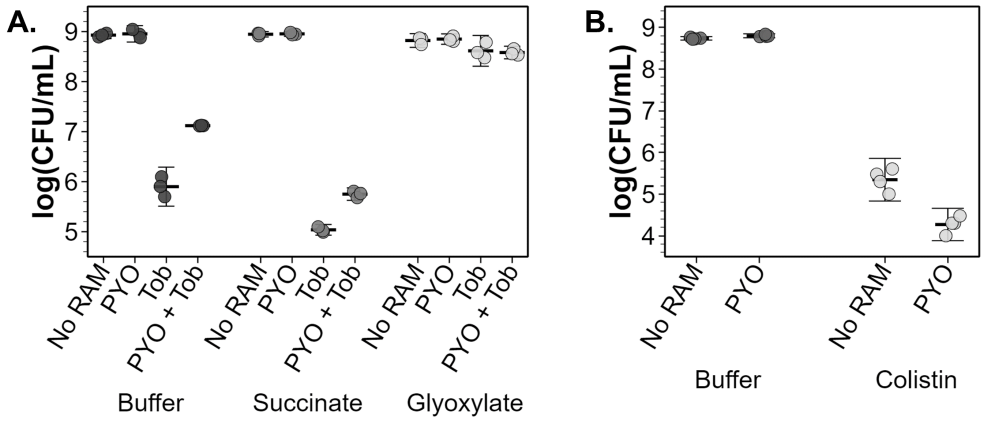

Figure S7. Succinate synergizes with tobramycin while glyoxylate protects against it, PYO synergizes with colistin, unlike tobramycin or ciprofloxacin. (A) Treatment of MOPS media cell suspensions with succinate increases tobramycin lethality and abolishes PYO's protective effect while glyoxylate increases survival. (B) PYO does not protect and lightly synergizes with colistin. (A, B) Log-transformed CFU/mL values of biological replicates. Error bars represent 95% confidence intervals. (A) 3 biological replicates per condition. (B) 4 biological replicates per condition. Antibiotic treatments were done for 2 hours following a 1-hour pre-treatment by addition of 100 μg/mL of tobramycin, or 10 μg/mL of colistin to suspensions.

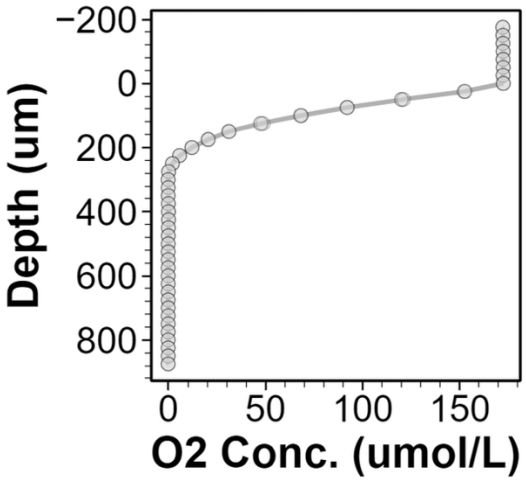

Figure S8. ABBAs have a steep O_2 gradient, with O_2 hitting undetectable levels within 300 μm of the ABBA surface. Representative biological replicate. Line represents the mean of 3 technical replicate measurements taken within seconds of one another with an O_2 micro-electrode probe. Circles represent the 3 technical replicates for each depth.

Chapter 3

PSEUDOMONAS AERUGINOSA RELIES ON A PHOSPHOKETOLASE TO SUPPORT ANAEROBIC SURVIVAL UNDER REDUCTIVE STRESS

Abstract

Across diverse contexts, bacteria experience loss of electron acceptors due to fluctuating environmental conditions, leading to growth-arrest and reductive stress. Yet, microbial metabolism has been primarily studied with cells growing under nutrient replete conditions. To study how cells preserve metabolic flux under reductively stressed growth-arrest, we explored how the opportunistic pathogen *Pseudomonas aeruginosa* remodels its metabolism under such conditions. During anaerobic survival on glucose, *P. aeruginosa* utilizes the upper Embden-Meyerhoff-Parnas pathway and pentose-phosphate pathway to generate metabolite precursors for a previously undescribed phosphoketolase (herein termed *xfp*) used to produce acetyl-P and indirectly ATP via subsequent acetate formation. This re-routing bypasses *P. aeruginosa*'s canonical glucose-catabolizing Entner-Doudoroff pathway (EDP) allowing for metabolic flux without exacerbating reductive stress. Moreover, anaerobic survival on diverse carbon sources triggers purine degradation and metabolite accumulation, requiring *xfp* to maintain metabolic balance and viability. Thus, our data suggest that phosphoketolases may play an additional role in ribonucleotide balance. This study expands our understanding of *P. aeruginosa*'s anaerobic survival strategies and serves as a reminder that large gaps remain in our understanding of growth arrest physiology even in well-studied model organisms, highlighting the potential for basic discovery in the realm of non-growth metabolism.

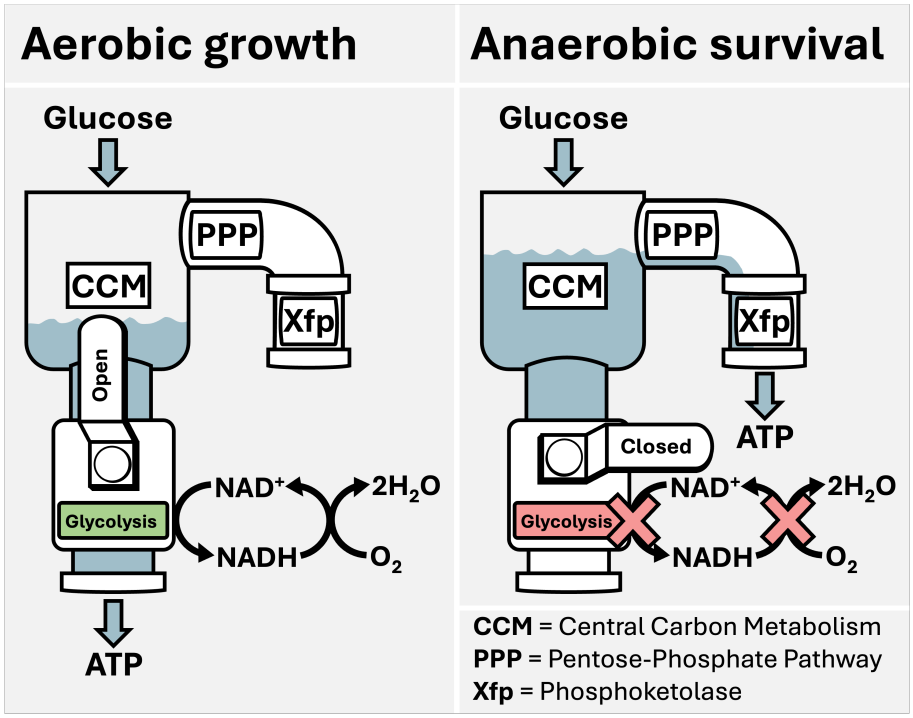

Graphical abstract: In *Pseudomonas aeruginosa,* oxidant limitation, and subsequent reductive stress, inhibits pathways such as glycolysis, leading to metabolite accumulation and flux into the pentose-phosphate pathway (PPP). Under these conditions, *P. aeruginosa* relies on a phosphoketolase (Xfp) to catalyze an alternative glucose degradation pathway, supporting ATP generation, metabolic homeostasis, and viability.

Introduction

Despite the immense diversity of metabolic strategies across the tree of life, the rules underpinning them are remarkably unified. All life must couple energy generation with energy expenditures (e.g. biosynthesis); a process accomplished via carefully managed redox reactions (Chubukov *et al.*, 2014). Loss of redox balance, such as an inability to consume excess reducing equivalents (i.e. reductive stress), leads to metabolic disruption, growth arrest, and even cellular death (Xiao and Loscalzo, 2020). From the

perspective of human biology, reductive stress is commonly thought to be purely detrimental due to its linkage to a variety of illnesses (Cantó, Menzies and Auwerx, 2015; Luo, Ma and Ye, 2024; Ying, 2008; Yang, Guo and Li, 2025). Yet, microorganisms are commonly found in oxidant-limited environments, such as in bioreactors, soil communities, and human infections (Silver, Lugo and Keller, 1999; Enfors *et al.*, 2001; Cowley *et al.*, 2015; Voroney and Heck, 2015; Bergkessel, Basta and Newman, 2016). While numerous studies have uncovered diverse fermentative metabolisms to support growth under reductive stress (Bartacek, Zabranska and Lens, 2007; Hackmann and Zhang, 2023; Hackmann, 2024; Thauer, Jungermann and Decker, 1977), we know far less about the metabolic strategies supporting growth-arrested survival in bacteria reliant on respiration for growth.

Within the metabolism field, a historic focus on bacterial growth has led to many organisms being defined as "non-fermentative" or "obligate aerobes" based on their inability to grow under oxidant-limited conditions. Yet many of these bacteria contain fermentation genes. For example, in the traditionally deemed "obligate aerobe" *Mycobacterium smegmatis,* cells can utilize fermentative hydrogen production to alleviate reductive stress and generate ATP during hypoxia-induced growth arrest (Berney *et al.*, 2014). A related phenomenon is observed in human biology, with hypoxia and mitochondrial dysfunction stimulating the Warburg effect, whereby glycolysis outpaces respiration leading to lactate production to consume excess reducing equivalents while maintaining ATP production (Warburg, 1925; Kukurugya, Rosset and Titov, 2024). Because bacteria that rely on aerobic respiration for growth can be challenged by oxygen limitation (Ciemniecki and Newman, 2020; Silver, Lugo and Keller, 1999; Voroney and

Heck, 2015), it is likely that these fermentative strategies to support non-growth survival in respiratory organisms may be more common than has been realized.

An alternative to consuming reducing equivalents to maintain metabolic flux under reductive stress is to use metabolic pathways that do not generate reducing equivalents. To test this idea, we turned to the "non-fermentative" pathogen *Pseudomonas aeruginosa,* known to survive for weeks in oxidant-limited growth-arrested states, herein termed "anaerobic survival" (Eschbach *et al.*, 2004). *P. aeruginosa* depends on respiration of molecular oxygen or via denitrification to support exponential growth (Gayon and Dupetit, 1886; Zumft, 1997); it is unable to grow exponentially in the absence of terminal electron acceptors. However, it can metabolize arginine and yeast extract for slight anaerobic growth or ferment pyruvate to support anaerobic survival (Vander Wauven *et al.*, 1984). In the case of the latter, pyruvate is metabolized to acetate via acetyl-CoA and acetyl-phosphate (acetyl-P) by the *ackA-pta* system, generating ATP and NADH. Meanwhile, generation of lactate from additional pyruvate molecules via *ldhA* regenerates NAD+ (Eschbach *et al.*, 2004) (FIG 1A).

On carbon sources such as glucose, *P. aeruginosa* also relies on *ackA-pta* for ATP generation and can persist in a non-growth state (Ciemniecki *et al.*, 2024; Glasser, Kern and Newman, 2014). However, glucose-surviving cells can only survive if they employ phenazines – self-made electron shuttles – to alleviate reductive stress (Ciemniecki *et al.*, 2024; Glasser, Kern and Newman, 2014). *P. aeruginosa* lacks a complete upper Embden-Meyerhoff-Parnas pathway (EMPP) for standard glycolysis and lacks the oxidative pentose-phosphate pathway (PPP) (Kohlstedt and Wittmann, 2019; Lessie and Phibbs, 1984). During aerobic growth, almost all glucose catabolic flux occurs first via oxidation

of glucose to gluconate, followed by further oxidation or its phosphorylation, eventually generating 6-phosphogluconate that feeds into the Entner-Duodoroff pathway (EDP) and lower EMPP (Kohlstedt and Wittmann, 2019). However, during anaerobic survival this glycolytic pathway would generate excess reducing equivalents ([$2e^-$]) via reduced ubiquinone from initial glucose oxidation, and NADPH or NADH from the lower EMPP (FIG 1A). Therefore, we predicted that under reductive stress *P. aeruginosa*'s glucose catabolic flux would shift towards the non-oxidative upper EMPP and PPP by way of glucose-6-phosphate (glucose-6P) and fructose-6-phosphate (fructose-6P).

Precedent for such metabolic re-routing in *P. aeruginosa* exists in the literature. Despite catabolizing glucose to gluconate during aerobic growth (generating reduced ubiquinone), during anaerobic growth on nitrate as a terminal electron acceptor, *P. aeruginosa* instead catabolized all measurable glucose to glucose-6P (Lessie and Phibbs, 1984). However, use of the lower EMPP to connect the PPP to acetate and ATP production would still generate excess reducing equivalents, unless paired with lactate production, limiting ATP and acetate yields (Fig 1A). An alternative non-oxidative path connecting the PPP to acetate production is via phosphoketolases, one such protein being previously discovered and purified from *P. aeruginosa* ATCC 15442 (Petrareanu *et al.*, 2014).

Phosphoketolases are thiamine-pyrophosphate-dependent enzymes that catalyze the phosphorolysis of fructose-6-phosphate (fructose-6P), xylulose-5-phosphate (xylulose-5P), and/or sedoheptulose-7-phosphate (sedoheptulose-7P), releasing 2 carbons from each substrate as acetyl-P and generating erythrose-4-

phosphate (erythrose-4P), glyceraldehyde-3-phosphate (glyceraldehyde-3P), or ribose-5-phosphate (ribose-5P), respectively (Krüsemann *et al.*, 2018; Sánchez *et al.*, 2010; Suzuki *et al.*, 2010). The activity and preference for each substrate differs across phosphoketolase homologs in different species. Phosphoketolases have been primarily studied for their role in natural product generation and in fermentative metabolisms such as hexose catabolism via the phosphoketolase pathway in some *Lactobacillus* species and the bifido-shunt in *Bifidobacterium* species, as well as pentose catabolism in *Clostridium acetobutylicum* (Aristilde *et al.*, 2015; Årsköld *et al.*, 2008; de Vries and Stouthamer, 1967; Liu *et al.*, 2012). Within *C. acetobutylicum*, phosphoketolases provide efficient non-oxidative pentose catabolism while supporting ATP generation. This metabolism bypasses pentose flux through the PPP or EMPP, avoiding rate-limiting enzymatic steps, carbon loss, and generation of additional reducing equivalents (Aristilde *et al.*, 2015; Liu *et al.*, 2012; Servinsky *et al.*, 2012). During energy-limited anaerobic survival in *P. aeruginosa*, a similar strategy would allow for continued ATP production while minimizing protein cost and reducing equivalent generation (FIG 1A). While *P. aeruginosa* contains many of the genes involved in the bifido-shunt, it is unable to consume excess reducing equivalents via ethanol generation through the enzyme ethanol dehydrogenase.

Intriguingly, the phosphoketolase gene of *P. aeruginosa* is regulated by the anaerobic transcription factor Anr and its regulatory small RNA *esrA*, indicating a potential role for phosphoketolases during anaerobic carbon metabolism in this organism (Ferrara *et al.*, 2021; Hammond *et al.*, 2015; Tribelli *et al.*, 2019). Accordingly, we set out to test the hypothesis that during anaerobic survival on glucose, metabolic flux diverts into the non-oxidative PPP, enabling Xfp to utilize PPP metabolites, such

as xylulose-5P, to form acetyl-P, ultimately leading to acetate and ATP production, while avoiding additional production of reducing equivalents (FIG 1A).

Results

P. aeruginosa relies on a phosphoketolase during anaerobic survival on glucose under reductive stress

Evidence in support of our hypothesis, that during anaerobic survival *P. aeruginosa* catabolizes glucose via the non-oxidative PPP and a putative phosphoketolase, came from a preliminary transposon-sequencing (Tn-seq) screen performed in our lab using *P. aeruginosa* UCBPP-PA14 (PA14) surviving anaerobically on glucose in the presence of phenazine-1-carboxylic acid (Saunders, 2020). Despite PA14 relying on the EDP for aerobic glucose catabolism, transposon insertions in the core EDP gene *edaA,* catalyzing the formation of glyceraldehyde-3P and pyruvate, or in the positive EDP regulator *hexR*, increased survival on glucose (FIG 1A) (Saunders, 2020). Meanwhile, transposon insertion in genes involved in the upper EMPP, the PPP gene transaldolase, the *ackA-pta* system, or a putative phosphoketolase (*PA14_17580*, here-in referred to as *xfp*), were all detrimental to PA14's survival (FIG 1A) (Saunders, 2020). While PA14's Xfp has not been purified and confirmed for phosphoketolase activity, its amino acid sequence is nearly identical to the previously purified phosphoketolase of *P. aeruginosa* strain ATCC 15442, with only two amino acid identities differing (SUPP FIG1). The Xfp of 15442 was confirmed to have *in vitro* enzymatic activity on both fructose-6P and xylulose-5P, with a strong preference for the latter (Petrareanu *et al.*, 2014). Therefore, we reasoned that PA14's Xfp might retain this catalytic capability, preferentially consuming xylulose-5P to generate glyceraldehyde-3P and acetyl-P, bridging the non-

oxidative PPP and acetate generation to support anaerobic survival and ATP production on glucose.

To determine whether the loss of *xfp* results in a survival deficit during reductively stressed anaerobic survival on glucose, we generated a clean deletion of *PA14_17580*. All experiments were performed in a phenazine-null mutant background (*Δphz*) to avoid alleviation of reductive stress by phenazines and better isolate a Xfp-dependent reductive stress survival mechanism. To test for survival, anoxic cell suspensions of *Δphz* and *ΔphzΔxfp* strains were sampled and plated for colony-forming units (CFUs) over time. Both strains maintained ~100% survival for the first 3 days of anaerobic survival, yet by day 5, *ΔphzΔxfp* CFUs dropped over 2 orders of magnitude, before plateauing between 10 and 15 days (FIG 1B). Meanwhile the parent strain *Δphz* maintained ~100% survival for 10 days before losing viability, plateauing to a similar level as the *xfp* mutant – 2 orders of magnitude lower than starting CFUs (FIG 1B). Complementation of *xfp* in the *ΔphzΔxfp* strain fully restored viability (SUPP FIG 2A). Additionally, there was no effect of the *xfp* mutation during anaerobic growth on glucose using KNO_3 as a terminal electron acceptor (SUPP FIG 2B). Finally, to confirm this effect was not due to the *Δphz* background, we additionally generated a *Δxfp* strain in the WT PA14 background, observing no statistical difference between it and the *ΔphzΔxfp* strain (SUPP FIG 2A).

To test our assumption that Xfp is only needed under conditions of reductive-stress, we repeated the experiment above in a 96-well plate equipped with electrodes, allowing us to determine if the addition of phenazines could rescue the *ΔphzΔxfp* strain.

Cells were given 200 μM, 50 μM, or 0 μM of phenazine-1-carboximide (PCN), an endogenous electron shuttle produced by PA14. Each well of the 96-well plate contained a working, reference, and counter electrode, enabling any PCN that is reduced by cells to be re-oxidized at the working electrode, allowing for dissipation of reducing equivalents. In support of our hypothesis that reductive stress causes the need for Xfp to maintain viability, we see that 200 μM of PCN rescues the survival of the *Δphz*Δ*xfp* strain (Fig 1C). Notably, the *Δphz* strain is unable to maintain 100% survival in the absence of PCN, yet 50 μM is enough to promote full viability. However, the *Δphz*Δ*xfp* strain still dies in the presence of 50 μM PCN, suggesting a greater demand for an electron acceptor to restore redox balance in the *xfp* mutant (Fig 1C). Together, these data suggests that Xfp and phenazines play complementary roles in allowing cells to maintain survival under reductive stress.

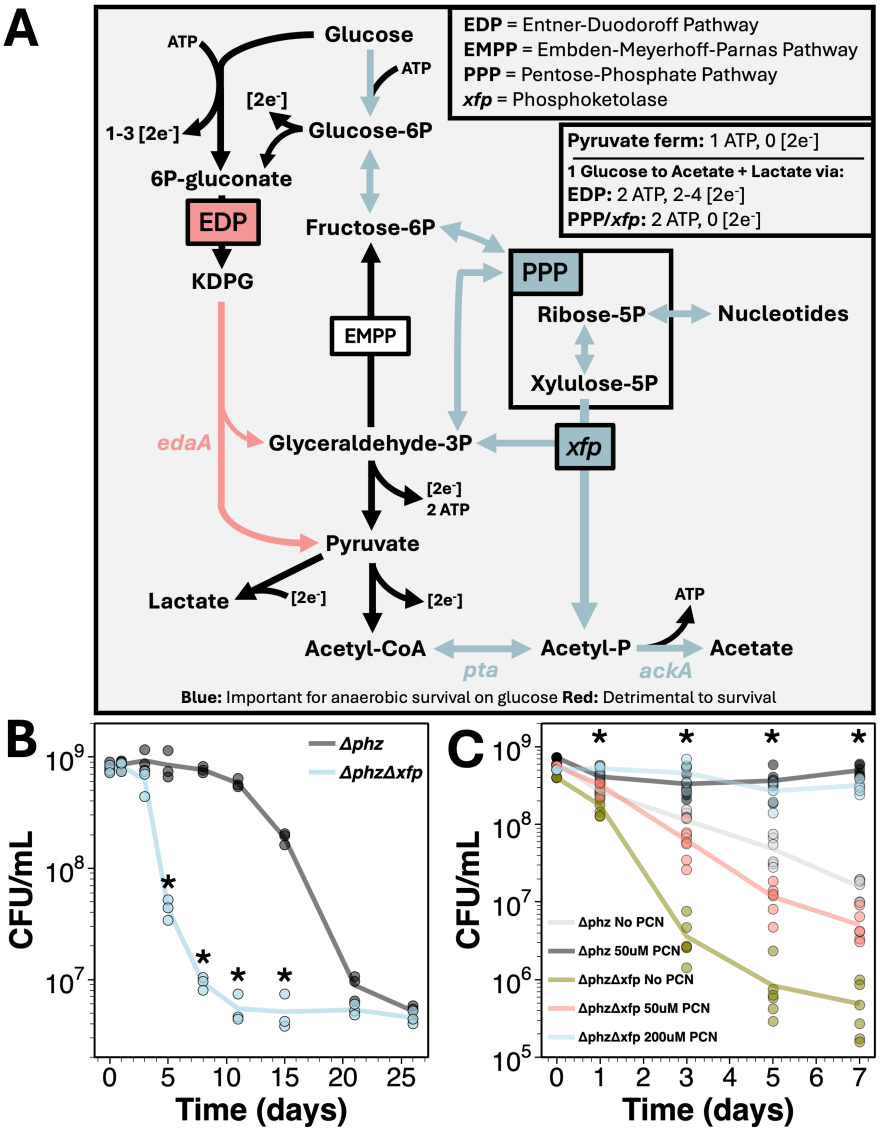

Figure 1. Mutation of PA14's *xfp* diminishes anaerobic survival on glucose but can be rescued by alleviation of reductive stress. (A) Condensed metabolic diagram highlighting the evidence behind our hypothesis that under reductive stress, glucose catabolic flux to acetate would be more favorable by way of the PPP than via the EDP. Blue arrows are pathways or genes that were important for anaerobic survival on glucose while red genes were detrimental (Saunders, 2020). All reducing equivalents are written as [2e$^-$] for simplicity. KDPG = 2-keto-3-deoxy-6-phosphogluconate. (B) Mutation of *xfp* leads to

a drop in anaerobic survival after 3 days in anoxic Balch tubes. Blue = *Δphz*. Grey = *ΔphzΔxfp*. (C) Addition of the electron shuttle phenazine-1-carboxamide (PCN) to increase reducing equivalent consumption rescues survival of the *xfp* mutant during anaerobic survival in a 96-well potentiostat system. Light grey = *Δphz* with no PCN, black = *Δphz* + 50 uM PCN, olive = *ΔphzΔxfp* with no PCN, light red = *ΔphzΔxfp* + 50 uM PCN, light blue = *ΔphzΔxfp* + 200 uM PCN. (B, C) Log transformed CFU per mL values. Carbon source is 20 mM glucose. Starting OD_{500nm} = 0.75. Dots are biological replicates, lines represent means. (B) n = 3 per condition. (C) n = 3-6 per condition. (B) * denotes p-value < 0.05 from independent two-tailed t-test comparing each strain for each say. (C) * denotes p-value < 0.05 from one-way ANOVA comparing all groups per day.

P. aeruginosa utilizes a phosphoketolase-mediated pathway for catabolism of glucose to acetate during anaerobic survival

To verify that PA14 can use its Xfp for glucose catabolism and acetate production, we performed pathway-diagnostic isotopic labelling experiments. Both *Δphz* and *ΔphzΔxfp* strains were incubated with 1-$^{13}C_1$-glucose and supernatants were removed on days 3/5/7 for the *Δphz* strain and on day 3 for *ΔphzΔxfp*. We then measured the relative abundance of acetate and the fraction that was ^{13}C labelled. PA14 relies on *ackA*-mediated ATP generation during anaerobic survival on glucose. Accordingly, if all 1-$^{13}C_1$-glucose is catabolized via the EDP and lower EMPP to form pyruvate and then acetate via *ackA-pta*, we expected all acetate would lack ^{13}C labelling due to loss of ^{13}C as CO_2 during formation of acetyl-CoA (FIG 2A). However, if 1-$^{13}C_1$-glucose were instead

catabolized via a bifido-shunt-like phosphoketolase-mediated metabolism, we predicted a fraction of the acetate would be ^{13}C labelled, specifically at the first carbon atom. As PA14 lacks the oxidative PPP, this latter possibility would require glucose to enter the PPP by way of glucose-6P and fructose-6P, where ^{13}C labelled fructose-6P is either directly processed by Xfp, or interconverted to xylulose-5P and/or sedoheptulose-7P, potential Xfp substrates. Cleavage of any of these three potential substrates by Xfp would thus be expected to release singly ^{13}C-labelled acetyl-P, which can then form acetate via *ackA* or acetyl-CoA via *pta,* all of which would be ^{13}C labelled in the first position (FIG 2A). However, the strong homology of PA14's Xfp to a previously purified *P. aeruginosa* phosphoketolase (Petrareanu *et al.*, 2014, SUPP FIG1) suggests a preference for xylulose-5P as a substrate, generating glyceraldehyde-3P and acetyl-P as products, denoted by red boxes in Figure 2A.

By day 3 of anaerobic survival, we observed no significant ^{13}C labelling of acetate from *ΔphzΔxfp* supernatants, meanwhile, ~20% of acetate from *Δphz* samples was singly ^{13}C labelled, increasing to ~40% by day 7 (FIG 2B). Additionally, by day 3, *Δphz* supernatants contained around twice the acetate of *ΔphzΔxfp* supernatants (FIG 2C). While acetate was primarily visible as the acetic acid molecular ion (CH_3COOH^+), in-source fragmentation also allowed detection of the second carbon atom in the form of carboxylic acid cations (HCO_2^+). Despite high levels of singly labelled acetate in *Δphz* supernatants, we were unable to detect substantial doubly ^{13}C labelled acetic acid or singly ^{13}C labelled carboxylic acid fragments. Taken together, these results indicate that acetate produced by *Δphz* cells from 1-$^{13}C_1$-glucose is singly ^{13}C labelled at the methyl

position. It is important to note that the fraction of ^{13}C labelled-acetate likely underestimates the contribution of Xfp to acetate generation, as Xfp substrates can also be generated from unlabeled endogenous carbon stores, or unlabeled glucose-derived fructose-6P or glyceraldehyde-3P. Regardless, these findings demonstrate that during anaerobic survival on glucose, PA14 can utilize an alternative glucose catabolic pathway for acetate production.

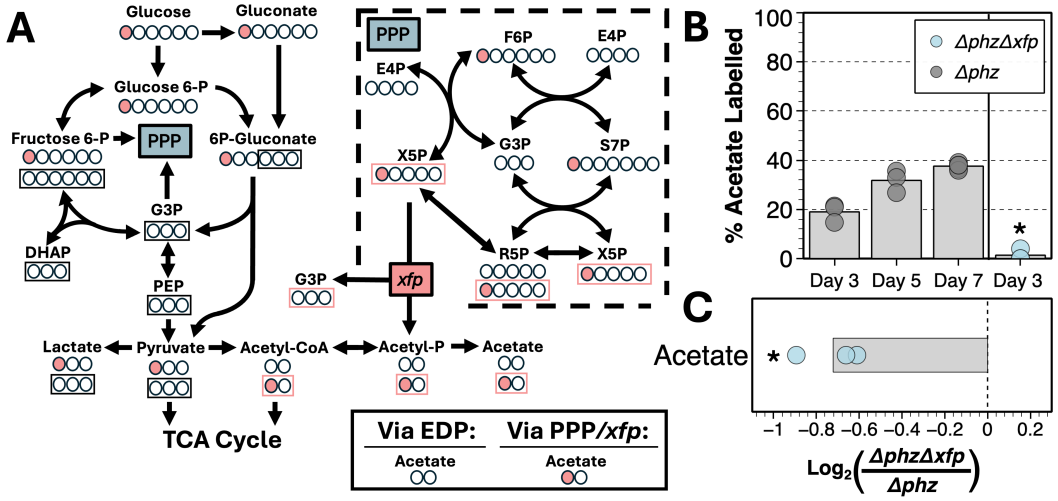

Figure 2. PA14 can utilize the PPP and its phosphoketolase to catabolize glucose to acetate. (A) Abridged central carbon metabolism diagram of PA14 showing initial incorporation/assimilation of 1-$^{13}C_1$-glucose to acetate either via the EDP (glucose → 6P-gluconate → G3P + pyruvate) and lower EMPP (G3P → pyruvate → acetate) or via the PPP (glucose → glucose 6-P → fructose 6-P → X5P) and Xfp activity (X5P → G3P + acetyl-P → acetate). Acetate via the EDP and lower EMPP would be unlabeled while acetate via the PPP and Xfp could be labelled in the first position. Red dots represent ^{13}C label. Black boxes = carbon from the 4,5,6 C atoms of 6P-gluconate. Red boxes = carbon from X5P.(B) Percent of ^{13}C labelled acetate in the parent strain and *xfp* mutant during of anaerobic survival on 20 mM 1-$^{13}C_1$-glucose. (C) Relative abundance of acetate

in the *xfp* mutant by day 3 of anaerobic survival on 20 mM glucose, normalized to the parent strain. (B,C) Points show individual biological replicates, n = 3. Grey = *Δphz*, blue = *ΔphzΔxfp*. (B) Bars show means of each group. (C) Bar shows mean of *ΔphzΔxfp* metabolite intensities normalized to the mean of *Δphz* levels. (A) PPP = pentose-phosphate pathway. DHAP = dihydroxyacetone phosphate. G3P = glyceraldehyde-3-phosphate. PEP = phosphoenolpyruvate. E4P = erythrose-4-phosphate. F6P = fructose-6-phosphate. X5P = xylulose-5-phosphate. R5P = ribose-5-phosphate. S7P = sedoheptulose-7-phosphate.

P. aeruginosa relies on Xfp for metabolic homeostasis of endogenous metabolites during anaerobic survival on glucose

Having established that PA14 can utilize a PPP and Xfp-mediated metabolism for acetate generation during anaerobic survival on glucose, we were curious whether Xfp played any additional roles in metabolic homeostasis. To test this, we repeated our anaerobic survival experiments, using the *Δphz* and *ΔphzΔxfp* strains, as well as a *ΔphzΔackAΔpta* strain – unable to generate acetate or acetyl-CoA from acetyl-P – and a *ΔphzΔackAΔptaΔxfp* strain. Loss of *ackA-pta* is less detrimental than loss of *xfp* and loss of all three genes is as detrimental as loss of *xfp* alone (Fig 3A). This suggests that both acetate and acetyl-CoA generation from Xfp-derived acetyl-P is dispensable early in survival, implying that Xfp plays an additional role under these conditions.

To identify this role, we repeated our 1-$^{13}C_1$-glucose experiment with the *Δphz* and *ΔphzΔxfp* strains, extracting intracellular metabolites and measuring their relative abundance and fraction of ^{13}C isotopic incorporation. On day 3, 60-80% of glucose-6P,

fructose-6P and sedoheptulose-7P were ^{13}C labelled in the *Δphz* strain, consistent with flux of glucose into the upper EMPP and PPP. However, in the *ΔphzΔxfp* strain we observed only 20-40% ^{13}C incorporation for these same metabolites (Fig 3B). Despite lower ^{13}C labelling in *ΔphzΔxfp* cells, upper EMPP and PPP metabolites were ~4-8 times higher than in *Δphz* cells (Fig 3C). The simultaneous low ^{13}C labelling of PPP-metabolites and ~4-8 times increase in their abundance in *ΔphzΔxfp* cells suggests input into the PPP, from glucose or endogenous carbon stores, outpaces PPP metabolite consumption. Additionally, as the increase in metabolite abundance is larger than the decrease in ^{13}C labelling for metabolites such as sedoheptulose-7P, these results may suggest that ^{13}C incorporation and PPP influx is faster in *ΔphzΔxfp* cells than *Δphz* cells for some metabolites.

As ^{13}C labelling of upper EMPP and PPP metabolites continued to increase by a few percent in the *Δphz* strain across the 7 days (SUPP FIG 3A/3B), we noted a decrease in the relative abundance of these metabolites by half (SUPP FIG 3C). The presence of doubly and triply ^{13}C labelled ribose-5P and sedoheptulose-7P in *Δphz* cells throughout survival suggests substantial cycling of glucose-derived metabolites through the PPP (FIG 2B, SUPP FIG 3B). The lack of detection of acetyl-CoA, absence of significant ^{13}C labelling of TCA cycle metabolites, and lack of detection of ^{13}C labelling of N-acetyl-glutamate, despite its significant consumption in *Δphz* cells throughout survival, leaves us unable to determine if any Xfp-derived acetyl-P is used to form acetyl-CoA (SUPP FIG 3A/3C/3D). Meanwhile a lack of pyruvate ^{13}C labelling, despite little change in its abundance over 7 days in *Δphz* cells suggests little flux out of the EDP (Fig

2B). However, EDP metabolites were undetectable so we cannot comment on levels of flux into the EDP.

To determine which metabolite differences were caused by anaerobic survival or *xfp* loss *per se*, we compared metabolite abundance in cells before and after the start of our survival experiment. Before anaerobic survival, the *ΔphzΔxfp* strain showed no dramatic differences in PPP metabolites compared to the *Δphz* strain, and though we observed some differences between the strains, such as 1.5-log decrease decrease in phenylalanine levels in *ΔphzΔxfp* cells, these differences were largely abolished after 3 days of anaerobic survival on glucose (SUPP FIG 4A/4B). Both strains individually showed an increase of up to 5-fold of upper EMPP, PPP, and TCA cycle metabolites during anaerobic survival compared to their levels beforehand, likely due to lower carbon utilization rates during growth arrest (FIG 3D/3E, SUPP FIG 4C/4D). These results indicate that anaerobic survival itself causes widespread central carbon metabolite accumulation, but that Xfp is important for balancing metabolite influx and consumption, specifically in the upper EMPP and PPP.

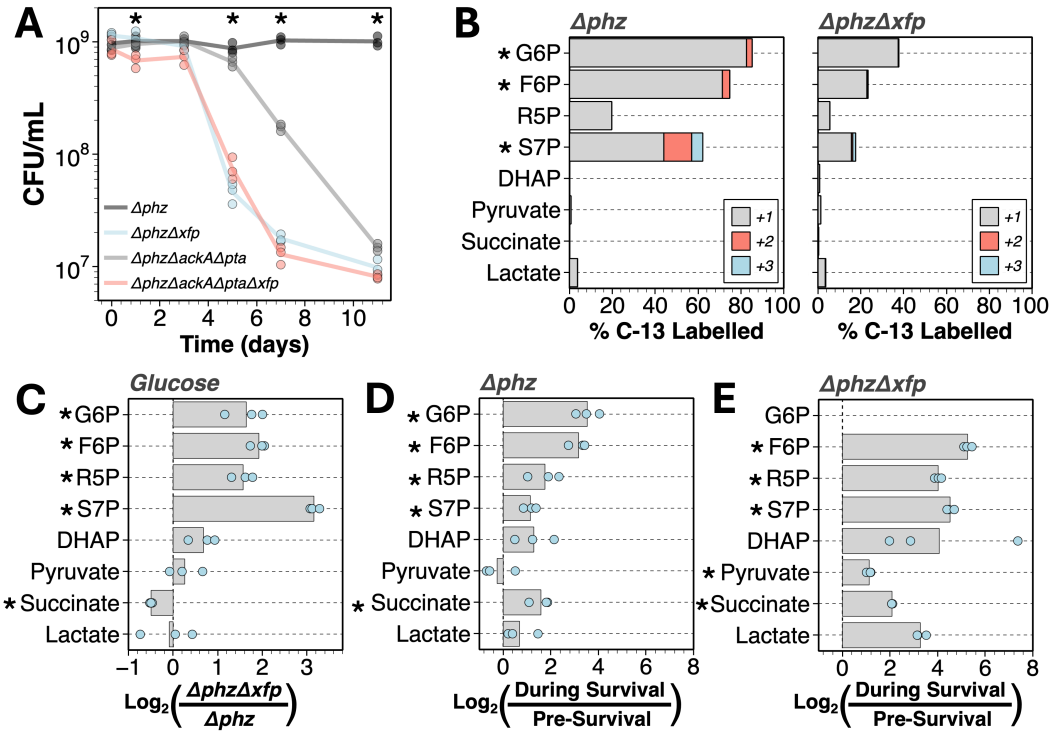

Figure 3: Xfp plays a role in metabolic homeostasis and consumption of endogenous metabolites to support catabolic flux from glucose. (A) Log-transformed CFU/mL values showing loss of the acetate generating system *ackA-pta* does not increase the survival deficit caused by *xfp* mutation. Lines = means, dots = replicates, n = 3. * denotes $p < 0.05$ from one-way ANOVA comparing means across all groups per day. (B) Percent of isotopically labelled metabolites in the parent strain and *xfp* mutant. Bars = mean of 3 biological replicates. Grey = singly labelled. Red = doubly labelled. Blue = triply labelled. (C) Log_2 transformed *ΔphzΔxfp* metabolite intensities normalized to the mean of *Δphz* metabolite intensities. Bars = means of *ΔphzΔxfp* normalized intensities, dots = replicates, n = 3. (D, E). Log_2 transformed metabolite intensities from *Δphz* samples (D) or *ΔphzΔxfp* samples (E) after 3 days of survival normalized to mean metabolite levels of the same strain before survival, bars = means, dots = independent replicates, n = 3.

(B, C, D, E) * denotes p-value < 0.05 from an independent two-tailed t-test comparing means between strains (B, C) or between pre- and post-survival metabolite levels within strains (D, E). G6P = glucose-6-phosphate. F6P = fructose-6-phosphate. R5P = ribose-5-phosphate, which is in equilibrium with xylulose-5-phosphate. S7P = sedoheptulose-7-phosphate. DHAP = dihydroxyacetone phosphate, which is in equilibrium with glyceraldehyde-3-phosphate.

P. aeruginosa's Xfp maintains metabolic homeostasis and viability during anaerobic survival on diverse carbon sources and in the absence of exogenous carbon

The accumulation of unlabeled EMPP and PPP metabolites in *ΔphzΔxfp* cells from presumptive metabolism of endogenous carbon stores suggested that the *ΔphzΔxfp* strain might exhibit similar phenotypes when provided with carbon sources other than glucose. Accordingly, we repeated our survival experiments on a variety of carbon sources or the absence of an exogenous carbon source. By Day 7 of anaerobic survival the *ΔphzΔxfp* mutant showed over 10-fold lower CFUs on all carbon sources except for pyruvate, as well as in the no carbon condition (Fig 4A). Additionally, by day 3, we observed mean metabolite levels of upper EMPP and PPP ~2 to 16 times higher in the *ΔphzΔxfp* strain during survival on succinate, glutamate and in the absence of exogenous carbon, but not on pyruvate (FIG 4B). Differences in some conditions between strains were non-significant due to variation in individual replicate metabolite values (SUPP FIG 5A). Each carbon source had unique differences between strains (SUPP FIG 5A). Metabolite measurements were not made during survival on glycerol, fructose, or butyrate.

Compared to their individual metabolite levels before anaerobic survival, both strains showed general increases in EMPP, PPP and TCA cycle metabolites in all conditions including pyruvate, likely due to lower carbon utilization during growth arrest (SUPP FIG 6A/6B). These data further support that metabolite accumulation is a general phenotype of transitioning from aerobic growth to anaerobic survival, but that, as survival continues, Xfp prevents further accumulation of upper EMPP and PPP metabolites. Notably, while trends in metabolite differences between the two strains were the same across all conditions except pyruvate, the magnitude of these changes was different for each nutrient condition (SUPP FIG 7). Therefore, different carbon sources likely cause varying levels of carbon influx into the PPP and its related pathways, leading to unique metabolic pressure, potentially explaining the variable importance of Xfp on promoting survival (FIG 4A).

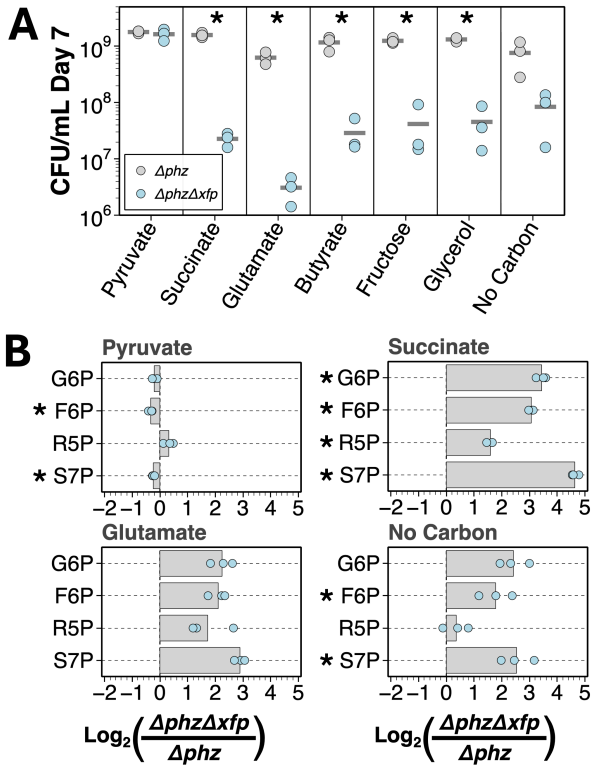

Figure 4. Xfp is important for viability and PPP metabolite homeostasis during anaerobic survival on various carbon sources, but not pyruvate. (A) CFU/mL of the *xfp* mutant and parent strain after 7 days of anaerobic survival on different carbon sources or in the absence of an exogenous carbon source. Grey = *Δphz*, blue = *ΔphzΔxfp*. (B) Log_2 transformed *ΔphzΔxfp* metabolite intensities normalized to the mean *Δphz* metabolite intensities after 3 days of survival on specified carbon sources. (A, B) Bar/dash = mean, dots = independent replicates, n = 3. (A, B) * denotes p-value < 0.05 from an independent two-tailed t-test comparing the means of each strain per metabolite per condition. G6P = glucose-6-phosphate. F6P = fructose-6-phosphate. R5P = ribose-5-phosphate. S7P = sedoheptulose-7-phosphate. All carbon sources were at a final concentration for 120 mM of total carbon (ex. 20 mM fructose, 40 mM pyruvate, etc.)

Anaerobic survival triggers purine degradation and Xfp is essential for maintaining ribonucleotide homeostasis

Because several studies have observed widespread RNA degradation during nutrient starved growth arrest in diverse bacteria (Deutscher, 2003; Himeoka *et al.*, 2022), we hypothesized that release of ribose-5-phosphate during ribonucleotide degradation might explain the accumulation of unlabeled metabolites in the PPP. This notion was bolstered by the fact that studies in mitochondria have shown increased PPP flux and accumulation of ribonucleotides after induction of reductive stress (Wu *et al.*, 2024; Yang *et al.*, 2022; Yang, Guo and Li, 2025). Moreover, directly upstream of PA14's *xfp* genes are two hypothetical proteins – *PA14_17550* and *PA14_17570* – with homology to LOG-family proteins and MBL-fold metallo-hydrolases with potential RNA and

ribonucleotide degradative functions respectively (Baier and Tokuriki, 2014; Dzurová *et al.*, 2015; Seo *et al.*, 2016).

To test this hypothesis, we measured xanthine – a purine nucleobase degradation product – before and after anaerobic survival under various conditions. After 3 days of anaerobic survival, xanthine levels were ~4 to 32 times higher in both the *Δphz* and *ΔphzΔxfp* strains across all conditions compared to their pre-survival levels (FIG 5A). Before and during survival both strains show similar xanthine levels relative to each other, albeit with slight elevation in the *ΔphzΔxfp* strain generally (FIG 5A, SUPP FIG 8A). Therefore, this data suggests that, irrespective of Xfp activity, anaerobic survival may trigger purine ribonucleotide degradation and xanthine accumulation, in addition to promoting flux into the PPP via ribose-5P. Alternatively, lowered xanthine consumption (via inhibition of ribonucleotide salvage or xanthine degradation to uric acid) could explain these results.

We further hypothesized that buildup of PPP metabolites in the *ΔphzΔxfp* strain during survival would potentially dysregulate ribonucleotide levels by inhibiting further ribose-5P release during ribonucleotide degradation. After 3 days of anaerobic survival on glucose, ribonucleotides levels were over 4 times higher in the *ΔphzΔxfp* strain compared to *Δphz* cells, except for ATP and dUMP (FIG 5B). Ribonucleotide levels were similarly elevated in *ΔphzΔxfp* cells after 3 days of survival in the absence of an exogenous carbon source, on glutamate, or on succinate compared to *Δphz* cells (FIG 5C, SUPP FIG 8B). However, loss of *xfp* did not change ribonucleotide levels during survival on pyruvate (FIG 5C, SUPP FIG 8B), similar to its lack of effect on the

accumulation of upper PPP metabolites (FIG 4B). Notably, while trends were similar across conditions, metabolite levels and the effect of *xfp* mutation occurred at different magnitudes for different nutrient conditions (SUPP FIG 9). This observed increase in ribonucleotide levels in *ΔphzΔxfp* cells compared to *Δphz,* cells despite both strains having similar xanthine levels, may suggest faster ribonucleotide polymer (e.g. RNA) breakdown in *ΔphzΔxfp* cells to form ribonucleotide monomers, but an inhibition of further degradation; alternatively, it may point to increased ribonucleotide biosynthesis. Follow-up studies are needed to distinguish between these possibilities. Regardless, our data suggest that Xfp plays a role in ribonucleotide homeostasis.

To determine if, as seen with PPP and upper EMPP metabolite levels, ribonucleotide accumulation generally occurred upon transition to anaerobic survival, irrespective of *xfp,* we compared the metabolite levels of each strain during survival to their own levels before survival began. Compared to before survival, ribonucleotide levels only generally increased by 2 times or more in *Δphz* cells during survival on glucose, but not on other substrates, compared to *Δphz* cells before survival began (SUPP FIG 10A/10B). In contrast, ribonucleotide levels were generally ~2 to 64 times higher in *ΔphzΔxfp* cells during survival on all substrates except pyruvate compared to *ΔphzΔxfp* cells before survival began (SUPP FIG 10C). Both strains individually showed lower ATP levels during survival compared to before on all substrates except for pyruvate and showed large increases upwards of 64 times higher in dUMP levels during survival on pyruvate (SUPP FIG 10B/10C). Therefore, while xanthine accumulation and loss of ATP occur during anaerobic survival irrespective of *xfp,* ribonucleotide

accumulation is generally specific to *ΔphzΔxfp* cells. As ribonucleotide accumulation is only correlated with PPP metabolite accumulation in *ΔphzΔxfp* cells, this suggests a role for Xfp in mediating ribonucleotide degradation and/or recycling.

Overall, our data reveal that anaerobic survival triggers purine degradation and PPP metabolite accumulation, necessitating Xfp to maintain homeostasis of these metabolite pools during survival on non-pyruvate carbon sources. We hypothesize that Xfp is necessary because consumption of accumulated PPP metabolites by other pathways would be inhibited under reductive stress, such as the EDP or lower EMPP, or require substantial energetic costs, such as ribonucleotide biosynthesis (FIG 5D). Meanwhile during survival on pyruvate, compared to survival in other nutrient conditions, a relatively higher adenylate charge and/or lower reductive stress conditions could make non-Xfp pathways for metabolite consumption viable, abolishing a need for Xfp activity to maintain metabolic balance. Finally, the increase in AMP and ADP, but not ATP levels in the *ΔphzΔxfp* strain compared to *Δphz* cells, suggests that Xfp plays a role in maintaining the cellular energy state as such changes would lead to a lower adenylate charge, which could inhibit functions such as biosynthesis or nutrient transport.

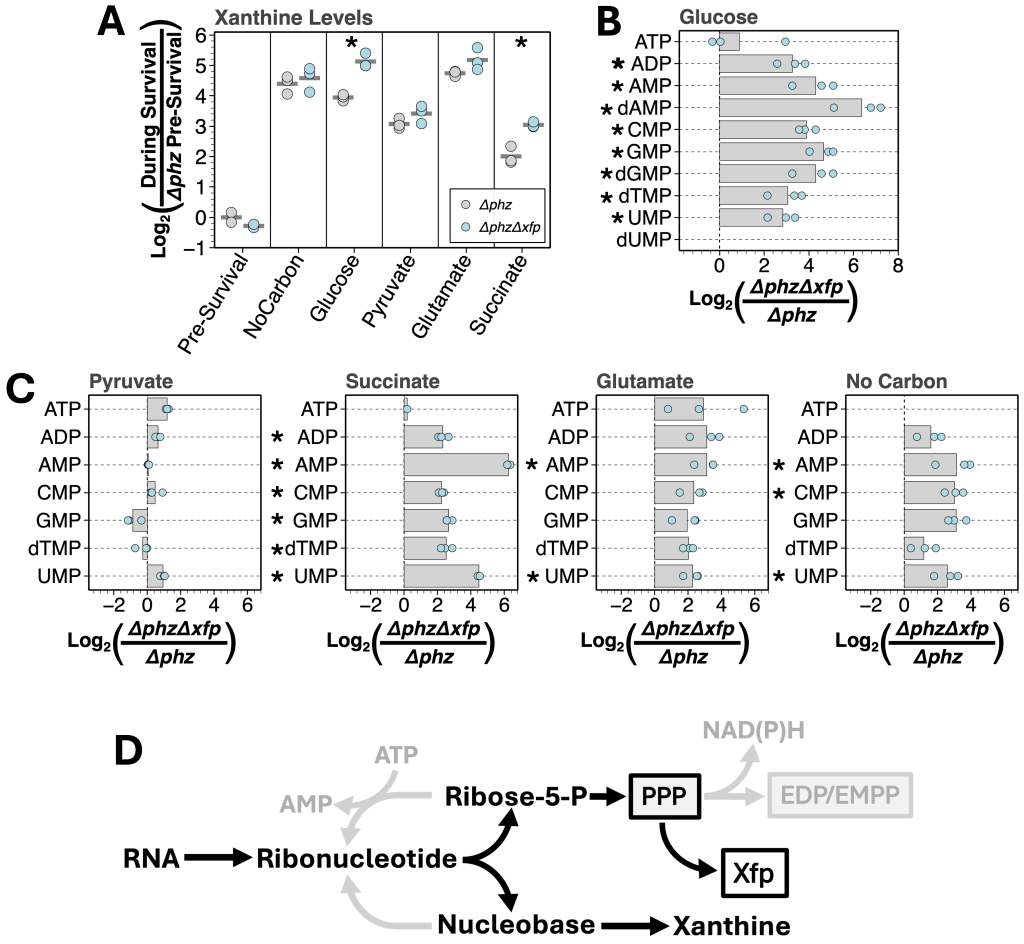

Figure 5. Ribonucleotide salvage occurs during anaerobic survival on all conditions irrespective of *xfp,* but Xfp is important for maintaining ribonucleotide homeostasis under all nutrient conditions except pyruvate. (A) Log_2 transformed xanthine intensities after 3 days of anaerobic survival on various carbon sources, normalized to the mean xanthine level in *Δphz* strain before survival. Grey = *Δphz,* blue = *ΔphzΔxfp*. (B, C) Log_2 transformed *ΔphzΔxfp* metabolite intensities normalized to mean *Δphz* metabolite intensities after 3 days of anaerobic survival on various carbon sources. (A, B, C) Dashes/bars = mean. Dots = independent replicates, n = 3. * denotes p-value < 0.05 from an independent two-tailed t-test comparing the means of each strain per metabolite

per condition. All carbon sources were at a final concentration for 120 mM of total carbon (ex. 20 mM glucose, 40 mM pyruvate, etc.) (D) Condensed metabolic diagram of ribonucleotide salvage showing that ribonucleotide degradation produces ribose-5P and nucleobases, the former enters the PPP where it can exit via ATP-costly ribonucleotide biosynthesis, reducing equivalent-generating EDP/EMPP pathways, or via PA14's Xfp. Nucleobases can either be consumed via ribonucleotide biosynthesis or be further degraded to form xanthine. Black arrows represent pathways that would be uninhibited during energy-limited reductive stress survival while grey arrows/pathways are those we believe would be inhibited during anaerobic survival.

Discussion

Bacteria are commonly found in growth-arrested states, however, the metabolic networks supporting survival under such conditions are understudied even in model organisms such as *P. aeruginosa*. Based on studies performed during active growth, *P. aeruginosa* has been assumed to only catabolize glucose via the EDP (Kohlstedt and Wittmann, 2019; Lessie and Phibbs, 1984), yet here we show that during anaerobic survival it relies on the PPP and a phosphoketolase-dependent pathway, allowing it to mitigate metabolic dysregulation and death. While phosphoketolases occur across the bacterial tree of life, hitherto, their study has focused almost entirely on their role in fermentative metabolisms in obligate anaerobes or their use in natural product generation and synthetic biology (Årsköld *et al.*, 2008; Bogorad, Lin and Liao, 2013; Bruinsma *et al.*, 2023; de Vries and Stouthamer, 1967; Fleige, Kroll and Steinbüchel, 2011; Krüsemann *et al.*, 2018; Liu *et al.*, 2012; Sánchez *et al.*, 2010). Our contribution to bacterial physiology in this study has been to demonstrate that phosphoketolases can

also support viability and ribonucleotide homeostasis during oxidant-limited growth arrest in a historically deemed "non-fermentative" or "obligately aerobic" bacterium. Because cancer cell mitochondria experience reductive stress-induced metabolic disruptions similar to those observed in our system, our findings embody the principle of "unity in biochemistry" first articulated by Albert Kluyver over a century ago (Kluyver, 1924).

It is noteworthy that routing of metabolism through the PPP and a phosphoketolase to support anoxic sugar catabolism is shared between fermentative obligate anaerobes, such as Bifidobacterium, Lactobacillus, or Clostridia species, and *P. aeruginosa,* which cannot grow fermentatively (Aristilde *et al.*, 2015; Årsköld *et al.*, 2008; de Vries and Stouthamer, 1967; Liu *et al.*, 2012; Sánchez *et al.*, 2010). It reinforces the view that the conceptual divide between "fermenters" and "non-fermenters", or "obligate aerobes" as *P. aeruginosa* is commonly but erroneously called, requires reconsideration. Further research investigating whether Xfp-products can be used as electron acceptors would clarify whether *P. aeruginosa* is capable of Xfp-mediated fermentation decoupled from growth. Moreover, we show *P. aeruginosa* carries out significant purine degradation during anaerobic survival and reveal an additional role for phosphoketolases in maintaining ribonucleotide homeostasis within this context. Ribonucleotide recycling is a metabolic necessity for various bacteria during growth-arrest, especially during nutrient starvation (Condon, 2007; Deutscher, 2003; Himeoka *et al.*, 2022); yet whether phosphoketolases facilitate this process in other bacteria during growth arrest remains to be determined. However, the importance of phosphoketolases to support PPP flux and therefore generation of ribonucleotide precursors in various

species during fermentative of sugars supports the feasibility of such a role (Aristilde *et al.*, 2015; Aristilde, 2017; Årsköld *et al.*, 2008; de Vries and Stouthamer, 1967; Sánchez *et al.*, 2010). Regardless, as research into the biology of growth arrest increases, particularly as induced by oxidant limitation, our ability to identify metabolic strategies that transcend historical growth-oriented classifications and taxonomic distance will improve.

In this vein, we speculate that organisms such as *P. aeruginosa* may have evolved to survive but not grow under reductive stress. *P. aeruginosa* prefers non-fermentative easily respirable carbon sources (such as organic acids as opposed to sugars), lacks a few key fermentative genes while containing others, and is unable to use the major NADPH-producing oxidative PPP (Eschbach *et al.*, 2004; Lessie and Phibbs, 1984; McGill *et al.*, 2021). Meanwhile, it also produces phenazines (diffusible electron shuttles) that support non-growth maintenance metabolisms in the absence of terminal electron acceptors (Ciemniecki *et al.*, 2024; Glasser, Kern and Newman, 2014). Our discovery that a phosphoketolase supports anaerobic survival, but not growth, furthers this speculation and demonstrates the multitude of complementary strategies this bacterium uses to survive oxidant limitation. Such a strategy might act to bolster stress tolerance under such conditions, while conserving resources for use upon reintroduction of a terminal electron acceptor.

Under energy limited anaerobic survival conditions, the upper EMPP and PPP may represent a metabolite "reservoir" with Xfp acting as a release valve. The non-oxidative PPP represents the only cyclable central carbon metabolic network in PA14 that produces no reducing equivalents or requires ATP expenditure. Yet, all exits from

the PPP (except by way of Xfp) all quickly generate reducing equivalents – lower EMPP – or require ATP expenditure – biosynthesis (FIG 5D) (Kohlstedt and Wittmann, 2019). Extensive use of such cycling is supported by the presence of doubly or triply labelled PPP and upper EMPP metabolites in *Δphz* cells during anaerobic survival on glucose (FIG 3B, SUPP FIG 3B). Therefore, while Xfp can stimulate energy conservation via substrate phosphorylation during acetate production, we suggest that Xfp's primary role is to maintain metabolic homeostasis via consumption of accumulated metabolites in the PPP. This conclusion is supported by the lower survival of *Δxfp* strains on glucose compared to strains lacking only *ΔackAΔpta*. However, further quantitative flux analysis is required to test this hypothesis. Previous studies in the obligate anaerobe *C. acetobutylicum* have suggested that phosphoketolase-mediated catabolism of pentoses is faster and requires fewer enzymatic steps than catabolism via other PPP enzymes such as transaldolase (Aristilde *et al.*, 2015; Liu *et al.*, 2012). Therefore, it is plausible that during energy-limited anaerobic survival in *P. aeruginosa* such a phosphoketolase-based metabolism may act as an enzymatically "cheaper" and faster way to consume PPP metabolites than other pathways.

The dispensability of Xfp during survival on pyruvate but not on other substrates, can also be rationalized (FIG 4A). Pyruvate fermentation does not generate reductive stress because it is redox-balanced (Eschbach *et al.*, 2004; Glasser, Kern and Newman, 2014); it also generates a relatively high adenylate charge ratio and its products (acetate and lactate) can be effluxed to prevent accumulation. Together, these features would enable the cell to maintain balanced PPP metabolism via non-Xfp-mediated pathways (Fig 5D). In contrast, we observed a substantial portion of PPP flux and

metabolite accumulation from endogenous carbon stores, one potential source being ribonucleotides. This build-up appears inherent to anaerobic survival, independent of whether Xfp is present, yet Xfp serves to prevent further accumulation and lethality. The survival patterns seen for the parent and *xfp* mutant in the presence of different carbon sources indicate that during anaerobic survival, carbon metabolism acts as a double-edged sword, with increased catabolic flux fueling energy conservation, and production of biosynthetic precursors, but at the cost of increased reductive stress, leading to increased pressure on the PPP and metabolite accumulation.

A case in point that illustrates this phenomenon is the importance of balanced ribonucleotide recycling, for which the PPP is vital (Condon, 2007; Deutscher, 2003; Himeoka *et al.*, 2022). The PPP produces ribose-5P for ribonucleotide biosynthesis and accepts ribose-5P during ribonucleotide degradation (FIG 5D). During anaerobic survival in *P. aeruginosa,* purine degradation occurs in an Xfp-independent manner, evidenced by significant increases to xanthine levels (up to ~64 times higher) across strains and conditions, yet we hypothesize that Xfp ensures the cell's ability to maintain ribonucleotide homeostasis. In fluctuating environments, cells remodel their transcriptome and ribose-5P is generated as a consequence of RNA degradation (Guo and Gross, 2014). Because the rate of ribonucleotide degradation during energy-limited growth-arrest likely outpaces the rate of energetically costly ribonucleotide biosynthesis, ribose-5P accumulation would require Xfp to prevent inhibition of ribonucleotide recycling or other catabolic/anabolic flux through the PPP. Catabolism of carbon sources such as glucose during anaerobic survival would then emphasize this role by causing additional PPP metabolite accumulation on top of accumulation via

ribonucleotide degradation. This capability of Xfp to regulate these pathways is supported by the absence of PPP metabolite accumulation despite increases to xanthine and ribonucleotide levels in *Δphz* cells during anaerobic survival on glucose. While further work is required to determine Xfp's substrate(s), its homology to a preferentially xylulose-5P degrading phosphoketolase (Petrareanu *et al.*, 2014), and its role in modulating ribonucleotide levels, suggests that xylulose-5P may be a primary substrate in this organism (SUPP FIG1).

In this vein, an intriguing hypothesis is that Xfp's consumption of ribose-5P, via its equilibration with xylulose-5P, could support redox balance via NAD^+ consumption. Degradation of NAD+ and NADP+, releasing AMP and ribose-5P, may represent a strategy to gain increased control over the cellular redox state (Gazzaniga *et al.*, 2009; Gossmann *et al.*, 2012). Lower levels and/or lack of detection of NADH, NADPH, glutathione, and glutathione disulfide in cells surviving on glucose compared to pyruvate may hint at degradation of redox pools as a general cellular strategy to combat reductive stress. However, the pathways to accomplish such degradation are poorly understood in *P. aeruginosa.*

Alternatively, regulation of PPP metabolite levels by Xfp could avoid energetically costly futile cycling and biosynthesis. During reductive stress and hypoxia, cancer cells have been shown to increase PPP flux and dramatically accumulate ribonucleotides (Wu *et al.*, 2024; Yang, Guo and Li, 2025). In one study the authors suggest that reductive stress deregulates ribonucleotide biosynthesis, leading to *de novo* purine biosynthesis and ATP consumption (Yang, Guo and Li, 2025). Meanwhile, a separate study found that reductive stress led to ribonucleotide accumulation via the far

less costly purine salvage pathway, with the resulting increase in ribonucleotide monophosphates inhibiting *de novo* biosynthesis preventing further energy expenditure (Wu *et al.*, 2024). Additionally, recent work in the cyanobacterium *Synechococcus elongatus* found an Xfp homolog supports survival during light-dark transitions by consuming Calvin-Benson-Bassham cycle metabolites to prevent ATP-consuming futile cycling, albeit at the cost of lower carbon fixation (Lu *et al.*, 2023). In tandem with previous studies in *C. acetobutylicum* suggesting phosphoketolases can act as metabolic "shortcuts" to limit enzymatic costs while hastening pentose catabolism, we speculate that PA14's Xfp consumption of PPP metabolites could avoid futile and energetically costly biosynthesis (Aristilde *et al.*, 2015; Liu *et al.*, 2012; Lu *et al.*, 2023; Servinsky *et al.*, 2012). Such a function could explain why loss of *xfp* is lethal, with buildup of PPP metabolites forcing biosynthesis, draining ATP and disrupting the adenylate charge. Further testing will determine whether this is in fact the case for PA14 and possibly other bacteria.

In summary, our discovery that Xfp facilitates the maintenance of metabolic homeostasis during anaerobic survival under reductive stress remind us of the adage that "an ounce of prevention is worth a pound of cure". Though we have highlighted Xfp's role in facilitating ribonucleotide homeostasis in *P. aeruginosa* PA14, given that the PPP and acetyl-P derived compounds are integral to many other anabolic processes, it is possible that Xfp could also play a role in amino acid or fatty acid metabolisms, processes known to support bacterial survival during growth arrest (Bergkessel, Basta and Newman, 2016). Additionally, generation of acetyl-P by Xfp may serve as a vital signaling molecule. The parallels seen in the mitochondria literature, where reductively stressed mitochondria are reported to increase ribonucleotide salvage, amino acid biosynthesis,

and lipogenesis (Wu *et al.*, 2024; Yang, Guo and Li, 2025), serve as a powerful reminder of the potential to identify overarching principles of metabolism that span the domains of life as we open our studies of metabolites to include the biology of growth arrest.

Methods

Strains, culture conditions, and reagents

All strains used can be found in the Supplemental Table 1. All strains were derived from *P. aeruginosa* UCBPP-PA14 (DKN263, laboratory strain). The *Δphz* strain lacks the *phzA1-G1*, *phzA2-G2* operons, as well as *phzH, phzS,* and *phzM* genes (Meirelles *et al.*, 2021). Cells were streaked from 20% glycerol -80 C freezer stocks onto Difco LB 1.5% agar plates (BD Biosciences) and grown overnight at 37 C. *ΔphzΔackAΔpta* strain lacked the *phzA1-G1* and *phzA2-G2* operons as well as the *ackA* and *pta* genes (Glasser, Kern and Newman, 2014). The *ΔphzΔxfp* (this study) strain lacked all genes of the *Δphz* strain including *PA14_17580* encoding a putative phosphoketolase. The *ΔphzΔackAΔptaΔxfp* (this study) gene lacked all genes of the *ΔphzΔackAΔpta* strain including *PA14_17580*.

Mutant generation and complementation

All plasmids and primers used can be found in the Supplemental Table 1. Primers were ordered from Integrated DNA technologies. For mutant generation we utilized allelic exchange. Plasmids were synthesized using Gibson assembly (NEB) (Gibson *et al.*, 2009). The plasmid pMQ30 (Shanks *et al.*, 2006) was digested with SmaI, 1 kb regions flanking *PA14_17580* were inserted, and the plasmid was transformed into *E. coli* S17 and conjugated into *P. aeruginosa* PA14. PA14 conjugates were selected on LB + 70

ug/mL gentamicin and 20 ug/mL of chloramphenicol. Final mutants were then selected on LB + 10% sucrose and no NaCl. Complementation was done by addition of *PA14_17580* to the multicloning site of pJM220 (Choi and Schweizer, 2006) under control of a L-rhamnose inducible promoter and transformed into *E. coli* S17. *PA14_17580* was then inserted in trans at the attTn7 site of PA14.

Balch tube anaerobic survival assays and viability measurements

Planktonic cultures were made with 7 mL of Difco LB and grown for 20 hours at 37 C at 250 RPM to reach late stationary phase, OD_{500nm} ~ 5. A MOPS minimal media (MM) was used for all experiments (100 mM anhydrous MOPS, 9.3 mM NH_4Cl, 3.7 mM KH_2PO_4, 1 mM $MgSO_4$, 30 uM $FeSO_4$ dissolved in EDTA, and 1x HAquil trace metals mix lacking $FeCl_3$ (Martocello, Morel and McRose, 2019). Cell suspensions for all experiments were prepared by washing stationary phase cells 3x at 10,000 xg for 10 minutes at 4 C with resuspension in MOPS MM, then resuspended to a final volume of 200 uL, the OD_{500nm} measured, and the suspension diluted to an OD_{500nm} of ~75. Cell suspensions were then transferred to an anaerobic Coy Chamber with an atmosphere of N_2 and ~1.5-2.5 % H_2. Cell suspensions were diluted 5x with N_2 sparged MOPS MM. N_2 sparged MOPS MM, 250 uL of N_2 sparged carbon sources, and 250 uL of cell suspensions were added to Balch tubes to reach a final concentration of OD_{500nm} = 0.75 of cells and 120 mM carbon atoms (ex. 20 mM glucose or 40 mM pyruvate) in a final volume of 5 mL. Balch tubes were then stoppered and crimped before being removed from the Coy Chamber and left to incubate at 30 C at 250 RPM. All Balch tubes, pipettes, and stoppers used were left to passively degas for 5+ days before their use above. Sparging occurred for 30+ minutes in all steps.

To measure CFU/mL of anaerobically surviving cells in Balch tubes, 1 mL syringes with a INSERT GAUGE needle were fully filled and emptied 5 times under a steady flow of N_2 to remove oxygen, then inserted into Balch tubes and ~ 200 uL withdrawn and placed in a 96 well plate (Fischer). To confirm no large inputs of oxygen during this, a Balch tube prepared above was given resazurin which is reduced to colorless by cells and re-oxidized by oxygen, turning a bright pink. No pink was seen when inserting or withdrawing media for CFU sampling. Samples were serially-diluted at 10x dilution steps, then 5 uL was platted onto Difco LB + 1.5% agar plates and left to incubate overnight at 37 C before CFUs were counted.

96-well potentiostat anaerobic survival assays

Cell suspensions were prepared as in Balch tube experiments, but added to a 96-well electrochemical plate at a final cell OD_{500nm} of 0.75, with 20 mM glucose, set concentrations of phenazine-1-carboxamide (PCN), and MOPS MM to a final volume of 200 uL. PCN was solubilized in DMSO. Samples given 0 uM PCN were given an equal volume of DMSO as a vehicle control. Plates were sealed using both a slit-seal cover (BioChromato #R80.120.00) and an aluminum seal cover (DiversifiedBiotech #ALUM-1000). Each well contained a screen-printed carbon working electrode and counter electrode, and Ag/AgCl reference electrode. The plate was incubated at 33 C without shaking in a custom 96-potentiostat system developed at the National Institute for Materials Science, Japan. Every well's working electrode was held at a constant 0 mV vs Ag/AgCl. On set days, the aluminum seal was removed and wells mixed by pipetting 150 uL several times. 10 uL was removed and transferred to a 96 well plate and CFUs measured as described above for Balch tube experiments.

Metabolite extractions

On select days of anaerobic survival in Balch tubes, the full 7 mL cell suspension (OD_{600} = 0.75) was collected by vacuum filtration onto Whatman 0.22 um nylon filters. Flow-through was collected and frozen at -80 C for downstream measurement of acetate. For collection of intracellular metabolites, filters were dunked upside down in 2 mL cold quenching solution of 40/40/20 methanol/acetonitrile/water (v/v) and incubated at -20 C for 30 minutes. Quenching solution was pipetted up and down over the filter to remove cell debris and the cell suspension was transferred into 2-mL tubes followed by centrifugation at 10,000 *g* at 4 C for 5 minutes. The supernatant (200 μL) was aliquoted and dried on ice under flow of N_2. Dried samples were stored at -80 C until analysis.

Intracellular metabolite quantification

Intracellular metabolites were quantified based on an established metabolomics protocol using UHPLC (Thermo Fisher Scientific Dionex UltiMate 3000) coupled to high-resolution mass spectrometry (Thermo Fisher Scientific Q Exactive quadrupole-Orbitrap) operating in negative mode (Aristilde *et al.*, 2017). For LC we used an Acquity UPLC BEH C18 Column (particle size 1.7 um, 2.1 mm x 100 mm) maintained at 25 C with an injection volume of 10 uL. The eluents consisted of 97:3 (v/v) water:methanol with 15 mM acetic acid and 10 mM tributylamine (eluent A) and methanol (eluent B)(Aristilde *et al.*, 2017). The flow rate was 0.18 mL min^{-1} (Aristilde *et al.*, 2017). Relative intensities and the fraction of ^{13}C isotopologues of each metabolite was analyzed using the Metabolomic Analysis and Visualization Engine (MAVEN) software (2011.6.17) (Clasquin, Melamud and Rabinowitz, 2012). IsoCor v2.2.0 was used to correct for natural abundance of ^{13}C (Millard *et al.*, 2019).

Determination of ^{13}C incorporation into acetate

Extracellular supernatant samples were thawed and diluted 20:1 (sample:acid) with 1M H_2SO_4. Low pH assured efficient transfer of acetate as acetic acid in the gas phase processes involved in GC-MS analysis. Samples were analyzed with an Agilent 6890 gas chromatograph coupled to a Waters GCT Premier time-of-flight mass spectrometer operating in electron impact positive ion mode. Samples (500 nL) were injected via a split/splitless injector operated in in split mode (20:1) at 250 C. A Phenomenex Focusliner (single taper with wool) (p/n AG0-4680) was installed in the injector. The instrument was tuned to 6000 resolution (m/Δm) and continuous accurate mass calibration was maintained by locking the mass axis to the $C_4F_9^+$ (218.98508 m/z) ion obtained by continuous admission of perfluorotributylamine via the reference reservoir. Spectra were recorded from 33 to 400 m/z beginning at 2.3 minutes until 10 minutes. Separation of acetate from other components of the sample was achieved on a ZB-FFAP column (Phenomenex, Torrance, CA) 30m x 0.32mm ID x 0.25 microns operated at a constant flow of 0.8 mL/min. Initial column temperature was 100 C for 2 minutes increasing to 124 C at 8 C/min, then increasing to 180 C at 25 C with a final hold for 3 minutes. Acetic acid was eluted at 6.9 minutes. Masslynx and QuanLynx (Version 4.1) software was employed for data processing using peak areas of 60, 61, and 62 m/z for un-labelled, singly ^{13}C-labelled, and doubly ^{13}C-labelled acetic acid, respectively. HCO2+ ions resulting from in-source fragmentation of acetic acid were used to determine labeling at the carboxylate carbon based on the areas of the peaks 45 and 46 m/z for un-labelled and singly ^{13}C labelled fragments, respectively. Ratios of peak areas of

labelled to unlabeled ions were used to estimate relative amounts of ^{13}C labelling without further correction.

Statistical analysis and data visualization

Unpaired two-tailed t-test was applied to determine difference of means between two groups while on-qay analysis of variance (ANOVA) was employed to evaluate difference of means between more than two conditions. Tukey's honestly significant difference test was used for pairwise comparisons following a significant ANOVA result. P-value threshold for all tests set at 0.05. All data was analyzed and processed in a Python (3.13.2) using Pandas (2.2.3), NumPy (2.1.3), SciPy (1.15.2), and Statsmodels (0.14.4). All plotting was done using Bokeh (2.2.3). Homology between the phosphoketolase amino acid sequences of *P. aeruginosa* UCBPP-PA14 and *P. aeruginosa* ATCC 15442 was done using Benchling (https://benchling.com).

Acknowledgements

We would like to thank the various Newman lab members for their advice throughout the project. We thank Dr. Xiayou Shan (Caltech – Newman Lab) for assistance in initial hypothesis generation and Dr. Scott Saunders (UT Southwestern) for the preliminary tn-seq screen used to generate our hypothesis. This work was supported by grants from the NIH (2R01AI127850-06A1).

Data Availability Statement

Metabolomics MS data are freely available through the MetaboLights depository (https://www.ebi.ac.uk/metabolights/) under accession (MTBLS13293).

References

Aristilde, L. *et al.* (2015) "Hierarchy in Pentose Sugar Metabolism in Clostridium acetobutylicum," *Applied and Environmental Microbiology*, 81(4), pp. 1452–1462. Available at: https://doi.org/10.1128/AEM.03199-14.

Aristilde, L. *et al.* (2017) "Glyphosate-Induced Specific and Widespread Perturbations in the Metabolome of Soil Pseudomonas Species," *Frontiers in Environmental Science*, 5. Available at: https://doi.org/10.3389/fenvs.2017.00034.

Aristilde, L. (2017) "Metabolite labelling reveals hierarchies in Clostridium acetobutylicum that selectively channel carbons from sugar mixtures towards biofuel precursors," *Microbial Biotechnology*, 10(1), pp. 162–174. Available at: https://doi.org/10.1111/1751-7915.12459.

Årsköld, E. *et al.* (2008) "Phosphoketolase Pathway Dominates in Lactobacillus reuteri ATCC 55730 Containing Dual Pathways for Glycolysis," *Journal of Bacteriology*, 190(1), pp. 206–212. Available at: https://doi.org/10.1128/jb.01227-07.

Baier, F. and Tokuriki, N. (2014) "Connectivity between Catalytic Landscapes of the Metallo-β-Lactamase Superfamily," *Journal of Molecular Biology*, 426(13), pp. 2442–2456. Available at: https://doi.org/10.1016/j.jmb.2014.04.013.

Bartacek, J., Zabranska, J. and Lens, P.N.L. (2007) "Developments and constraints in fermentative hydrogen production," *Biofuels, Bioproducts and Biorefining*, 1(3), pp. 201–214. Available at: https://doi.org/10.1002/bbb.17.

Bergkessel, M., Basta, D.W. and Newman, D.K. (2016) "The physiology of growth arrest: uniting molecular and environmental microbiology," *Nature Reviews*

Microbiology, 14(9), pp. 549–562. Available at: https://doi.org/10.1038/nrmicro.2016.107.

Berney, M. *et al.* (2014) "An obligately aerobic soil bacterium activates fermentative hydrogen production to survive reductive stress during hypoxia," *Proceedings of the National Academy of Sciences*, 111(31), pp. 11479–11484. Available at: https://doi.org/10.1073/pnas.1407034111.

Bogorad, I.W., Lin, T.-S. and Liao, J.C. (2013) "Synthetic non-oxidative glycolysis enables complete carbon conservation," *Nature*, 502(7473), pp. 693–697. Available at: https://doi.org/10.1038/nature12575.

Bruinsma, L. *et al.* (2023) "Increasing cellular fitness and product yields in Pseudomonas putida through an engineered phosphoketolase shunt," *Microbial Cell Factories*, 22(1), p. 14. Available at: https://doi.org/10.1186/s12934-022-02015-9.

Cantó, C., Menzies, K.J. and Auwerx, J. (2015) "NAD+ Metabolism and the Control of Energy Homeostasis: A Balancing Act between Mitochondria and the Nucleus," *Cell Metabolism*, 22(1), pp. 31–53. Available at: https://doi.org/10.1016/j.cmet.2015.05.023.

Choi, K.-H. and Schweizer, H.P. (2006) "mini-Tn7 insertion in bacteria with single attTn7 sites: example Pseudomonas aeruginosa," *Nature Protocols*, 1(1), pp. 153–161. Available at: https://doi.org/10.1038/nprot.2006.24.

Chubukov, V. *et al.* (2014) "Coordination of microbial metabolism," *Nature Reviews Microbiology*, 12(5), pp. 327–340. Available at: https://doi.org/10.1038/nrmicro3238.

Ciemniecki, J.A. *et al.* (2024) "Mechanistic study of a low-power bacterial maintenance state using high-throughput electrochemistry," *Cell*, 187(24), pp. 6882-6895.e8. Available at: https://doi.org/10.1016/j.cell.2024.09.042.

Ciemniecki, J.A. and Newman, D.K. (2020) "The Potential for Redox-Active Metabolites To Enhance or Unlock Anaerobic Survival Metabolisms in Aerobes," *Journal of Bacteriology*, 202(11), p. 10.1128/jb.00797-19. Available at: https://doi.org/10.1128/jb.00797-19.

Clasquin, M.F., Melamud, E. and Rabinowitz, J.D. (2012) "LC-MS Data Processing with MAVEN: A Metabolomic Analysis and Visualization Engine," *Current Protocols in Bioinformatics*, 37(1), p. 14.11.1-14.11.23. Available at: https://doi.org/10.1002/0471250953.bi1411s37.

Condon, C. (2007) "Maturation and degradation of RNA in bacteria," *Current Opinion in Microbiology*, 10(3), pp. 271–278. Available at: https://doi.org/10.1016/j.mib.2007.05.008.

Cowley, E.S. *et al.* (2015) "Pediatric Cystic Fibrosis Sputum Can Be Chemically Dynamic, Anoxic, and Extremely Reduced Due to Hydrogen Sulfide Formation," *mBio*, 6(4), p. 10.1128/mbio.00767-15. Available at: https://doi.org/10.1128/mbio.00767-15.

Deutscher, M.P. (2003) "Degradation of Stable RNA in Bacteria *," *Journal of Biological Chemistry*, 278(46), pp. 45041–45044. Available at: https://doi.org/10.1074/jbc.R300031200.

Dzurová, L. *et al.* (2015) "The three-dimensional structure of 'Lonely Guy' from Claviceps purpurea provides insights into the phosphoribohydrolase function of

Rossmann fold-containing lysine decarboxylase-like proteins," *Proteins: Structure, Function, and Bioinformatics*, 83(8), pp. 1539–1546. Available at: https://doi.org/10.1002/prot.24835.

Enfors, S.-O. *et al.* (2001) "Physiological responses to mixing in large scale bioreactors," *Journal of Biotechnology*, 85(2), pp. 175–185. Available at: https://doi.org/10.1016/S0168-1656(00)00365-5.

Eschbach, M. *et al.* (2004) "Long-Term Anaerobic Survival of the Opportunistic Pathogen Pseudomonas aeruginosa via Pyruvate Fermentation," *Journal of Bacteriology*, 186(14), pp. 4596–4604. Available at: https://doi.org/10.1128/jb.186.14.4596-4604.2004.

Ferrara, S. *et al.* (2021) "The Small RNA ErsA Impacts the Anaerobic Metabolism of Pseudomonas aeruginosa Through Post-Transcriptional Modulation of the Master Regulator Anr," *Frontiers in Microbiology*, 12, p. 691608. Available at: https://doi.org/10.3389/fmicb.2021.691608.

Fleige, C., Kroll, J. and Steinbüchel, A. (2011) "Establishment of an alternative phosphoketolase-dependent pathway for fructose catabolism in Ralstonia eutropha H16," *Applied Microbiology and Biotechnology*, 91(3), pp. 769–776. Available at: https://doi.org/10.1007/s00253-011-3284-5.

Gayon, U. (1845-1929) A. du texte and Dupetit, G.A. du texte (1886) *Recherches sur la réduction des nitrates par les infiniment petits / par MM. U. Gayon et G. Dupetit ; Station agronomique de Bordeaux*. Available at: https://gallica.bnf.fr/ark:/12148/bpt6k9366473 (Accessed: November 11, 2025).

Gazzaniga, F. *et al.* (2009) "Microbial NAD Metabolism: Lessons from Comparative Genomics," *Microbiology and Molecular Biology Reviews*, 73(3), pp. 529–541. Available at: https://doi.org/10.1128/mmbr.00042-08.

Gibson, D.G. *et al.* (2009) "Enzymatic assembly of DNA molecules up to several hundred kilobases," *Nature Methods*, 6(5), pp. 343–345. Available at: https://doi.org/10.1038/nmeth.1318.

Glasser, N.R., Kern, S.E. and Newman, D.K. (2014) "Phenazine redox cycling enhances anaerobic survival in Pseudomonas aeruginosa by facilitating generation of ATP and a proton-motive force," *Molecular Microbiology*, 92(2), pp. 399–412. Available at: https://doi.org/10.1111/mmi.12566.

Gossmann, T.I. *et al.* (2012) "NAD+ biosynthesis and salvage – a phylogenetic perspective," *The FEBS Journal*, 279(18), pp. 3355–3363. Available at: https://doi.org/10.1111/j.1742-4658.2012.08559.x.

Guo, M.S. and Gross, C.A. (2014) "Stress-Induced Remodeling of the Bacterial Proteome," *Current Biology*, 24(10), pp. R424–R434. Available at: https://doi.org/10.1016/j.cub.2014.03.023.

Hackmann, T.J. (2024) "The vast landscape of carbohydrate fermentation in prokaryotes," *FEMS Microbiology Reviews*, 48(4), p. fuae016. Available at: https://doi.org/10.1093/femsre/fuae016.

Hackmann, T.J. and Zhang, B. (2023) "The phenotype and genotype of fermentative prokaryotes," *Science Advances*, 9(39), p. eadg8687. Available at: https://doi.org/10.1126/sciadv.adg8687.

Hammond, J.H. *et al.* (2015) "Links between Anr and Quorum Sensing in Pseudomonas aeruginosa Biofilms," *Journal of Bacteriology*, 197(17), pp. 2810–2820. Available at: https://doi.org/10.1128/jb.00182-15.

Himeoka, Y. *et al.* (2022) "Distinct Survival, Growth Lag, and rRNA Degradation Kinetics during Long-Term Starvation for Carbon or Phosphate," *mSphere*, 7(3), pp. e01006-21. Available at: https://doi.org/10.1128/msphere.01006-21.

Kluyver, A.J. (1924) "Unity and diversity in the metabolism of micro-organisms." Available at: https://lib.guides.umbc.edu/ld.php?content_id=46752710.

Kohlstedt, M. and Wittmann, C. (2019) "GC-MS-based 13C metabolic flux analysis resolves the parallel and cyclic glucose metabolism of *Pseudomonas putida* KT2440 and *Pseudomonas aeruginosa* PAO1," *Metabolic Engineering*, 54, pp. 35–53. Available at: https://doi.org/10.1016/j.ymben.2019.01.008.

Krüsemann, J.L. *et al.* (2018) "Artificial pathway emergence in central metabolism from three recursive phosphoketolase reactions," *The FEBS Journal*, 285(23), pp. 4367–4377. Available at: https://doi.org/10.1111/febs.14682.

Kukurugya, M.A., Rosset, S. and Titov, D.V. (2024) "The Warburg Effect is the result of faster ATP production by glycolysis than respiration," *Proceedings of the National Academy of Sciences*, 121(46), p. e2409509121. Available at: https://doi.org/10.1073/pnas.2409509121.

Lessie, T.G. and Phibbs, P.V. (1984) "ALTERNATIVE PATHWAYS OF CARBOHYDRATE UTILIZATION IN PSEUDOMONADS," *Annual Review of Microbiology*, 38(1), pp. 359–388. Available at: https://doi.org/10.1146/annurev.mi.38.100184.002043.

Liu, L. *et al.* (2012) "Phosphoketolase Pathway for Xylose Catabolism in Clostridium acetobutylicum Revealed by 13C Metabolic Flux Analysis," *Journal of Bacteriology*, 194(19), pp. 5413–5422. Available at: https://doi.org/10.1128/jb.00713-12.

Lu, K.-J. *et al.* (2023) "An ATP-sensitive phosphoketolase regulates carbon fixation in cyanobacteria," *Nature Metabolism*, 5(7), pp. 1111–1126. Available at: https://doi.org/10.1038/s42255-023-00831-w.

Luo, M., Ma, X. and Ye, J. (2024) "Reductive stress—a common metabolic feature of obesity and cancer," *Acta Pharmaceutica Sinica. B*, 14(12), pp. 5181–5185. Available at: https://doi.org/10.1016/j.apsb.2024.08.034.

Martocello, D.E., Morel, F.M.M. and McRose, D.L. (2019) "H-Aquil: a chemically defined cell culture medium for trace metal studies in Vibrios and other marine heterotrophic bacteria," *BioMetals*, 32(6), pp. 819–828. Available at: https://doi.org/10.1007/s10534-019-00215-2.

McGill, S.L. *et al.* (2021) "Pseudomonas aeruginosa reverse diauxie is a multidimensional, optimized, resource utilization strategy," *Scientific Reports*, 11(1), p. 1457. Available at: https://doi.org/10.1038/s41598-020-80522-8.

Meirelles, L.A. *et al.* (2021) "Bacterial defenses against a natural antibiotic promote collateral resilience to clinical antibiotics," *PLOS Biology*, 19(3), p. e3001093. Available at: https://doi.org/10.1371/journal.pbio.3001093.

Millard, P. *et al.* (2019) "IsoCor: isotope correction for high-resolution MS labeling experiments," *Bioinformatics*, 35(21), pp. 4484–4487. Available at: https://doi.org/10.1093/bioinformatics/btz209.

Petrareanu, G. *et al.* (2014) "Phosphoketolases from Lactococcus lactis, Leuconostoc mesenteroides and Pseudomonas aeruginosa: dissimilar sequences, similar substrates but distinct enzymatic characteristics," *Applied Microbiology and Biotechnology*, 98(18), pp. 7855–7867. Available at: https://doi.org/10.1007/s00253-014-5723-6.

Sánchez, B. *et al.* (2010) "Bacterial and Eukaryotic Phosphoketolases: Phylogeny, Distribution and Evolution," *Journal of Molecular Microbiology and Biotechnology*, 18(1), pp. 37–51. Available at: https://doi.org/10.1159/000274310.

Saunders, S. (2020) "Phenazine survival TnSeq." CaltechDATA. Available at: https://data.caltech.edu/records/bdfca-9rp28 (Accessed: November 11, 2025).

Seo, H. *et al.* (2016) "Structural basis for cytokinin production by LOG from Corynebacterium glutamicum," *Scientific Reports*, 6(1), p. 31390. Available at: https://doi.org/10.1038/srep31390.

Servinsky, M.D. *et al.* (2012) "Arabinose is metabolized via a phosphoketolase pathway in Clostridium acetobutylicum ATCC 824," *Journal of Industrial Microbiology and Biotechnology*, 39(12), pp. 1859–1867. Available at: https://doi.org/10.1007/s10295-012-1186-x.

Shanks, R.M.Q. *et al.* (2006) "Saccharomyces cerevisiae-Based Molecular Tool Kit for Manipulation of Genes from Gram-Negative Bacteria," *Applied and Environmental Microbiology*, 72(7), pp. 5027–5036. Available at: https://doi.org/10.1128/AEM.00682-06.

Silver, W.L., Lugo, A.E. and Keller, M. (1999) "Soil oxygen availability and biogeochemistry along rainfall and topographic gradients in upland wet tropical

forest soils," *Biogeochemistry*, 44(3), pp. 301–328. Available at: https://doi.org/10.1007/BF00996995.

Suzuki, R. *et al.* (2010) "Crystal Structures of Phosphoketolase: THIAMINE DIPHOSPHATE-DEPENDENT DEHYDRATION MECHANISM *," *Journal of Biological Chemistry*, 285(44), pp. 34279–34287. Available at: https://doi.org/10.1074/jbc.M110.156281.

Thauer, R.K., Jungermann, K. and Decker, K. (1977) "Energy conservation in chemotrophic anaerobic bacteria," *Bacteriological Reviews*, 41(1), pp. 100–180. Available at: https://doi.org/10.1128/br.41.1.100-180.1977.

Tribelli, P.M. *et al.* (2019) "Core regulon of the global anaerobic regulator Anr targets central metabolism functions in Pseudomonas species," *Scientific Reports*, 9(1), p. 9065. Available at: https://doi.org/10.1038/s41598-019-45541-0.

Vander Wauven, C. *et al.* (1984) "Pseudomonas aeruginosa mutants affected in anaerobic growth on arginine: evidence for a four-gene cluster encoding the arginine deiminase pathway," *Journal of Bacteriology*, 160(3), pp. 928–934. Available at: https://doi.org/10.1128/jb.160.3.928-934.1984.

Voroney, R.P. and Heck, R.J. (2015) "The Soil Habitat," in *Soil Microbiology, Ecology and Biochemistry*. Elsevier, pp. 15–39. Available at: https://doi.org/10.1016/B978-0-12-415955-6.00002-5.

de Vries, W. and Stouthamer, A.H. (1967) "Pathway of Glucose Fermentation in Relation to the Taxonomy of Bifidobacteria," *Journal of Bacteriology*, 93(2), pp. 574–576. Available at: https://doi.org/10.1128/jb.93.2.574-576.1967.

Warburg, O. (1925) "The Metabolism of Carcinoma Cells1," *The Journal of Cancer Research*, 9(1), pp. 148–163. Available at: https://doi.org/10.1158/jcr.1925.148.

Wu, Z. *et al.* (2024) "Electron transport chain inhibition increases cellular dependence on purine transport and salvage," *Cell Metabolism*, 36(7), pp. 1504-1520.e9. Available at: https://doi.org/10.1016/j.cmet.2024.05.014.

Xiao, W. and Loscalzo, J. (2020) "Metabolic Responses to Reductive Stress," *Antioxidants & Redox Signaling*, 32(18), pp. 1330–1347. Available at: https://doi.org/10.1089/ars.2019.7803.

Yang, R. *et al.* (2022) "Identification of purine biosynthesis as an NADH-sensing pathway to mediate energy stress," *Nature Communications*, 13(1), p. 7031. Available at: https://doi.org/10.1038/s41467-022-34850-0.

Yang, R., Guo, Z. and Li, B. (2025) "NADH reductive stress drives metabolic reprogramming," *Trends in Cell Biology*, 0(0). Available at: https://doi.org/10.1016/j.tcb.2025.07.005.

Ying, W. (2008) "NAD+/NADH and NADP+/NADPH in Cellular Functions and Cell Death: Regulation and Biological Consequences," *Antioxidants & Redox Signaling*, 10(2), pp. 179–206. Available at: https://doi.org/10.1089/ars.2007.1672.

Zumft, W.G. (1997) "Cell biology and molecular basis of denitrification," *Microbiology and Molecular Biology Reviews*, 61(4), pp. 533–616. Available at: https://doi.org/10.1128/mmbr.61.4.533-616.1997

Xfp amino acid sequence alignment between *P. aeruginosa* UCBPP-PA14 and *P. aeruginosa* ATCC 15442

```
                1                                                                   75
UCBPP-PA14 Xfp MSQILPSQDELLAHAAAEPAFAAWLQGHGPLQHSAETRAAVFRTAHQLVQAGLQPDLASVYQLFRALDRLTASAL
ATCC 15442 Xfp MSQILPSQDELLAHAAAEPAFAAWLQGHGPLQHSAETRAAVFRTAHQLVQAGLQPDLASVYQLFRALDRLTASAL

.....

               76                                                                  150
UCBPP-PA14 Xfp RIVVHMTYARRIRLDGQPLQAEDFKTQPEGHTGGALNMVPAYAGYLALNVLTGKTRAWLMGQGHCVVAIDALNVL
ATCC 15442 Xfp RIVVHMTYARRIRLDGQPLQAEDFKTQPEGHTGGALNMVPAYAGYLALNVLTGKTRAWLMGQGHCVAAIDALNVL

.....

               151                                                                 225
UCBPP-PA14 Xfp TGNLHPEQERAYADGEEGLNRLLQDFYGYAQAPNGAPAAPLGSHVNPHTAGGIAEGGYLGFAELQYAHMPLPGET
ATCC 15442 Xfp TGNLHPEQERAYADGEEGLNRLLQDFYGYAQAPNGAPAAPLGSHVNPHTAGGIAEGGYLGFAELQYAHMPLPGET

.....

               226                                                                 300
UCBPP-PA14 Xfp LVAFLSDGAAEEQRGSDWIPRWWRAEDCGAALPVMIANGRRIEQRTELGTHEGLEGFKLHLRRCGFDPISFDGRD
ATCC 15442 Xfp LVAFLSDGAAEEQRGSDWIPRWWRAEDCGAALPVMIANGRRIEQRTELGTHEGLEGFKLHLRRCGFDPISFDGRD

.....

               301                                                                 375
UCBPP-PA14 Xfp PAAFVCTLWEMEQRLERRVQEKNSGILRYPLPIPYGIAETVKGFGFYGAGSNAAHNLPLPGNPHNDEQARQLFNQ
ATCC 15442 Xfp PAAFVCTLWEMEQRLERRVQEKNSGILRYPLPIPYGIAETVKGFGFYGAGSNAAHNLPLPGNPHNDEQARQLFNQ

.....

               376                                                                 450
UCBPP-PA14 Xfp HANELWVEPEALELARRLFAEQRGERPLERDNPLALRHPIEPIIPPLRYRDDPCSPMAALDRFYTELVEANPDLR
ATCC 15442 Xfp HANELWVEPEALELARRLFAEQRGERPLERDNPLALRHPIEPIIPPLRYRDDACSPMAALDRFYTELVEANPDLR

.....

               451                                                                 525
UCBPP-PA14 Xfp ARVGNPDELASNRLGGVLKALKHRVSEPESELESVSGRVITALNEEAVVSACLANQGGLNLVASYEAFCVKMLGA
ATCC 15442 Xfp ARVGNPDELASNRLGGVLKALKHRVSEPESELESVSGRVITALNEEAVVSACLANQGGLNLVASYEAFCVKMLGA

.....

               526                                                                 600
UCBPP-PA14 Xfp VRQTLIFARQQKEVGRPAGWLGWPLVATSHTWENGKNQQSHQDTTFCEALLGEMSDMVRVLFPADHNSALALLPT
ATCC 15442 Xfp VRQTLIFARQQKEVGRPAGWLGWPLVATSHTWENGKNQQSHQDTTFCEALLGEMSDMVRVLFPADHNSALALLPT

.....

               601                                                                 675
UCBPP-PA14 Xfp IYRSRGQLACLVIPKRDRPMVFDAVQAERLARDGAILVEERCGSDPLLLIANGSYQLEQMRRAAQRLAEAGQAYR
ATCC 15442 Xfp IYRSRGQLACLVIPKRDRPMVFDAVQAERLARDGAILVEERCGSDPLLLIANGSYQLEQMRRAAQRLAEAGQAYR

.....

               676                                                                 750
UCBPP-PA14 Xfp LVYLQEPGRFRAPRDRWEVEAVADEALVERLFPDSHERRVLLTHMRAEVARGHLWPILPDARRTSVLGYRNRGGT
ATCC 15442 Xfp LVYLQEPGRFRAPRDRWEVEAVADEALVERLFPDSHERRVLLTHMRAEVARGHLWPILPDARRTSVLGYRNRGGT

.....

               751                                                 801
UCBPP-PA14 Xfp LDEAGMQFANRACWGNVLAACARLMEVPRTALLTPEEAAAVAGKGDPALLR
ATCC 15442 Xfp LDEAGMQFANRACWGNVLAACARLMEVPRTALLTPEEAAAVAGKGDPALLR

.....
```

Figure S1. Amino acid sequence of the phosphoketolase gene from *Pseudomonas aeruginosa* UCBPP-PA14 aligned against the amino acid sequence of the phosphoketolase gene from *Pseudomonas aeruginosa* ATCC 15442.

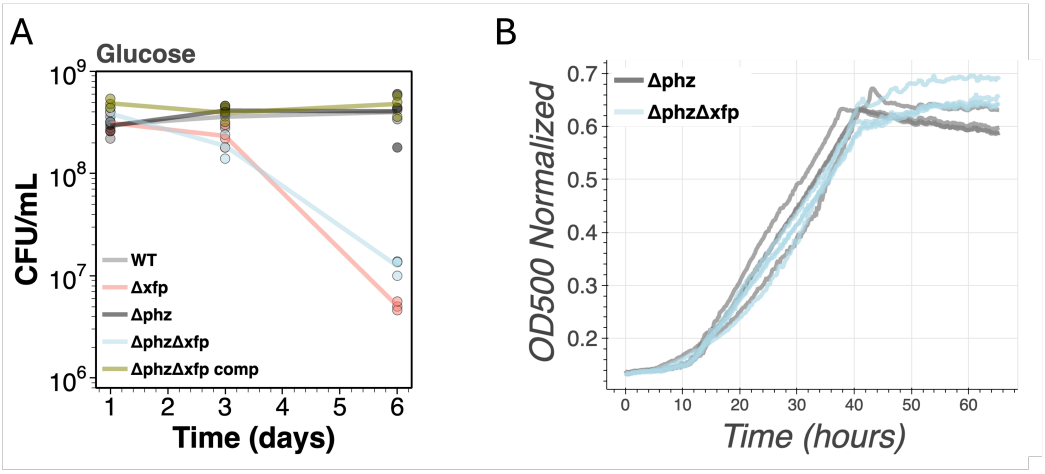

Figure S2. (A) CFU/mL of WT PA14 (grey), *Δxfp* (red), *Δphz* (black), *ΔphzΔxfp* (blue), *ΔphzΔxfp* + *xfp* (*ΔphzΔxfp* comp) (green) in the attB site during anaerobic survival with 20 mM glucose. Lines = means, dots = biological replicates, n = 3. (B) Anaerobic growth curves of *Δphz* and *ΔphzΔxfp* in the same MOPS MM + 20 mM glucose used for survival assays with the addition of 100 mM KNO3 to allow for growth. Grey = *Δphz*, blue = *ΔphzΔxfp*. Line = independent replicates. n = 3.

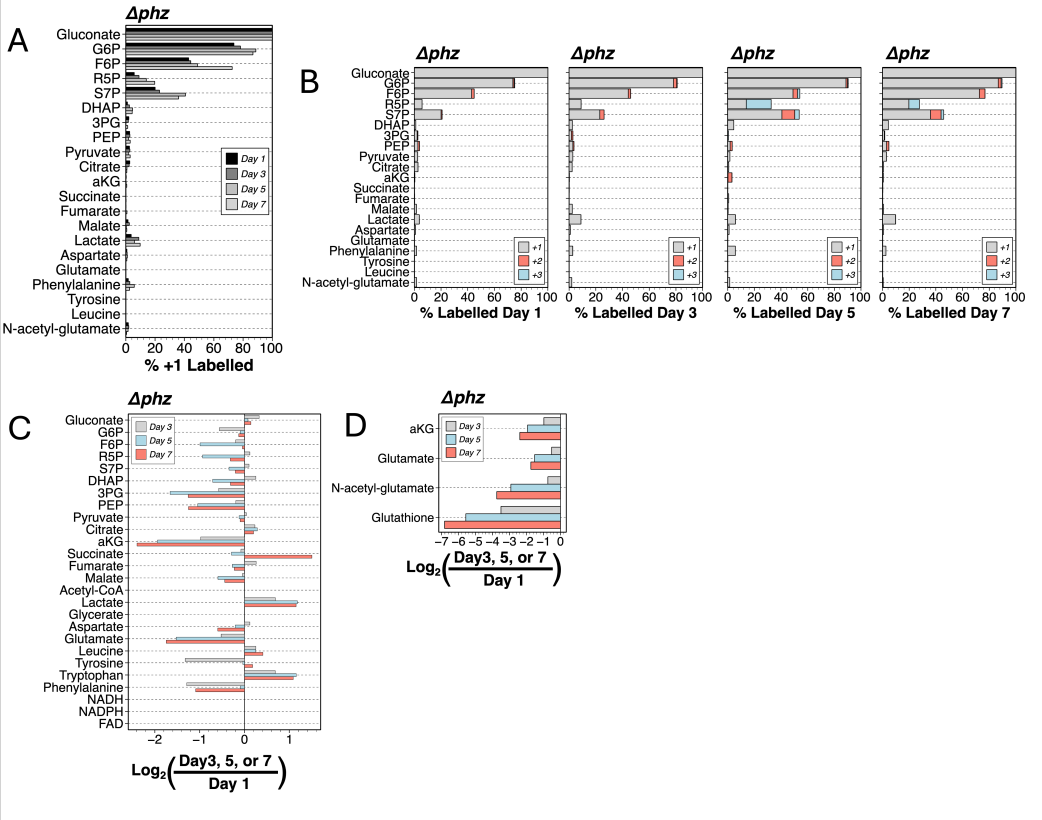

Figure S3. (A) Fraction of metabolites singly labelled with ^{13}C in *Δphz* cells on days 1, 3, 5, 7 of anaerobic survival on 20 mM 1-$^{13}C_1$-glucose. (B) Same samples as A, but showing doubly and triply labelled fractions in red and blue respectively. (C, D) Log_2 transformed metabolite intensities in *Δphz* cells during anaerobic survival on 1-$^{13}C_1$-glucose across days 3, 5, 7, normalized to metabolite levels on Day 1. (A, B, C, D) Bars represent means of 3 biological replicates. n = 3.

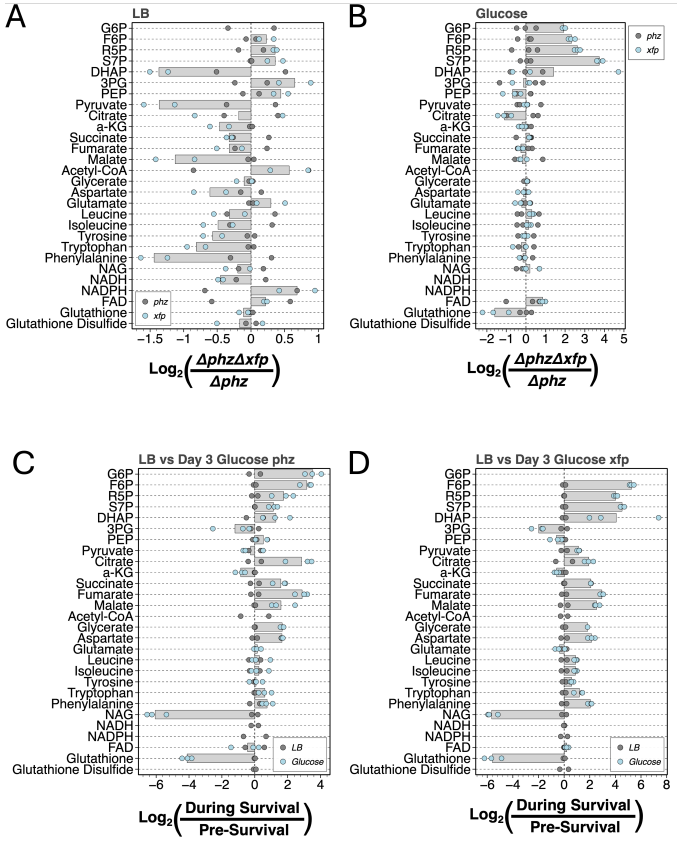

Figure S4. (A, B) Log_2 transformed metabolite levels from *Δphz* (grey) or *ΔphzΔxfp* (blue) normalized to the mean metabolite level of *Δphz* cells after LB pre-growth (A) before survival began, or after 3 days of survival on glucose (B). Bars = mean *ΔphzΔxfp* normalized metabolite levels. Grey dots = independent *Δphz* replicates, blue dots = independent *ΔphzΔxfp* replicates. n = 3. (C, D). Log_2 transformed metabolite levels during survival on glucose normalized to the mean metabolite levels after LB-pregrowth before survival began. Samples taken from *Δphz* cells (C) or *ΔphzΔxfp* cells (D). Bars = mean metabolite intensities during anaerobic survival on glucose, grey dots = independent replicates of samples before survival began, blue dots = independent replicates of samples after survival on glucose. n = 3.

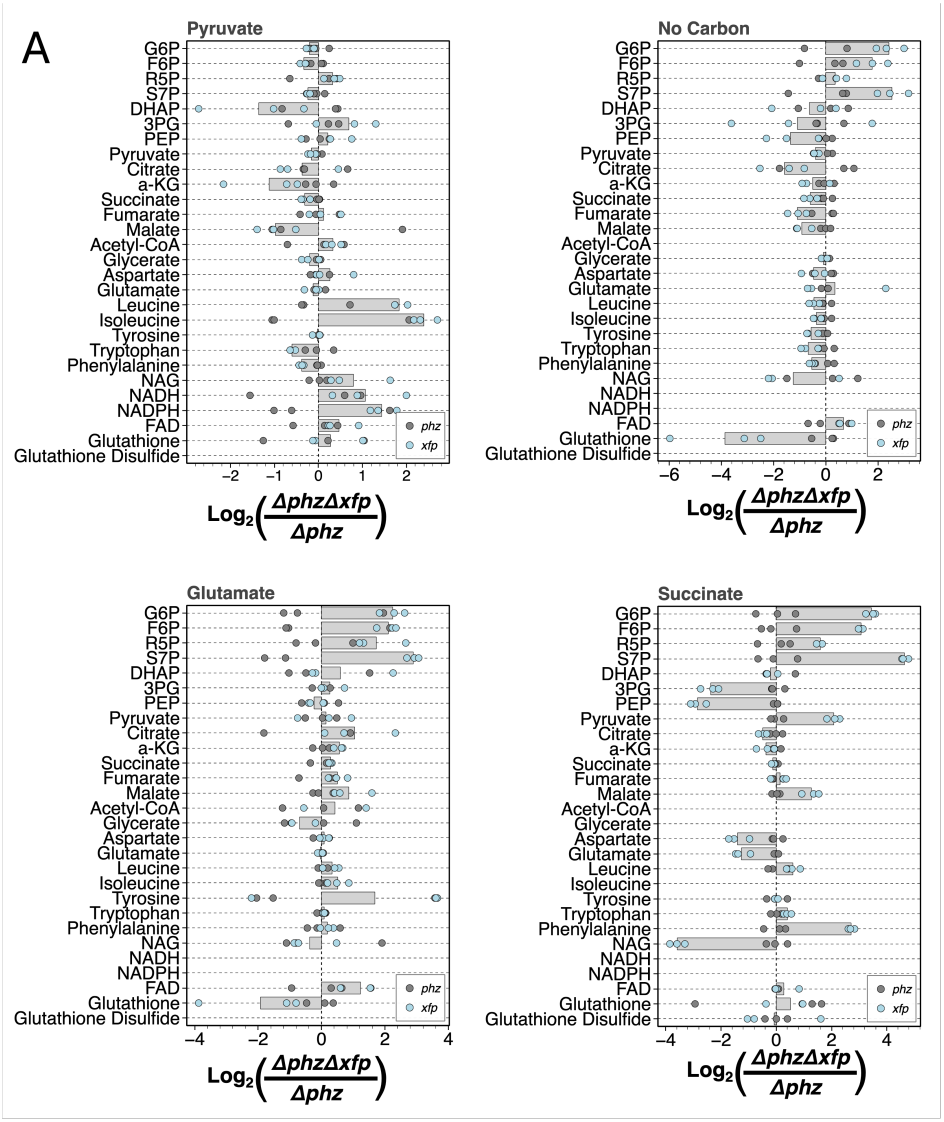

Figure S5. (A) Log_2 transformed metabolite levels from *Δphz* (grey) or *ΔphzΔxfp* (blue) normalized to the mean metabolite level of *Δphz* cells during survival on pyruvate, the absence of exogenous carbon (No Carbon), glutamate, or succinate. Bars = mean *ΔphzΔxfp* normalized metabolite levels. Grey dots = independent *Δphz* replicates, blue dots = independent *ΔphzΔxfp* replicates. n = 3.

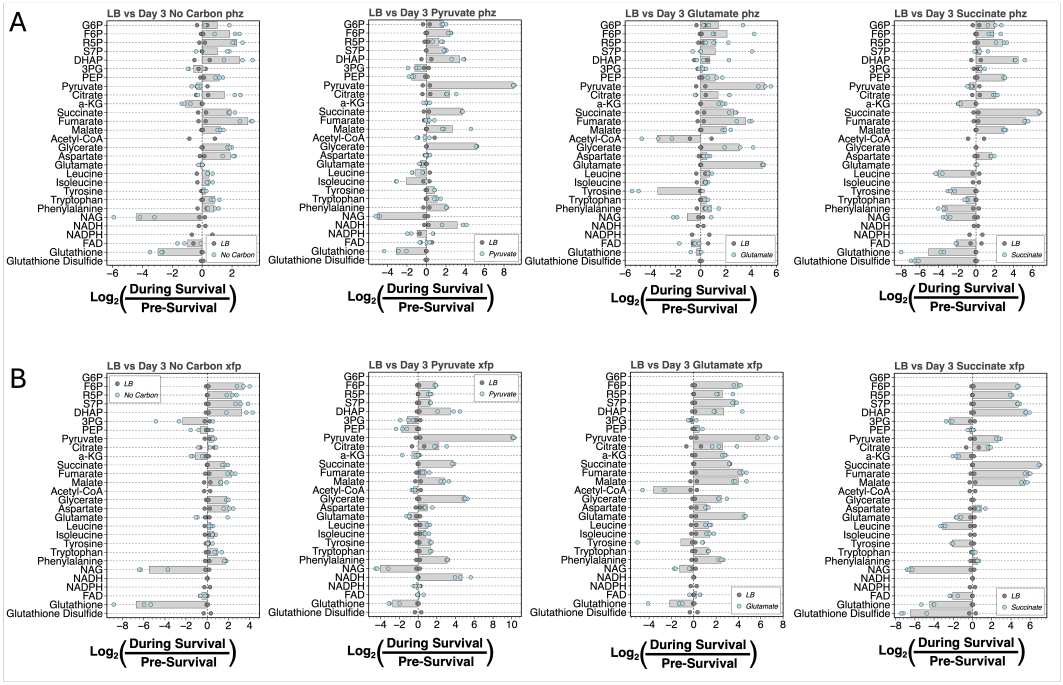

Figures S6. (A, B). Log_2 transformed metabolite levels during anaerobic survival in the absence of exogenous carbon (No Carbon), pyruvate, glutamate, or succinate, normalized to the mean metabolite levels after LB-pregrowth before survival began. Samples taken from *Δphz* cells (A) or *ΔphzΔxfp* cells (B). Bars = mean metabolite intensities during anaerobic survival, grey dots = independent replicates of samples before survival began, blue dots = independent replicates of samples after survival on glucose. n = 3.

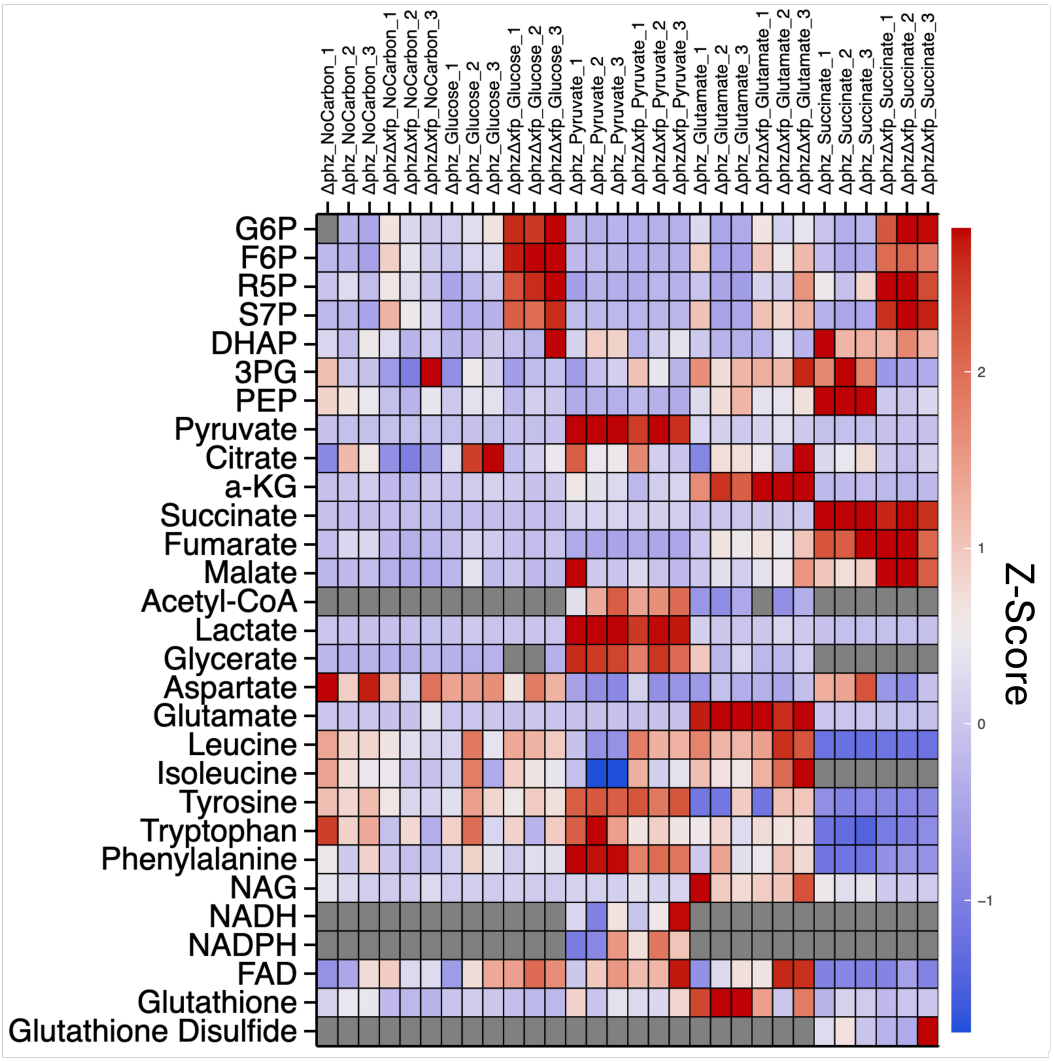

Figure S7. Heatmap showing metabolite levels in both strains across all carbon source conditions. Colors represent Z-score calculated based on the mean and standard deviation of each metabolite across all conditions.

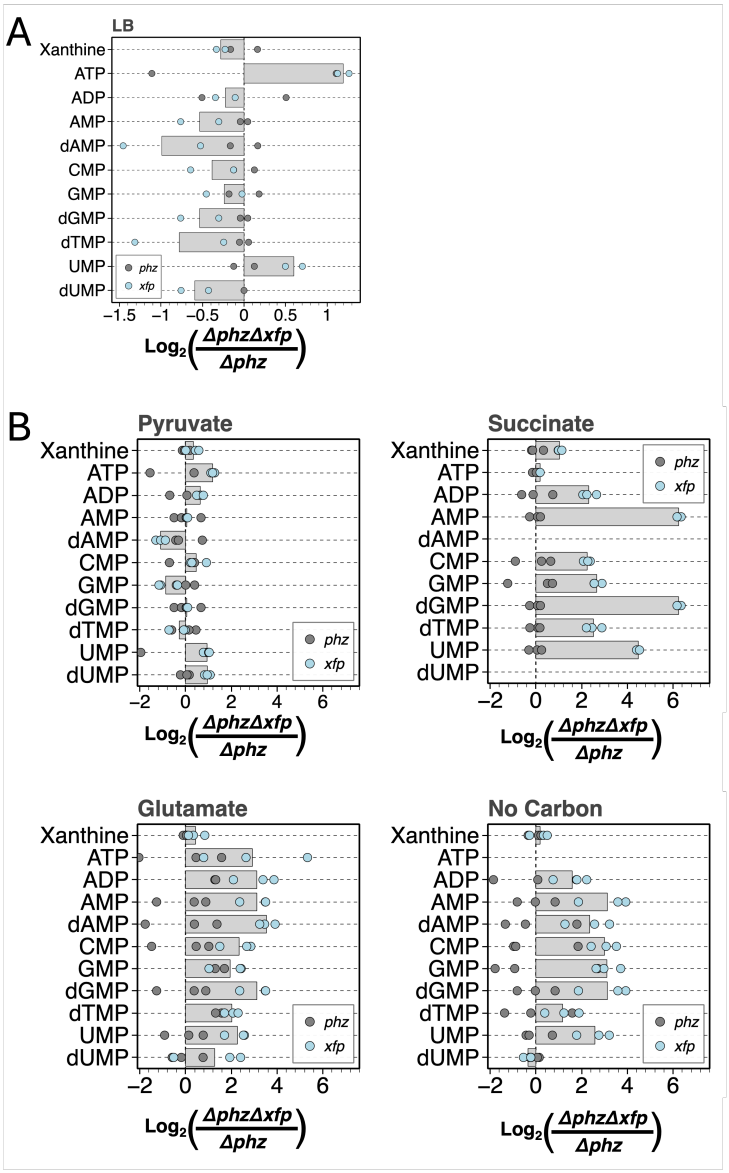

Figure S8. (A) Log_2 transformed metabolite levels of *Δphz* or *ΔphzΔxfp* cells during survival on glucose normalized to the mean metabolite levels in the *Δphz* strain, or during survival on pyruvate, succinate, glutamate, or no exogenous carbon (No Carbon) (B). Bars = mean metabolite intensities in the *ΔphzΔxfp* strain. Grey dots = independent replicates of *Δphz* cells, blue dots = independent replicates of *ΔphzΔxfp* cells. n = 3.

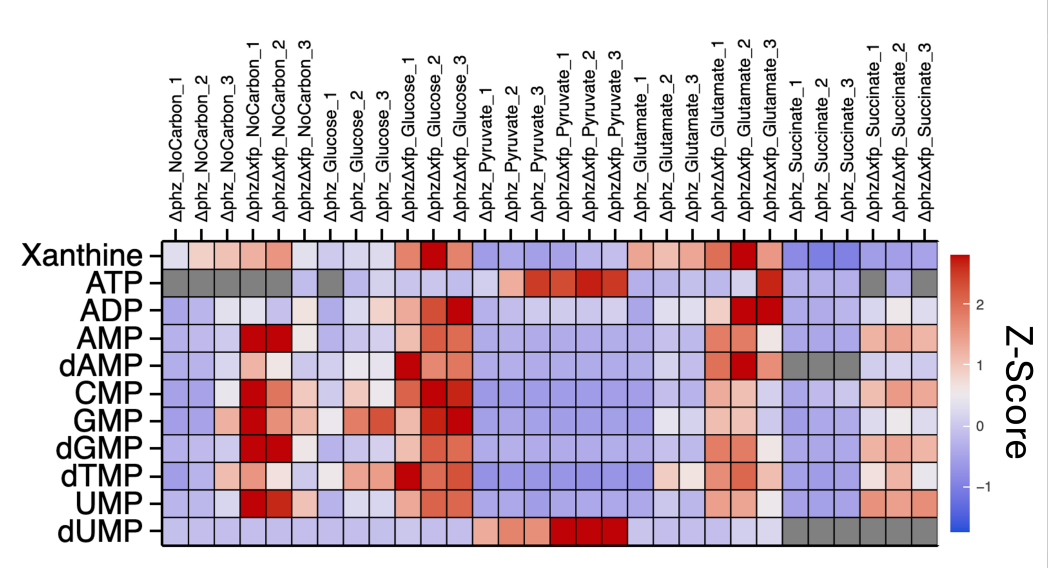

Figure S9. Heatmap showing metabolite levels in both strains across all carbon source conditions. Colors represent Z-score calculated based on the mean and standard deviation of each metabolite across conditions.

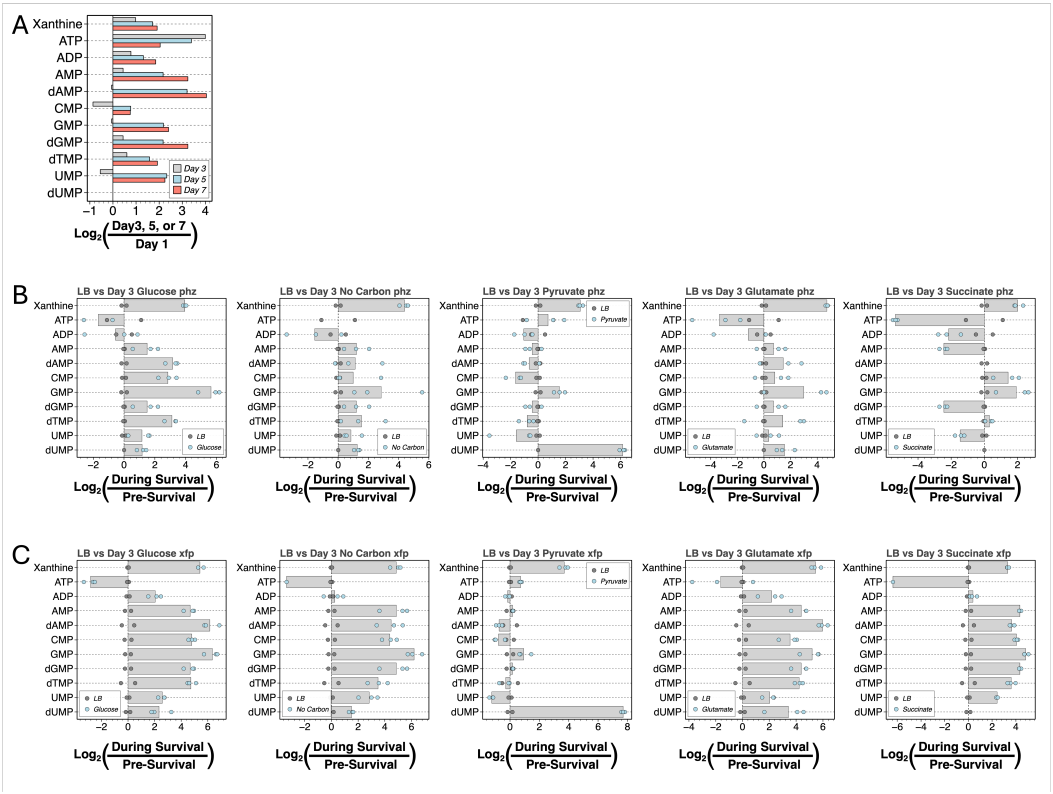

Figure S10. (A) Log_2 transformed metabolite levels in *Δphz* cells during survival on glucose on days 3, 5, and 7, normalized to the mean metabolite level in *Δphz* cells on day 1. Bars represent mean normalized metabolite intensity on day 3 (grey), day 5 (blue), or day 7 (red). n = 3. (B, C). Log_2 transformed metabolite levels during anaerobic survival on glucose, in the absence of exogenous carbon (No Carbon), pyruvate, glutamate, or succinate, normalized to the mean metabolite levels after LB-pregrowth before survival began. Samples taken from *Δphz* cells (A) or *ΔphzΔxfp* cells (B). Bars = mean metabolite intensities during anaerobic survival, grey dots = independent replicates of samples before survival began, blue dots = independent replicates of samples after survival on glucose. n = 3.

C h a p t e r 4

PHOSPHOKETOLASES SUPPORT RIBONUCLEOTIDE HOMEOSTASIS AND SURVIVAL UNDER ANAEROBIC GROWTH ARREST ACROSS DIVERSE BACTERIAL SPECIES

Abstract

Microbial metabolism primarily has been explored during exponential growth where nutrients and oxidants are replete. Yet bacteria are commonly challenged with oxidant-limitation, with many species such as *Pseudomonas aeruginosa* unable to grow in the absence of respiration. To survive anaerobically, cells must rewire their metabolism to support energy conservation and macromolecule turnover. We recently showed that *P. aeruginosa* uses a phosphoketolases protein to promote anaerobic survival, catalyzing a glucose catabolic pathway reminiscent of growth metabolisms in obligate anaerobes. However, our previous results also hinted at a role for this protein in supporting ribonucleotide homeostasis, an unrecognized role for phosphoketolases. In this study, we test and support this hypothesis. We find that anaerobic survival triggers ribonucleotide degradation, necessitating this phosphoketolase to consume released sugars to maintain metabolic balance in the pentose-phosphate pathway (PPP). Through co-feeding of ribose and glucose, we find alteration of this balance can alleviate the need for this phosphoketolase and that these two carbon sources serve different roles in supporting survival. This work points to the PPP and ribonucleotide salvage pathway as being important to sustaining anaerobic survival in *P. aeruginosa*. We demonstrate that phosphoketolases support anaerobic survival in other aerobic bacteria from diverse

Orders. Finally, we suggest that phosphoketolases serve a previously unappreciated role in mediating ribonucleotide homeostasis across diverse bacterial taxa.

Introduction

Regardless of species, all cells rely on the flow of electrons, from source to sink, to support metabolic flux for biosynthesis and energy conservation (1). An imbalance in this flux, such as oxidant-limitation or an inability to consume excess reducing equivalents (i.e. reductive stress) leads to metabolic dysregulation, growth arrest, and even cellular death (2, 3). Within human biology, reductive stress is highly detrimental and linked to various illnesses (3–6). However, many microbes routinely encounter and thrive under such conditions. While diverse fermentative pathways have long been known to support oxidant-limited growth, far less is known about the metabolism of historically classified "non-fermentative" bacteria (7–10). These organisms, such as the pathogen *Pseudomonas aeruginosa*, are reliant on terminal electron acceptors, such as molecular oxygen or nitrate, to fuel metabolic flux, energy conservation, and division (11, 12). Yet, across ecosystems from soil communities to human infections, such "non-fermentative" bacteria survive long periods of oxidant-limitation in growth-arrested states, herein termed "anaerobic survival" (13–17). The low metabolic rates underlying such survival are thought to provide heightened tolerance to stressors such as clinical antibiotics (18). Moreover, recent studies have found that several of these bacteria rely on fermentation pathways to support anaerobic survival (19, 20). Therefore, by investigating the metabolic strategies underlying anaerobic survival we may be able to discover unifying principles that bridge "non-fermentative" and "fermentative" organisms.

As a case in point, bacteria surviving anaerobically must maintain a basal level of metabolic flux (17). Energy must be generated to support repair of macromolecules or transcriptomic overhaul. Meanwhile the pathways to support ATP generation from substrate-level phosphorylation (SLP) and production of biosynthetic precursors must be redox balanced. Therefore, cells must walk a tightrope. Excess reducing equivalents, such as NADH, would inhibit many catabolic ATP generating pathways leading to carbon accumulation. One strategy to regain balance is the use of pathways to consume these reducing equivalents, as occurs during biosynthesis or the production of fermentation products (8, 19). However, these pathways typically exact an energetic price. An alternative strategy is to use metabolic pathways that avoid producing reducing equivalents all together. Previously, our group investigated such a strategy, using the opportunistic pathogen *Pseudomonas aeruginosa* (21). Despite being deemed a "non-fermentative" bacterium, *P. aeruginosa* can survive anaerobically for weeks by fermenting pyruvate or arginine (19, 22). In the case of the former pathway, pyruvate is metabolized to acetyl-CoA, then acetyl-phosphate (acetyl-P), and finally acetate via the *ackA*-pta system, generating ATP via SLP and NADH. Production of lactate with an additional pyruvate molecule regenerates NAD+. While *P. aeruginosa* also relies on *ackA* for anaerobic survival on carbon sources such as glucose, cells are unable to maintain a balanced redox state compared to survival on pyruvate without the help of phenazines, endogenous electron acceptors (23, 24).

During aerobic growth, *P. aeruginosa* catabolizes glucose through the Entner-Duodoroff pathway (EDP) and lower Embden-Meyerhoff-Parnas pathway (EMPP), lacking both a complete upper EMPP and the oxidative pentose-phosphate pathway

(PPP) (25, 26). In this regime, glucose catabolic flux occurs first via its oxidation to gluconate, followed by further oxidation or phosphorylation, eventually producing 6-phosphogluconate that feeds into the EDP and lower EMPP, eventually producing pyruvate (25). However, this glycolytic pathway generates excess reducing equivalents via reduced ubiquinone from initial oxidation to gluconate, and NADPH or NADH from the EDP and lower EMPP. Previously we showed that during anaerobic survival of the *P. aeruginosa* strain UCBPP-PA14 (PA14), this redox imbalance leads glucose catabolic flux to instead divert towards the non-oxidative PPP by way of glucose-6-phosphate (glucose-6P) and fructose-6-phosphate (fructose-6P) (21). Furthermore, PA14 relies on a phosphoketolase protein (*PA14_17580*), herein termed *xfp*, to consume PPP metabolites, supporting anaerobic glucose catabolism to acetate, metabolite balancing, and survival.

Phosphoketolases are thiamine-pyrophosphate-dependent enzymes that catalyze the phosphorolysis of fructose-6P, xylulose-5-phosphate (xylulose-5P), and/or sedoheptulose-7-phosphate (sedoheptulose-7P), releasing 2 carbon from each substrate as acetyl-P and generating erythrose-4-phosphate (erythrose-4P), glyceraldehyde-3-phosphate (glyceraldehyde-3P), or ribose-5P, respectively (27–29). Phosphoketolases are well studied for their role in supporting fermentative hexose metabolism such as the bifido-shunt in *Bifidobacterium* species or pentose fermentation in *Clostridium acetobutylicum* (30–33). In *C. acetobutylicum*, phosphoketolases provide efficient pentose catabolism to support ATP generation, avoiding rate-limiting steps such transaldolase or transketolase reactions in the PPP to ensure metabolite balance (30, 33, 34). That such a metabolism

is shared by obligate anaerobes for growth and PA14 for anaerobic survival points to shared strategies across bacteria for metabolic flux under oxidant-limitation.

While phosphoketolases are well known to regulate PPP metabolite balance, their role in mediating ribonucleotide pools has been less explored (35). As seen in mitochondria during reductive stress, anaerobic survival of PA14 triggers ribonucleotide degradation (21). Furthermore, loss of *xfp* leading to a widespread accumulation of ribonucleotides and PPP metabolites during anaerobic survival (21). Immediately upstream of the *xfp* gene in the PA14 genome are two hypothetical proteins – *PA14_17550* and *PA14_17570* – with homology to Lonely Guy (LOG) family proteins and Metallo-Beta-Lactamase (MBL) fold-containing proteins with potential RNA and ribonucleotide degradative functions respectively (36–38). Use of these enzymes for ribonucleotide degradation would lead to input into the PPP. Therefore, we predicted that PA14 relies on Xfp to maintain metabolic balance during survival-triggered ribonucleotide turnover via Xfp's consumption of xylulose-5P, in equilibrium with the ribonucleotide precursor and degradation product ribose-5P (21, 39). Of note, ribonucleotides are vital for the synthesis of RNA, DNA, NAD+, peptidoglycan, signaling molecules, and help define the cellular energy charge. Therefore, maintaining ribonucleotide homeostasis underpins the capacity to survive across diverse cells (6, 40–42). In this study, we sought to both gain further clarity on Xfp's role in mediating ribonucleotide balance in PA14 and test if these functions are generalizable to other phosphoketolase-bearing bacteria unable to grow fermentatively.

Results

Degradation and salvage of ribonucleotide derivatives during anaerobic survival necessitates Xfp to support metabolic homeostasis and viability

To confirm the role of Xfp in supporting anaerobic survival on glucose and its effect on ribonucleotide levels, we utilized a clean deletion of the *xfp* gene *PA14_17580* within a phenazine-null mutant background strain (*Δphz*). Using this strain allowed us to avoid variability due to rescue of reductive stress by phenazines and better elucidate Xfp-dependent survival mechanisms. We pre-grew the *Δphz* and *ΔphzΔxfp* strain aerobically in LB and then washed them using a MOPS-buffered minimal media with glucose as the sole carbon source. Cell suspensions were incubated anoxically in Balch tubes sparged with N_2 gas at 30 C. Sampling every few days and plating for colony-forming units (CFUs) aerobically to measure viability, we reproduced our previous phenotype showing that loss of *xfp* leads to a drop in viability by 2 orders of magnitude after 3 days of anaerobic survival (FIG 1A). Additionally, by extracting intracellular metabolites from both strains after 3 days of survival, we saw a 4-32x increase in PPP metabolite and ribonucleotide levels in the *ΔphzΔxfp* strain compared to *Δphz* cells (FIG 1B). Given our previous findings that accumulated PPP metabolites in *ΔphzΔxfp* cells are not from catabolism of isotopically labeled glucose (21), we predicted that accumulated ribonucleotides are from degradation of macromolecules such as RNA rather than *de novo* biosynthesis.

To test this hypothesis, we cultured *Δphz* and *ΔphzΔxfp* cells aerobically in a MOPS-buffered minimal medium with glucose as the carbon source and ^{15}N-labelled

NH_4Cl as the sole nitrogen-source. Cells were then washed and transferred to anaerobic incubation conditions, with glucose as the carbon source and unlabeled NH_4Cl as the nitrogen source. Intracellular metabolites were sampled before the switch from $^{15}NH_4Cl$ to unlabeled NH_4Cl, 30 minutes after (Day 0), and on days 1, 3, and 7 of anaerobic survival. If accumulated ribonucleotides were produced via *de novo* biosynthesis, we expected their labelling to match that of aspartate and glutamate pools used to source the nitrogen for the purine precursor IMP and pyrimidine precursor UMP. In contrast, during degradation of ribonucleotide derivatives, such as RNA, we expect ribonucleotides would be cleaved to release ribose-5P or ribose-1P and their nitrogenous bases. In the case of purines, adenine and guanine bases would be converted to hypoxanthine and xanthine. For pyrimidines, cytosine would be converted to uracil, while uracil and thymine would be reductively degraded. Therefore, if ribonucleotide degradation were occurring, we would expect all ribonucleotides and xanthine to be ^{15}N labelled. However, cells also contain the ribonucleotide salvage pathway that uses released nitrogenous bases and ribose-5P to resynthesize ribonucleotides, avoiding much of the energetic cost of *de novo* biosynthesis. During ribonucleotide salvage, ribose-5P and nitrogenous bases (xanthine, hypoxanthine, or uracil) are consumed to produce the purine precursor IMP or the pyrimidine precursor UMP via several enzymatic steps. Accordingly, if ribonucleotides are produced from degradation of ribonucleotide derivatives or synthesis via the salvage pathway, the entire metabolite pool should be fully labelled. An increase in ^{15}N-labelled IMP abundance should suggest use of the salvage pathway for resynthesis of ribonucleotides.

Within the first 30 minutes of anaerobic survival following the switch from $^{15}NH_4Cl$ to unlabeled NH_4Cl, we observed almost all xanthine being fully unlabeled in both strains as well as at least 20% of ribonucleotides other than UMP being unlabeled (FIG 1C/D, FIG S1A/B, FIG S2A/B). Similarly, all measured amino acid pools had a significant unlabeled fraction. This suggested rapid incorporation of NH_4Cl and a continuation of rapid metabolism upon transitioning cells to survival conditions. We were unable to detect IMP and GMP within this first time point. However, by Day 1 of anaerobic survival this trend shifted dramatically. Between day 0 to day 1, we observed a 4-16x increase in xanthine and ribonucleotide abundance in both strains (FIG 1E/F). Meanwhile, close to the entirety of ribonucleotide and xanthine pools were ^{15}N-labelled, while amino acid pools remained relatively stable (FIG 1C/D, FIGS1/S2). This trend continued throughout days 3 and 7 of survival. This suggests that most ribonucleotides being released during survival are from degradation of derivative compounds such as RNA. However, the increase in IMP abundance throughout survival in both strains also suggests a level of ribonucleotide biosynthesis via the salvage pathway (FIG S1E/F). We also observed slight differences between strains, with *ΔphzΔxfp* cells showing a less 14N incorporation in the first 30 minutes and steady increase in 14N accumulation in amino acid pools, potentially suggesting increased biosynthesis or use of these metabolites (FIG 1C/D, FIG S1/S2).

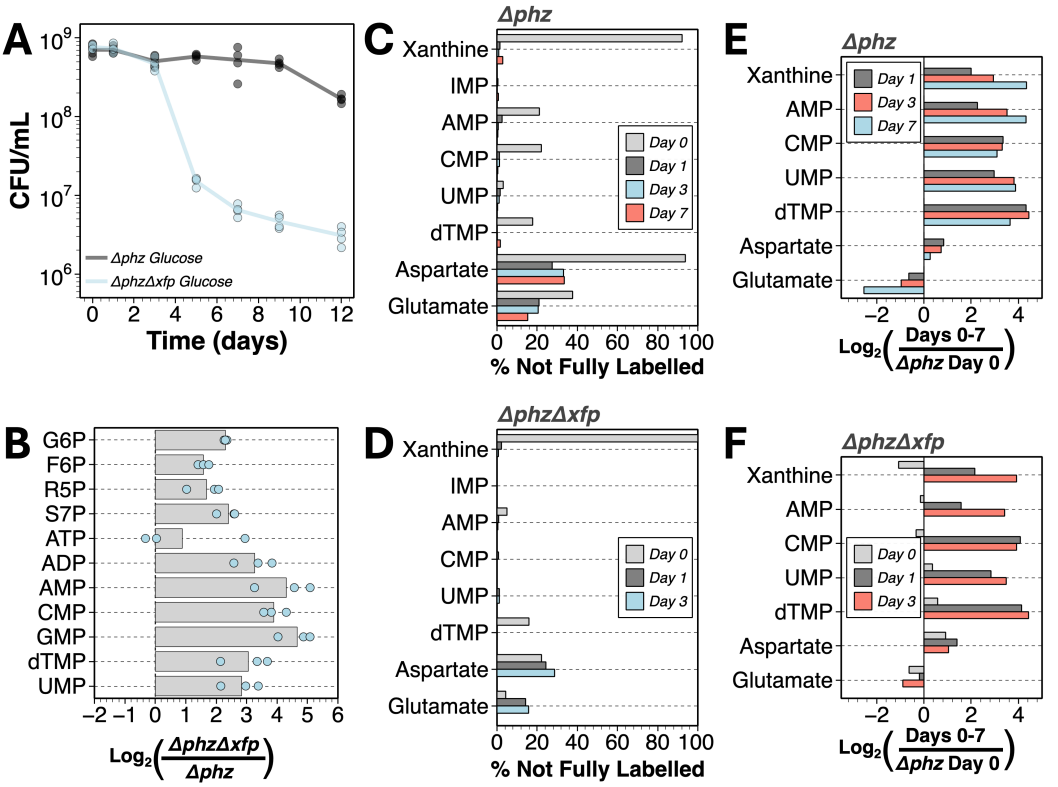

Figure 1: During anaerobic survival, PA14 exhibits metabolic signs of ribonucleotide degradation and salvage, with Xfp playing a role to maintain metabolic homeostasis under these conditions. (A) Log-transformed CFU/mL values showing loss of *xfp* leads to a anaerobic survival deficit. Lines = means, dots = replicates, n = 4. (B) Log2-fold change of relative metabolite abundance in *ΔphzΔxfp* cells compared to *Δphz* cells after 3 days of anaerobic survival. Bars = means, dots = replicates, n = 3. (C, D) Percent of metabolites lacking ^{15}N-labelling in at least 1 nitrogen atom, bars = means of 3 biological replicates. Colors denote day of anaerobic survival. C = *Δphz*, D = *ΔphzΔxfp*. (E, F) Log2-fold change of relative metabolite abundances in *Δphz* (E) or *ΔphzΔxfp* cells (F) after 0, 1, 3, or 7 days of anaerobic survival normalized to the Day 0 abundance in *Δphz* cells. G6P = glucose-6-phosphate. F6P = fructose-6-phosphate. R5P = ribose-5-

phosphate, which is in equilibrium with xylulose-5-phosphate. S7P = sedoheptulose-7-phosphate.

Ribose addition complements anaerobic survival and metabolic dysregulation in the PA14 *xfp* mutant

Building on our results indicating that Xfp supports anaerobic survival by coordinating metabolic input to the PPP from ribonucleotide degradation and glucose catabolism, we were curious how altering relevant metabolite pools would affect survival. Towards this end, we used ribose. Ribose is first phosphorylated to the PPP metabolite, and ribonucleotide precursor/degradation product, ribose-5P. Because Xfp affects glucose catabolic flux through the PPP, PPP metabolite abundance, and ribonucleotide abundance, we predicted addition of ribose, and therefore increase in ribose-5P, would alter the need for Xfp to balance these metabolic pools. For example, previous studies have shown that co-feeding bacteria hexose and pentose sugars segregates their catabolic pathways (30). Alternatively, in some bacteria, the abundance of ribose-5P can dramatically alter the directionality of flux within, into, and out of the PPP (43, 44). In our condition, such an effect might alleviate pressure on the PPP by inhibiting flux into the PPP from glucose catabolism or macromolecule degradation.

To test the effect of ribose on anaerobic Xfp necessity, we repeated our survival experiments, providing *Δphz* and *ΔphzΔxfp* cells with 20 mM of glucose isotopically labelled in the first position (1-^{13}C-glucose), 24 mM ribose, or 20 mM 1-^{13}C-glucose + 24 mM ribose. Compared to cells given only glucose, survival on ribose alone was indistinguishable between *Δphz* and *ΔphzΔxfp,* with the survival of *ΔphzΔxfp* increasing while *Δphz* decreased (FIG 2A). Meanwhile, during survival on 20 mM 1-^{13}C-glucose +

24 mM ribose, both strains survived better than on glucose alone, with the *ΔphzΔxfp* mutant being similar to the survival of the parent strain until a slight drop in viability around day 12 (FIG 2C). This effect was dose dependent as 2.4 mM ribose in addition to 20 mM glucose only minorly complemented the survival of the *ΔphzΔxfp* strain, whereas 0.24 mM ribose had no effect (FIG S3A).

To better understand the effect of ribose supplementation, we measured metabolic abundance and ^{13}C isotopic incorporation from catabolized 1-^{13}C-glucose. Similar to our viability results, after 3 days of anaerobic survival on ribose or glucose + ribose, both strains were far more similar in their metabolite abundance profiles than during survival on glucose alone (FIG 2B, FIG S3C). However, ribonucleotides accumulated more in the *ΔphzΔxfp* strain during anaerobic survival on ribose alone compared to the *Δphz* strain (FIG 2B). Additionally, we observed about 1/4th the amount of lower EMPP metabolites such as phosphoenolpyruvate in *ΔphzΔxfp* cells during survival on ribose alone compared to the *Δphz* strain. When comparing the metabolite abundances of both strains during survival on both 1-^{13}C-glucose + ribose, we see almost no difference (FIG 2D). However, when tracking ^{13}C incorporation, we see distinct patterns between strains.

During anaerobic survival on 1-^{13}C-glucose alone, the *ΔphzΔxfp* strain had higher PPP metabolite abundance but lower ^{13}C labelling in these metabolites than the *Δphz* strain, suggesting influx into the PPP of endogenous unlabeled carbon stores such as ribonucleotides (FIG 2E). During survival on both 1-^{13}C-glucose and ribose, ^{13}C labelling of glucose-6P and fructose-6P for both strains was comparable to that seen for

Δphz cells surviving on 1-^{13}C-glucose alone (FIG 2E). Suggesting lower flux of unlabeled carbon stores into the upper EMPP. However, ^{13}C-labelling of sedoheptulose-7P fell from ~60% in *Δphz* cells surviving on glucose alone to ~30% in *Δphz* cells surviving on glucose + ribose despite similar metabolite abundances across conditions (FIG 2E). Meanwhile, *ΔphzΔxfp* cells showed increased ^{13}C-labelling of sedoheptulose-7P from ~20% during survival on glucose to ~50% during survival on glucose + ribose, yet lower abundance of this metabolite when co-fed glucose + ribose (FIG 2E).This may suggest contribution of both glucose and ribose to sedoheptulose-7P in the *Δphz* strain but higher glucose contribution in the *ΔphzΔxfp* strain. However, it is unclear why this is the case. In both strains we see higher isotopic labelling of DHAP, pyruvate, and lactate during survival on glucose + ribose compared to glucose alone, suggesting higher flux of glucose into the lower EMPP, EDP, and/or cycling through gluconeogenesis (FIG 2E, FIG S5).

To better understand the effect of ribose on cellular metabolism independent of Xfp, we compared metabolite levels on each carbon mixture within each strain. In contrast to survival on glucose alone, when given ribose, both strains individually showed higher xanthine levels, lower TCA cycle metabolite levels, and lower PPP metabolite levels, apart from ribose-5P (FIG S3C). While ribonucleotide levels were similar in *ΔphzΔxfp* cells between survival on glucose vs ribose alone, in the *Δphz* strain we observed upwards of 16x the amount of ribonucleotides during survival on ribose alone (FIG S3C). Therefore, survival of the *ΔphzΔxfp* strain on either glucose or ribose leads to ribonucleotide accumulation, while such accumulation is only seen in *Δphz* cells

during survival on ribose alone. Moreover, survival on ribose alone for either strain appears to decouple ribose-5P levels from those of the PPP or downstream metabolic pathways. Therefore, we suggest that ribose alleviates the need for Xfp to buffer the PPP metabolite pool, but triggers ribonucleotide accumulation irrespective of Xfp activity.

To better understand why co-feeding of glucose + ribose leads to such higher anaerobic survival, we compared metabolite levels during co-feeding with survival on either glucose or ribose for each strain independently. During survival on glucose + ribose, both strains showed higher levels of ribose-5P and xanthine, as well as lower levels of lower EMPP and TCA cycle metabolites compared to survival on glucose (FIG S4B/E). Additionally, compared to survival on ribose alone, both strains showed lower levels of ribonucleotides and higher PPP metabolite levels (FIG S4C/F). Meanwhile, *Δphzℤ Δxfp* cells showed a dramatic lowering of ribonucleotide levels during survival on glucose + ribose vs glucose alone, matching ribonucleotide levels of *Δphzℤ* cells. These results suggest that when co-fed glucose and ribose, cells can maintain ribonucleotide turnover without accumulation of PPP metabolites and ribonucleotides. Lower abundance of EMPP and TCA cycle metabolite levels despite higher ^{13}C-labelling of the former may suggest increased flux through the EDP.

To determine whether co-feeding of 1-^{13}C-glucose and ribose was increasing acetate production in both strains – suggesting higher ATP production and catabolic flux – we extracted supernatants during anaerobic survival and measured both relative acetate abundance and approximate percent of acetate singly labelled with ^{13}C. Catabolism of 1-^{13}C-glucose via the EDP and lower EMPP to generate acetate would

lead to loss of the ^{13}C-label during decarboxylation of pyruvate. However, if glucose is instead catabolized through the PPP and Xfp, acetate should be singly labelled (21). After 3 days of anaerobic survival on 1-^{13}C-glucose, *Δphz* cells show ~10-20% acetate labelling, while *ΔphzΔxfp* cells produce under half the acetate with minimal ^{13}C-labelling (FIG 2F/G). Meanwhile, during survival on both glucose + ribose, we see that both *Δphz* and *ΔphzΔxfp* cells produce similar levels of acetate exceeding that of *Δphz* cells surviving on glucose alone (FIG 2F). We observed lower ^{13}C-labelling of acetate in *Δphz* cells on glucose + ribose than glucose alone, with still no discernable ^{13}C-labelling in *ΔphzΔxfp* cells (FIG 2G). This supports previous hypotheses that Xfp is acting primarily on xylulose-5P (21, 39) and that this is predominantly produced from its equilibration with ribose-5P, not 1-^{13}C-glucose during co-feeding, which may hint at the use of ribonucleotides as an energy source. Additionally, it suggests that co-feeding of glucose + ribose allows for maintenance of metabolic flux through the PPP in an Xfp-independent manner.

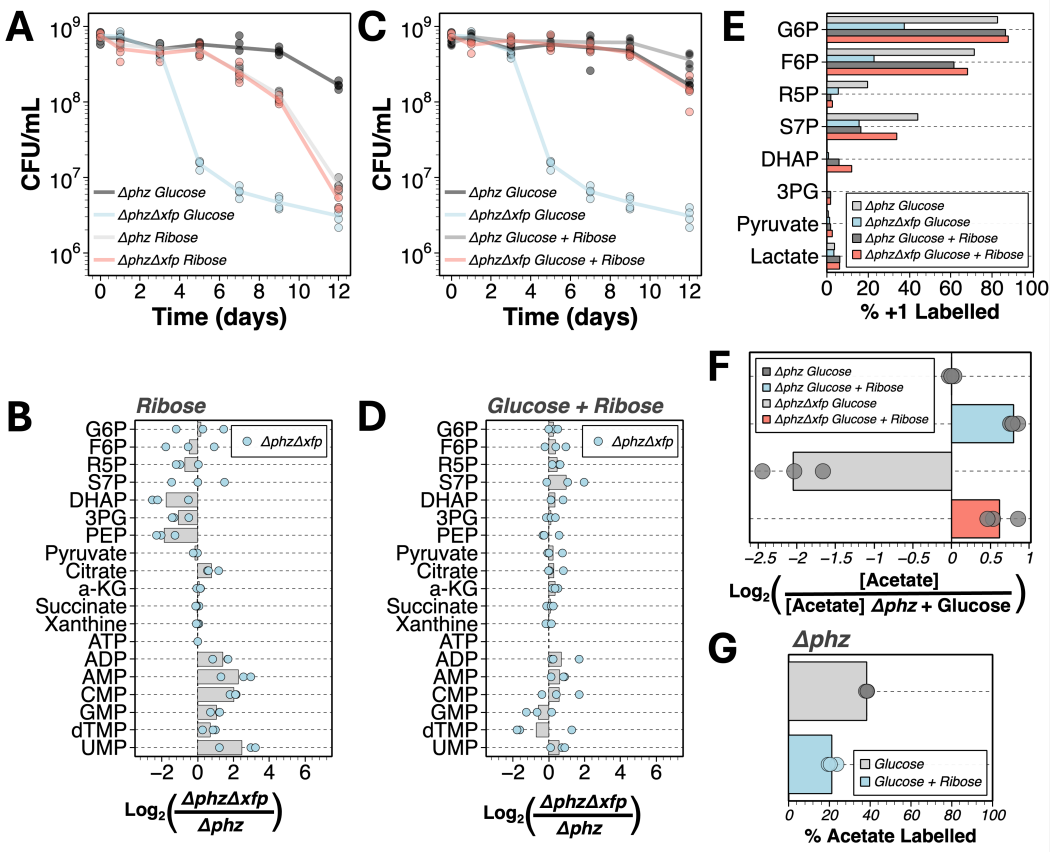

Figure 2: Addition of ribose to anaerobic survival conditions chemically complements *xfp* mutants and alters catabolic flux of 1-^{13}C-glucose. (A, C) Log-transformed CFU/mL values showing loss of *xfp* leads to an anaerobic survival deficit on glucose, but not on ribose (A) or glucose + ribose (C). *Δphz* cells survive worse on ribose (A) than on glucose or glucose + ribose (C). Lines = means, dots = biological replicates, n = 4. (B, D) Log2-fold change of relative metabolite abundance in *ΔphzΔxfp* cells normalized to *Δphz* cells after 3 days of anaerobic survival on ribose alone (B) or glucose + ribose (D), bars = means, dots = biological replicates, n = 3. (E) Percent of metabolites singly labelled with ^{13}C after 3 days of anaerobic survival on 1-^{13}C-glucose (grey/blue) or 1-^{13}C-glucose + ribose (black/red) in either *Δphz* cells (grey/black) or *ΔphzΔxfp* cells (blue/red). Bars =

means of 3 biological replicates. (F) Log2-fold change of acetate relative abundance in *Δphz* or *ΔphzΔxfp* cells after 3 days of anaerobic survival on glucose, or glucose + ribose normalized to acetate abundance in *Δphz* cells during survival on glucose. Bars = means, dots = biological replicates, n = 3. (G) Estimation of percent of acetate labelled with ^{13}C. Bars = means, dots = replicates, n = 3. G6P = glucose-6-phosphate. F6P = fructose-6-phosphate. R5P = ribose-5-phosphate, which is in equilibrium with xylulose-5-phosphate. S7P = sedoheptulose-7-phosphate. DHAP = dihydroxyacetone phosphate, which is in equilibrium with glyceraldehyde-3-phosphate. 3PG = 3-phosphoglycerate. PEP = phosphoenolpyruvate. a-KG = alpha-ketoglutarate.

Phosphoketolases support anaerobic survival in *Paraburkholderia graminis* and *Dyella japonica* as well as glucose catabolism in *P. graminis*

Our results show that in PA14, Xfp is essential for both survival and ribonucleotide homeostasis during oxidant-limited non-growth and that ribose can chemically complement these effects, potentially acting to segregate sugar catabolism as well as balance PPP and ribonucleotide flux. Phosphoketolases are found across bacteria, but their study has mostly focused on their role in growth metabolisms of anaerobes (28). Therefore, we wondered whether other bacterial species might utilize phosphoketolases for ribonucleotide homeostasis and maintenance of viability under anoxic non-growth conditions. We first generated a comprehensive collection of ~40,000 *xfp* homologs by exhaustively searching across ~200,000 non-redundant representative bacterial genomes. These homologs were spread across diverse taxa, such as *Actinomycetota*, containing the obligately anaerobic genus *Bifidobacterium*, and *Gammaproteobacteria*, containing *P. aeruginosa* (FIGURE 3A). From this list, we selected

Dyella japonica and *Paraburkholderia graminis*, two genetically-tractable species representing different Orders to test the generalizability of our results in *P. aeruginosa*.

Both *D. japonica* and *P. graminis* are Gram-negative plant-growth-promoting soil bacteria unable to grow in the absence of terminal electron acceptors. They both contain phosphoketolases, with *P. graminis* containing two distinct homologs. Both bacteria have distinct similarities and differences in central carbon metabolic structure compared to *P. aeruginosa*. Unlike *P. aeruginosa*, *D. japonica* contains both the EDP and a complete glycolytic EMPP pathway. Like *P. aeruginosa*, P. *graminis* lacks 6-phosphofructokinase and therefore, cannot use the EMPP for glucose catabolism and must rely on the EDP. Unlike *P.* aeruginosa, both strains contain the oxidative PPP, which converts 6-phosphogluconate to ribulose-5-phosphate while producing NAD(P)H. Finally, both strains include *ackA* homologs and would be able to produce acetate from Xfp-derived acetyl-P.

To investigate whether phosphoketolases play a role in anaerobic survival in these bacteria, we generated clean deletion mutants of the phosphoketolases in each species. When provided with glucose under anoxic conditions, *D. japonica* cells were generally unable to survive long-term oxidant-limitation like *P. aeruginosa*, with wild-type cells losing 3 orders of magnitude of viability over the course of 3 days (FIG 3B). However, loss of the phosphoketolase in *D. japonica* did exacerbate the survival defect, with these mutants showing 3 orders of magnitude lower viability than the wild-type strain by day 2 (FIG 3B). Wild-type *P. graminis* was able to survive anaerobically on glucose for 5 days with less than a 10-fold loss of viability. Interestingly, loss of one phosphoketolase homology (*xfp1*) led to a 3 order of magnitude loss in viability by day

5 of anaerobic survival, while deletion of the other homolog (*xfp2)* had no effect (FIG 3C). The double mutant *Δxfp1Δxfp2* showed similar loss of viability as the *Δxfp1* strain (FIG 3C). Both *xfp* homologs in *P. graminis* showed 65% sequence identity to one another. In both *D. japonica* and *P. graminis*, co-feeding with glucose and ribose did not chemically complement the lack of their phosphoketolases, and in fact seemed to lower the viability of the wild-type strains. Notably, unlike PA14, both *D. japonica* and *P. graminis* do not contain putative ribonucleotide processing genes flanking their *xfp* homologs, instead having *ackA* homologs like *Bifidobacterium animalis* or other obligate anaerobes that use phosphoketolases to support fermentative growth.

We next sought to determine if *P. graminis*, like *P. aeruginosa,* could use its phosphoketolase to catalyze glucose catabolism via the PPP to produce acetate by tracking the incorporation of 1-^{13}C-glucose. In *P. graminis*, catabolism of glucose to acetate could occur via several routes. In the first, glucose is catabolized through the EDP to produce pyruvate that is then decarboxylated to acetyl-CoA and converted into acetate. Through this pathway, the ^{13}C label would be lost as CO2 during this decarboxylation step (FIG 3D). Similarly, glucose can be catabolized via the EDP to 6-phosphogluconate then decarboxylated to ribulose-5-phosphate by the oxidative PPP, also losing the ^{13}C label as CO2 (FIG 3D). Therefore, any acetate generated by glucose catabolism via the EDP or via the oxidative PPP would be unlabeled. However, if *P. graminis* uses a similar pathway as discovered previously in *P. aeruginosa,* we would expect to see ^{13}C-labelled acetate (FIG 3D). This pathway requires glucose to be catabolized through the upper EMPP to fructose-6P and its interconversion to xylulose-5P or sedheptulose-7P in the PPP. Cleavage of any of these three putative phosphoketolase

substrates would release ^{13}C-labelled acetyl-P, thereby, generating ^{13}C-labelled acetate (FIG 3D). By day 2 of anaerobic survival we observed an estimated 40% of acetate is ^{13}C-labelled (FIG 3E). Meanwhile, both the *Δxfp1* and *Δxfp1Δxfp2* strains showed almost an order of magnitude lower acetate and minimal to no ^{13}C-labelling while the *Δxfp2* strain showed similar acetate production and ^{13}C labeling as the wild-type, matching our survival results (FIG 3E/F). Due to the presence of a catabolic EMPP in *D. japonica* we were unable to carry out a similar experiment in this organism. Together, our data show that, phosphoketolases promote anaerobic survival in *P. graminis* and *D. japonica* as well as support a glucose catabolic pathway in *P. graminis* reminiscent of fermentative growth metabolisms in obligate anaerobes. However, our inability to complement these mutants with ribose indicates that these phosphoketolases interface with the metabolic network of these organisms in different ways than in *P. aeruginosa*.

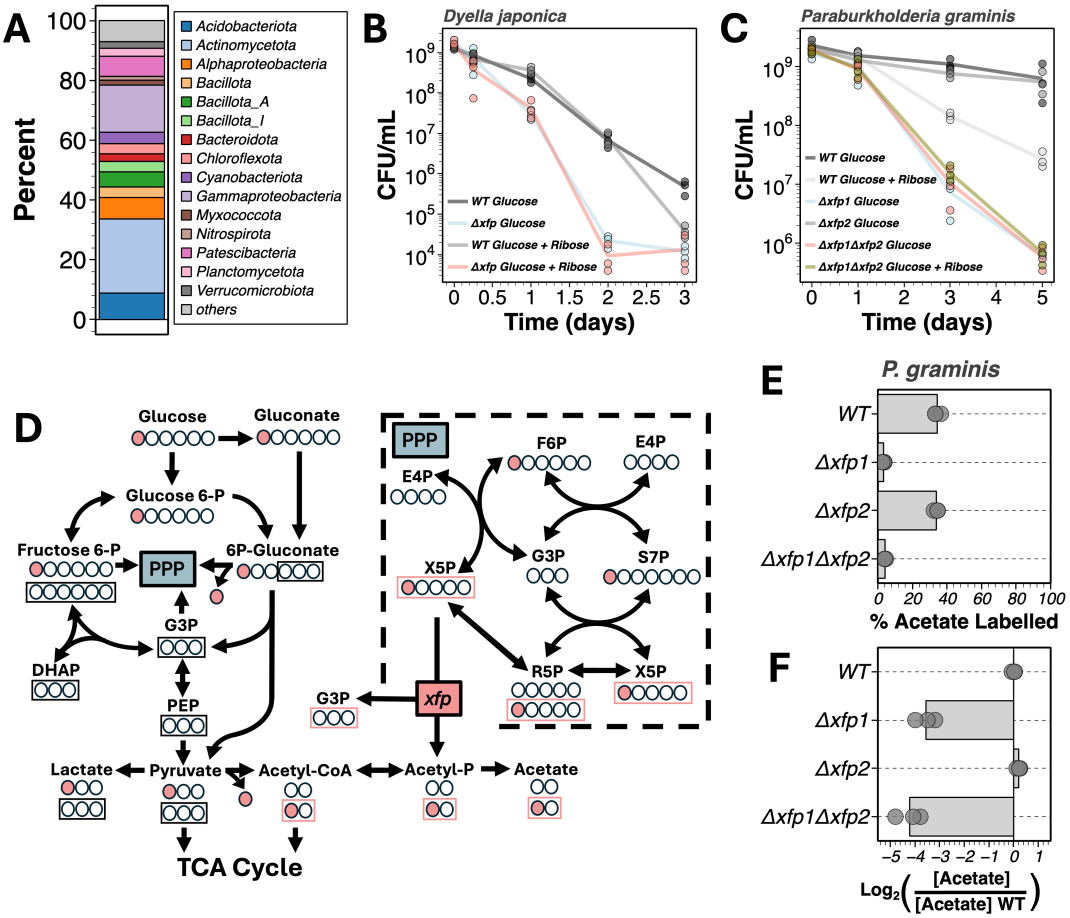

Figure 3: Phosphoketolases are spread across bacterial taxa and play a role in survival of *Dyella japonica* and *Paraburkholderia graminis* as well as glucose catabolism in *P. graminis*. (A) Percent of identified phosphoketolase homologs across different bacterial taxa. (B, C) Log-transformed CFU/mL from anaerobic survival of *D. japonica* (B) or *P. graminis* (C) during survival on glucose or glucose + ribose. Lines = means, dots = biological replicates, n = 3. (D) Central carbon metabolic diagram tracing catabolism of 1-^{13}C-glucose through the metabolism of *P. graminis*. Generation of acetate from 1-^{13}C-glucose via the EDP or through the oxidative PPP would lead to unlabeled acetate, generation of acetate from 1-^{13}C-glucose via the non-oxidative PPP via fructose-6P and Xfp would generate singly ^{13}C-labelled acetate. (E) Percent of acetate isotopically labelled after 2

days of anaerobic survival of 1-^{13}C-glucose in *P. graminis* strains. Bars = means, dots = replicates, n = 3. (F) Log2-fold change of acetate abundance after 2 days of anaerobic survival of *P. graminis* on 1-^{13}C-glucose normalized to acetate abundance in WT cells. Bars = means, dots = biological replicates. n = 3.

Use of phosphoketolases for ribonucleotide processing may be isolated to specific phosphoketolase homologs or the presence of flanking genes

To further distinguish between the phosphoketolase homologs in PA14, *P. graminis*, and other bacteria such as *B. animalis*, we returned to our library of ~40,000 Xfp homologs and constructed a phylogenetic tree based on amino acid sequence identity (Fig 4A). We found that classically studied phosphoketolase containing organisms like the bifidobacterium *B. animalis* and *P. graminis* reside within a large clade containing most of all phosphoketolases, shown in grey in Fig 4A. Notably, PA14's Xfp resides in a much smaller diverged clade primarily with homologs from Gammaproteobacteria and Alphaproteobacteria, shown in red (Fig 4A, Fig S6A). As shown previously, the phosphoketolase of *P. aeruginosa* contains an extra N-terminal sequence of unknown function compared to bifidobacterium phosphoketolases, likely explaining the divergence and motivating future biochemical studies (39).

Since co-localized genes often have functional relatedness because of genomic evolution, we examined a window of 5 genes upstream and downstream of phosphoketolase homolog within annotated genomes to hint at their potential physiological roles. As expected, within the larger Bifidobacterium-containing clade, one of those most frequent flanking genes was acetate/propionate kinases, homologs to PA14's *ackA* and a key gene in phosphoketolase-fermentation pathways. Meanwhile,

within the PA14-clade the majority of most frequent flanking genes, ignoring hypothetical proteins, were annotated as having ribonucleotide processing functions (FIG S6B). For instance, MBL fold metallo-hydrolases, such as PA14's *PA14_17570*, are known to cleave RNA into ribonucleotide monomers. Thymidine phosphorylase is used in ribonucleotide salvage, releasing thymine and 2-deoxy D-ribose-5-phosphate. Ribose-phosphate pyrophosphokinases produce PRPP from ribose-5-phosphate for use in synthesis of ribonucleotides or NAD+. LOG family proteins containing nucleotide 5-monophosphate nucleosidase activity, such as PA14's *PA14_17550*, are capable of cleaving ribonucleotides to release ribose-5-phosphate (FIG S6C) (36, 38, 45). Thus, while Xfp homologs from both clades may support anaerobic survival, PA14-clade homologs may be more closely associated with ribonucleotide homeostasis. Overall, these conserved patterns of genomic context across diverse species, including many environmentally important taxa well-known as obligate aerobes, such as nitrite oxidizing bacteria *Nitrobacter hamburgensis*, suggest a widespread role for Xfp (Fig 4B). Further comparing the clade assignment of Xfp sequences with a taxonomic tree based on 16S rRNA sequences (Fig 4C) indicates a clear pattern of horizontal gene transfer, raising an interesting hypothesis that gaining Xfp confers a fitness advantage under certain environmental conditions.

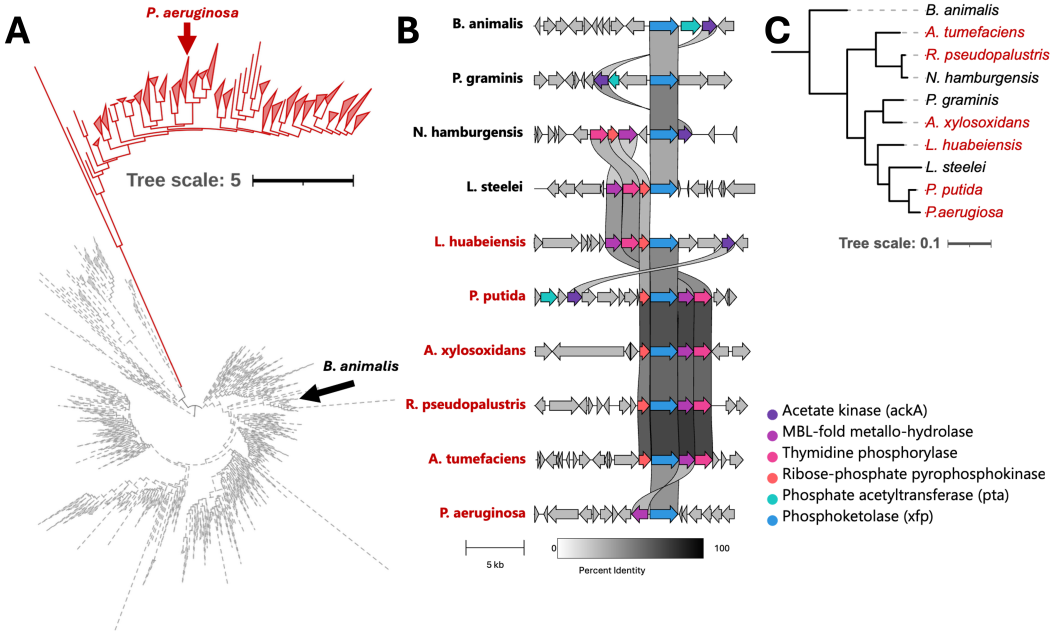

Figure 4: Phosphoketolase homologs diverge in their amino acid sequence identity, with *P. aeruginosa*'s Xfp sequence being more similar to homologs within a separate clade. Several ribonucleotide processing genes co-localize with phosphoketolase homologs across diverse bacteria, likely being shaped by horizontal gene transfer. (A) Phylogenetic tree based on amino acid sequence similarity between phosphoketolase homologs, where the position of *P. aeruginosa* and *Bifidobacterium animalis* are denoted. (B) Gene neighborhood diagrams showing the genes flanking the phosphoketolase gene of various species with environmental importance, such as nitrite oxidizing bacteria *N. hamburgensis*. (C) Phylogenetic tress based on 16S rRNA nucleotide sequence similarity of these species. (A, B, C) Red denotes phosphoketolases and their species where the amino acid sequence is more similar to *P. aeruginosa*'s while black denotes those not closely similar.

Discussion

Across various environments, microbes are commonly challenged by oxidant-limitation and growth arrest, requiring metabolic strategies to balance energy generation and biosynthesis to ensure survival. However, these strategies are poorly understood even in model organisms. Here we show that *P. aeruginosa* relies on a phosphoketolase to support metabolic homeostasis during ribonucleotide degradation and salvage under anaerobic survival. Additionally, we find that ribose complements loss of this phosphoketolase in a dose-dependent manner. We find that phosphoketolases are also essential for anaerobic survival in *P. graminis* and *D. japonica,* two bacteria also unable to grow fermentatively. This shared phenotype indicates that phosphoketolases play a potentially widespread role in tuning metabolic pools during non-growth survival under oxidant-limitation. Meanwhile, use of phosphoketolases for ribonucleotide homeostasis appears to be more specific, potentially restricted to phosphoketolases with high homology to PA14's own Xfp or with flanking ribonucleotide processing enzymes. That such a seemingly simple class of enzyme would play such a diversity of physiological roles across bacterial taxa exemplifies the flexibility of bacterial metabolism to use a unifying toolkit to solve a variety of challenges.

This work joins other studies that suggest that the classification of bacteria as "fermentative" or "non-fermentative" fails to capture the nuance of many of these organisms' anaerobic metabolic strategies (20, 46). Specific to our study, we discovered that *P. aeruginosa, P. graminis*, and likely *D. japonica* utilize a phosphoketolase-mediated sugar catabolism pathway that is shared by many fermentative obligate anaerobes such as Bifidobacterium or Clostridia species (28, 30–33). Notably, all three of the species

tested in this study contain different carbon catabolism pathways such as the presence or absence of a functional EMPP or oxidative PPP, yet all three relied on shared phosphoketolase proteins for anaerobic survival. Moreover, we identified a wide diversity of phosphoketolase-containing "non-fermentative" bacteria that must survive periods of oxidant-limitation within their ecological niches in soil communities or human infections. Therefore, it is interesting to speculate that across "non-fermentative" bacteria the unifying redox principles of metabolism dictate the need for such a metabolic shunt during anaerobic survival regardless of the species' catabolic strategies during aerobic growth. Future work should continue to test the generalizability of our discoveries to other species and alternative carbon sources.

At least within *P. aeruginosa,* anaerobic survival on pyruvate does not require the use of this phosphoketolase, while survival in the absence of an exogenous carbon source, or in the presence of carbon sources such as glycerol, succinate, fructose, or butyrate does (21). Therefore, PPP metabolite accumulation, catabolic inhibition due to reductive stress, and the need for phosphoketolases may only occur during catabolism of endogenous carbon stores or catabolism of carbon sources that strain the maintenance of redox balance while generating sufficient ATP. Future studies should expand beyond heterotrophic bacteria, with previous studies showing the use of phosphoketolases in the survival of cyanobacteria during light-dark transitions (47, 48). Due to the shared metabolites between the PPP and the Calvin cycle in phototrophic organisms, namely ribulose-5-phosphate which is in equilibrium with the Xfp substrate xylulose-5P, there are likely shared metabolic strategies between heterotrophs and

autotrophs to maintain balance of these metabolite pools in Xfp-dependent and independent regimes.

The presence of an N-terminal sequence in PA14's *xfp* gene not found in that of *B. animalis* or *Lactobacillus* species is a shared feature with that of Cyanobacterial phosphoketolases (39, 48). Previous studies found that the phosphoketolase of the Cyanobacterium *Synechococcus elongatus* binds ATP at its N-terminal, leading to its inhibition (48). While the residues responsible for this ATP-regulatory function are not found within PA14's Xfp, it is interesting to speculate that the N-terminal sequence of phosphoketolases within the PA14 clade similarly play a unique regulatory role, conferring a function for mediating ribonucleotide homeostasis. Additionally, within our dataset of Xfp homologs, there are at least 5658 non-redundant bacterial species with multiple Xfp homologs, such as seen with *P. graminis*. Within these species there are several which have homologs like those of PA14, Bifidobacterium species, and/or *Synechococcus elongatus*. The presence of duplicate Xfp homologs from multiple structural clades may support the use of each for separate physiological functions. In tandem with the occurrence of ribonucleotide processing genes flanking Xfp homologs across bacterial taxa, future studies should examine the biochemical functions of unique phosphoketolases as well as their ecological roles to better understand potential selective pressures behind the transfer of these genes between species. For example, within bacteria which had at least one Xfp homolog from the large structural clade and one from the PA14 clade, we saw an enrichment in Nitrospirota. This bacterial group is known for their "obligate aerobic" lifestyle and nitrite-oxidizing capabilities (49). Yet under hypoxia they show upregulation of putative fermentation genes (50). It would be

interesting to examine possible roles for these phosphoketolases in nitrogen-balance and comparison of these roles with the bacteria within this study.

The co-occurrence of thymidine phosphorylase genes with phosphoketolase proteins across our dataset, particularly those with similar homology to PA14's Xfp, is particularly notable. There is a large body of literature showing the increased expression and importance of these enzymes in supporting cancer cell survival and metabolism under hypoxia (45). Thymidine phosphorylases function to cleave pyrimidine deoxy nucleosides such as thymidine, a precursor of DNA biosynthesis. Therefore, they serve crucial functions in pyrimidine salvage and DNA repair. Within tumors, cancer cells must frequently survive periods of hypoxia or anoxia due to limited vascularization compared to healthy somatic cells. It is believed that under these conditions, thymidine phosphorylase acts to cleaves thymidine and other pyrimidines, releasing the ribose sugar for use as a nutrient source via its catabolism to glyceraldehyde-3P. While eukaryotic cells lack phosphoketolases, this hints at a conserved metabolic strategy across domains of life to survive oxidant-limitation and the importance of nucleotide homeostasis to do so, especially given similar results showing dramatic accumulation of ribonucleotides under hypoxia in cancer cells (40, 45, 51–53). While it is unclear whether bacteria such as *P. aeruginosa* are using such strategies for energy conservation or biosynthesis, it is possible that in our system cells are feeding on their own ribonucleotide pools such as rRNA or RNA/DNA released by cell lysis of neighboring bacteria. It is well documented that under growth arrest due to nutrient limitation, bacteria degrade their ribosomes to minimize maintenance costs (41, 42). Additionally, due to the limitations of using CFUs and 10-fold dilutions to measure viability, death of even 50% of the

population of *Δphz* cells surviving anaerobically appears similar to cells surviving at 100%. Therefore, future work should more carefully examine the source and use of such ribonucleotide pools during anaerobic survival.

Our measurements of ^{15}N incorporation into purine degradation product xanthine and the purine biosynthetic precursor IMP suggests that both ribonucleotide degradation and resynthesis via the salvage pathway are occurring. Determining the relative rates of each process could help confirm our hypothesis that Xfp in PA14 in essential for mediating metabolite homeostasis under ribonucleotide turnover. In fluctuating environments, cells must change their transcriptome requiring RNA degradation and re-synthesis, producing or consuming ribose-5P respectively (54). Because of the low metabolic rates intrinsic to anaerobic survival, the pace of ribonucleotide degradation likely outpaces that of ribonucleotide biosynthesis, leading to ribose-5P accumulation and further metabolic disruption, necessitating Xfp. However, why ribose complements *xfp* deletion is puzzling under this framework. Previous studies in *E. coli* have shown that increased ribose-5P levels lead to anabolic flux out of the PPP instead of catabolic, potentially minimizing accumulation of metabolites, aiding *ΔphzΔxfp* cells but at the cost of ATP-consumption from biosynthesis, harming *Δphz* cells during survival on ribose alone compared to glucose (44). During co-feeding of glucose + ribose, glucose catabolism could minimize the effects of this energetic cost.

Our observations that co-feeding cells 1-^{13}C-glucose + ribose increased ^{13}C-labelling of lower EMPP metabolites, increased acetate production in *ΔphzΔxfp* cells to that of *Δphz* cells, and lower upper TCA cycle metabolite levels, hints at a role for ribose

alleviates reductive stress in the presence of glucose. How this occurs, however, is unclear. During survival on glucose + ribose, there was no increase in ribonucleotide levels in either strain, but we did see heightened xanthine – a purine degradation product. It is interesting to speculate that ribonucleotide salvage may act to consume reducing equivalents, via generation of XMP from xanthine and ribose-5P, which can then form IMP to consume a reducing equivalent. Furthermore, biosynthesis of deoxy ribonucleotides, macromolecules such as RNA, and fresh NAD+ would also consume reducing equivalents or rebalance the redox state. However, such reactions would come at the cost of ATP. Within *Δphz* cells, Xfp-mediated cleavage of xylulose-5P would generate acetyl-P and glyceraldehyde-3P, both precursors for ATP generation via SLP. Meanwhile, in *ΔphzΔxfp* cells, the presence of ribose-5P would equilibrate with xylulose-5P, providing substrates for transketolase reactions in the PPP to generate glyceraldehyde-3P for ATP generation or gluconeogenic flux. The higher ^{13}C-labelling of sedoheptulose-7P in *ΔphzΔxfp* cells during survival on glucose + ribose potentially supporting such PPP metabolite cycling. Within both strains de-inhibition of glucose catabolism via the EDP and lower EMPP would also increase ATP generation via SLP. This might explain the heightened ^{13}C-labelling of pyruvate, lactate, acetate, and DHAP, in equilibrium with glyceraldehyde-3P, during survival on glucose + ribose.

In conclusion, our observations suggest there is still plenty of room for discovery of novel metabolic strategies to support anaerobic survival even in well studies organisms like *P. aeruginosa*. The similarities between our observation in *P. aeruginosa* and *D. japonica* or *P. graminis* as well as those seen during hypoxia in cancer cells suggests such

discoveries can have far reaching consequences and reiterates the conserved unifying principle of redox chemistry underlying metabolism.

Methods

Strains, culture conditions, and reagents

All strains can be found within Supplemental Table 1. All *P. aeruginosa* strains were derived from UCBPP-PA14 (DKN63, laboratory strain). The *Δphz* strain lacks the *phzA1-G1*, *phzA2-G2* operons, as well as *phzH, phzS,* and *phzM* genes (55). Cells were streaked from 20% glycerol -80 C freezer stocks onto Difco LB 1.5% agar plates (BD Biosciences) and grown overnight at 37 C. *D. japonica* and *P. graminis* were cultured on LB 1.5% agar with no NaCl. The *ΔphzΔxfp* (this study) strain lacked all genes of the *Δphz* strain including *PA14_17580*. *D. japonica* strains were derived from UNC79MFTsu3.2 (56). *P. graminis* strains were derived from an isolate taken from a wheat field (57).

Mutant generation

All primers and plasmids used can be found in Supplemental Table 1. All primers were sourced from Integrated DNA technologies. We used allelic exchange for mutant generation, first synthesizing plasmids with Gibson Assembly (NEB) (58). We digested the plasmid pMQ30 with SmaI and inserted 1kb regions flanking genes to be deleted, except for in the case of deletion of *xfp* in *D. japonica*, in which case the downstream flanking region was 500 bp (59). The resulting plasmid was transformed into *E. coli* S17 using heat shock, then conjugated into bacterial strain of choice. *P. aeruginosa* conjugates were selected on LB + 70 ug/mL of gentamicin and 20 ug/mL of chloramphenicol. For *D. japonica* we used LB with no NaCl, 20 ug/mL of gentamicin, and 6 ug/mL of

chloramphenicol. For *P. graminis* we used LB with no NaCl, 50 ug/mL of gentamicin, and 10 ug/mL of chloramphenicol. Final mutants were selected on LB + no NaCl + 10% sucrose.

Anaerobic survival assays and viability measurements

Overnight cultures were made with 7 mL of LB and grown for 20 hours at 37 C at 250 RPM to reach an OD_{500nm} of around 5. All experiments used a MOPS minimal media made of 100 mM anhydrous MOPS, 9.3 mM NH_4Cl, 3.7 mM KH_2PO_4, 1 mM $MgSO_4$, 30 uM $FeSO_4$ dissolved in EDTA, and 1x HAquil trace metals mix lacking $FeCl_3$ (60). For all anaerobic experiments, cells were washed 3x at 10,000 xg for 1 minutes at 4C then resuspended in MOPS minimal media to a concentration of OD_{500nm} of around 75. Concentrated cell suspensions were transferred to an anaerobic Coy Chamber with an atmosphere of N_2 + 1.5-2.5% H_2. Suspensions were diluted 5x with anoxic MOPS minimal media then 250 uL of diluted suspension was added to Balch tubes with 4.75 mL of MOPS minimal media with 120 mM of carbon (ex. 20 mM glucose) at a final cell concentration of OD_{500nm} of around 0.75 and a final volume of 5 mL. Balch tubes were then stoppered and removed from the Coy chamber and incubated at 30 C at 250 RPM. To measure viability, 1 mL syringes with 23-gauge 1-inch needles were fully filled and emptied 5 times under steady flow of N_2 to remove oxygen, before being inserted into Balch tubes and ~100 uL withdrawn and placed in 96-well plates (Fischer). Samples were then serially-diluted with 10x dilution steps with LB for *P. aeruginosa* or LB with no NaCl for *D. japonica* or *P. graminis*. For *P.* aeruginosa, 5 uL of samples were platted onto LB + 1.5% agar plates and incubated at 37 C overnight before CFUs were counted. For

D. japonica and *P. graminis*, we instead used LB with no NaCl + 1.5% agar plates and incubated at 30 C overnight.

Metabolite extractions

On described days, Balch tube cell suspensions were collected by vacuum filtration onto Whatman 0.22 um nylon filters. Flow-through was frozen at -80 C for measurement of acetate. Meanwhile, filters were dunked upside down in pre-chilled petri dishes with 2 mL cold solution of 40/40/20 methanol/acetonitrile/water and incubated at -20 C for 30 minutes. Solutions were then pipetted over filters to remove debris and suspensions transferred to 2-mL tubes and centrifuged at 4 C and 10,000 xg for 5 minutes. 200-400 uL supernatant was aliquoted and dried on ice under constant N_2 flow. Dried samples were stored at -80 C until analysis.

Intracellular metabolite quantification

We used a previously established protocol to quantify intracellular metabolites using UHPLC (Thermo Fisher Scientific Dionex UltiMate 3000) coupled with high-resolution mass spectrometry (Thermo Fisher Scientific Q Exactive quadrupled-Orbitrp) operating in negative mode. For LC we used an Acquity UPLC BEH C18 Column (particle size 1.7 um, 2.1 mm x 100 mm) maintained at 25 C with an injection volume of 10 uL. Eluents consisted of 97:3 (v/v) water:methanol with 15 mM acetic acid and 10 mM tributylamine (eluent A) and methanol (eluent B) (35). The flow rate was 0.18 mL min^{-1}. Relative intensities and the fraction of ^{13}C or ^{15}N isotopologues of each metabolite was analyzed using the Metabolomic Analysis and Visualization Engine (MAVEN) software (2011.6.17). IsoCor v2.2.0 was used to correct for natural abundance of ^{13}C or ^{15}N (61, 62).

Determination of ^{13}C incorporation into acetate

Supernatant samples were diluted 20:1 with 1M H_2SO_4 or 1M H_3PO_4 to ensure acetate was in the acetic acid form. We used an Agilent 6890 gas chromatograph with a Water GCT Premier time-of-flight ass spectrometer in elctron impact positive ion mode. 500 nL of sample was injected with a split/splitless injector in 20:1 split mode at 250 C. A Phenomenex Focusline p/n AG0-4680 was installed on the injector. Spectra were recorded from 33 to 400 m/z beginning at 2.3 minutes until 10 minutes. Separation of acetate from other components of the sample was achieved on a ZB-FFAP column (Phenomenex, Torrance, CA) 30m x 0.32mm ID x 0.25 microns operated at a constant flow of 0.8 mL/min. Initial column temperature was 100 C for 2 minutes increasing to 124 C at 8 C/min, then increasing to 180 C at 25 C with a final hold for 3 minutes. Acetic acid was eluted at 6.9 minutes. Masslynx and QuanLynx (Version 4.1) software was employed for data processing using peak areas of 60, 61, and 62 m/z for un-labelled, singly ^{13}C-labelled, and doubly ^{13}C-labelled acetic acid, respectively. Ratios of peak areas of labelled to unlabeled ions were used to estimate relative amounts of ^{13}C labelling without further correction.

Generation of phosphoketolase homolog library

To investigate the distribution of phosphoketolase across the bacterial domain, we analyzed 202,601 non-redundant bacterial genomes from the GlobDB collection (version 220, accessed October 2, 2024) (63). GlobDB integrates genomic resources from culturable isolates as well as environmental metagenomes, thereby providing a comprehensive and non-redundant representation of bacterial diversity. We used phosphoketolase sequences from *Pseudomonas aeruginosa* (NCBI protein accession

WP_003138037.1) and *Bifidobacterium animalis* (WP_012754421.1) as references. All protein sequences in GlobDB were first converted into the MMseqs2 database format with optimized memory usage (mmseqs createindex --split 0 --split-memory-limit 50G) (64). Homology searches were then performed with high sensitivity (-s 7.5). Rather than applying an arbitrary similarity cutoff during the search, we filtered hits post hoc by examining the distribution of alignment E-values and sequence coverage. We retained homologs with E-values < 1e-30 and alignment coverage > 90%, yielding 39,523 sequences homologous to the *B. animalis* reference and 1,671 homologs to the *P. aeruginosa* reference.

Generation of phosphoketolase amino acid sequence phylogenetic tree

To efficiently construct a high-quality multiple sequence alignment for this huge dataset, we adopted a centroid-based clustering strategy as developed before (65). Specifically, sequences were clustered with MMseqs2 (--cluster-mode 2 -c 0.8 --min-seq-id 0.7 -s 7.5) such that each cluster represented sequences with ≥70% pairwise identity. This reduced the dataset to 650 representative (centroid) sequences. These centroid sequences were aligned with MAFFT (version 7.505, --maxiterate 1000 --localpair) to generate a backbone alignment. The remaining sequences were subsequently added to this alignment using the --addfragments option in MAFFT (66). Based on this alignment, a phylogenetic tree was constructed using FastTree (version 2.1.11, FastTreeMP -lg -gamma), which applies maximum-likelihood methods with a gamma-distributed rate heterogeneity model and 1000 resamplings per split (67). This tree was visualized in iTOL using normal settings. For the main text figure, only annotated genomes were including and clades with an average branch length stance to their leaves of below 1.8

were collapsed for ease of visibility. The two furthest sides of the triangles from the origin of collapses clades is proportional to the distance of the node's closest and farthest child leaves.

Generation of 16S rRNA phylogenetic tree

For each strain, the entire genome was downloaded via NCBI as a FASTA file and input into barrnap version 1.2.1 using the online Galaxy GUI, to determine each species 16S rRNA sequences. Each sequence was combined into one FASTA file and imported into MEGA version 11 and aligned using default settings. The resulting alignment was used to generate a Maximum-Likelihood tree using default settings, with any gaps in the alignment being deleted. The resulting tree was visualized in iTOL.

Generation of gene neighborhood maps and flanking gene tables

For each of the 10 strains used in gene neighborhood mapping, a FASTA file containing ~20 kb surrounding each strain's phosphoketolase homolog was downloaded from NCBI and input into Prokka via the KBase online GUI for annotation, then exported as a GenBank file. The resulting GenBank files were then uploaded to the Clinker online GUI for generation of the map. To determine the genes flanking each species' phosphoketolase, we assembled a list of all annotated genomes containing an *xfp* homolog and their amino acid sequence as determined above. We then utilized BioPython to access their NCBI GenBank files, scanned all CDS translations for a match to their *xfp* homolog sequence, then pulled the information of the 5 CDS features upstream and downstream of this homolog, and saved the resulting information.

References

1. Chubukov V, Gerosa L, Kochanowski K, Sauer U. 2014. Coordination of microbial metabolism. Nat Rev Microbiol 12:327–340.

2. Xiao W, Loscalzo J. 2020. Metabolic Responses to Reductive Stress. Antioxidants & Redox Signaling 32:1330–1347.

3. Luo M, Ma X, Ye J. 2024. Reductive stress—a common metabolic feature of obesity and cancer. Acta Pharm Sin B 14:5181–5185.

4. Cantó C, Menzies KJ, Auwerx J. 2015. NAD+ Metabolism and the Control of Energy Homeostasis: A Balancing Act between Mitochondria and the Nucleus. Cell Metabolism 22:31–53.

5. Ying W. 2008. NAD+/NADH and NADP+/NADPH in Cellular Functions and Cell Death: Regulation and Biological Consequences. Antioxidants & Redox Signaling 10:179–206.

6. Yang R, Guo Z, Li B. 2025. NADH reductive stress drives metabolic reprogramming. Trends in Cell Biology 0.

7. Bartacek J, Zabranska J, Lens PNL. 2007. Developments and constraints in fermentative hydrogen production. Biofuels, Bioproducts and Biorefining 1:201–214.

8. Hackmann TJ. 2024. The vast landscape of carbohydrate fermentation in prokaryotes. FEMS Microbiol Rev 48:fuae016.

9. Hackmann TJ, Zhang B. 2023. The phenotype and genotype of fermentative prokaryotes. Science Advances 9:eadg8687.

10. Thauer RK, Jungermann K, Decker K. 1977. Energy conservation in chemotrophic anaerobic bacteria. Bacteriol Rev 41:100–180.

11. Gayon U (1845-1929) A du texte, Dupetit GA du texte. 1886. Recherches sur la réduction des nitrates par les infiniment petits / par MM. U. Gayon et G. Dupetit ; Station agronomique de Bordeaux. https://gallica.bnf.fr/ark:/12148/bpt6k9366473. Retrieved 11 November 2025.

12. Zumft WG. 1997. Cell biology and molecular basis of denitrification. Microbiol Mol Biol Rev 61:533–616.

13. Silver WL, Lugo AE, Keller M. 1999. Soil oxygen availability and biogeochemistry along rainfall and topographic gradients in upland wet tropical forest soils. Biogeochemistry 44:301–328.

14. Enfors S-O, Jahic M, Rozkov A, Xu B, Hecker M, Jürgen B, Krüger E, Schweder T, Hamer G, O'Beirne D, Noisommit-Rizzi N, Reuss M, Boone L, Hewitt C, McFarlane C, Nienow A, Kovacs T, Trägårdh C, Fuchs L, Revstedt J, Friberg PC, Hjertager B, Blomsten G, Skogman H, Hjort S, Hoeks F, Lin H-Y, Neubauer P, van der Lans R, Luyben K, Vrabel P, Manelius Å. 2001. Physiological responses to mixing in large scale bioreactors. Journal of Biotechnology 85:175–185.

15. Cowley ES, Kopf SH, LaRiviere A, Ziebis W, Newman DK. 2015. Pediatric Cystic Fibrosis Sputum Can Be Chemically Dynamic, Anoxic, and Extremely Reduced Due to Hydrogen Sulfide Formation. mBio 6:10.1128/mbio.00767-15.

16. Voroney RP, Heck RJ. 2015. The Soil Habitat, p. 15–39. *In* Soil Microbiology, Ecology and Biochemistry. Elsevier.

17. Bergkessel M, Basta DW, Newman DK. 2016. The physiology of growth arrest: uniting molecular and environmental microbiology. Nat Rev Microbiol 14:549–562.

18. Lopatkin AJ, Stokes JM, Zheng EJ, Yang JH, Takahashi MK, You L, Collins JJ. 2019. Bacterial metabolic state more accurately predicts antibiotic lethality than growth rate. Nat Microbiol 4:2109–2117.

19. Eschbach M, Schreiber K, Trunk K, Buer J, Jahn D, Schobert M. 2004. Long-Term Anaerobic Survival of the Opportunistic Pathogen Pseudomonas aeruginosa via Pyruvate Fermentation. J Bacteriol 186:4596–4604.

20. Berney M, Greening C, Conrad R, Jacobs WR, Cook GM. 2014. An obligately aerobic soil bacterium activates fermentative hydrogen production to survive reductive stress during hypoxia. Proceedings of the National Academy of Sciences 111:11479–11484.

21. Horak RD, Zhou N, Thalhammer KO, Dalleska NF, Aristilde L, Newman DK. 2026. Pseudomonas aeruginosa Relies on a Phosphoketolase to Support Anaerobic Survival Under Reductive Stress. Molecular Microbiology 125:361–374.

22. Vander Wauven C, Piérard A, Kley-Raymann M, Haas D. 1984. Pseudomonas aeruginosa mutants affected in anaerobic growth on arginine: evidence for a four-gene cluster encoding the arginine deiminase pathway. Journal of Bacteriology 160:928–934.

23. Glasser NR, Kern SE, Newman DK. 2014. Phenazine redox cycling enhances anaerobic survival in Pseudomonas aeruginosa by facilitating generation of ATP and a proton-motive force. Molecular Microbiology 92:399–412.

24. Ciemniecki JA, Ho C-L, Horak RD, Okamoto A, Newman DK. 2024. Mechanistic study of a low-power bacterial maintenance state using high-throughput electrochemistry. Cell 187:6882-6895.e8.

25. Kohlstedt M, Wittmann C. 2019. GC-MS-based 13C metabolic flux analysis resolves the parallel and cyclic glucose metabolism of *Pseudomonas putida* KT2440 and *Pseudomonas aeruginosa* PAO1. Metabolic Engineering 54:35–53.

26. Lessie TG, Jr PVP. 1984. ALTERNATIVE PATHWAYS OF CARBOHYDRATE UTILIZATION IN PSEUDOMONADS. Annual Review of Microbiology 38:359–388.

27. Krüsemann JL, Lindner SN, Dempfle M, Widmer J, Arrivault S, Debacker M, He H, Kubis A, Chayot R, Anissimova M, Marlière P, Cotton CAR, Bar-Even A. 2018. Artificial pathway emergence in central metabolism from three recursive phosphoketolase reactions. The FEBS Journal 285:4367–4377.

28. Sánchez B, Zúñiga M, González-Candelas F, De Los Reyes-Gavilán CG, Margolles A. 2010. Bacterial and Eukaryotic Phosphoketolases: Phylogeny, Distribution and Evolution. Microb Physiol 18:37–51.

29. Suzuki R, Katayama T, Kim B-J, Wakagi T, Shoun H, Ashida H, Yamamoto K, Fushinobu S. 2010. Crystal Structures of Phosphoketolase: THIAMINE DIPHOSPHATE-DEPENDENT DEHYDRATION MECHANISM *. Journal of Biological Chemistry 285:34279–34287.

30. Aristilde L, Lewis IA, Park JO, Rabinowitz JD. 2015. Hierarchy in Pentose Sugar Metabolism in Clostridium acetobutylicum. Applied and Environmental Microbiology 81:1452–1462.

31. Årsköld E, Lohmeier-Vogel E, Cao R, Roos S, Rådström P, van Niel EWJ. 2008. Phosphoketolase Pathway Dominates in Lactobacillus reuteri ATCC 55730 Containing Dual Pathways for Glycolysis. Journal of Bacteriology 190:206–212.

32. de Vries W, Stouthamer AH. 1967. Pathway of Glucose Fermentation in Relation to the Taxonomy of Bifidobacteria. Journal of Bacteriology 93:574–576.

33. Liu L, Zhang L, Tang W, Gu Y, Hua Q, Yang S, Jiang W, Yang C. 2012. Phosphoketolase Pathway for Xylose Catabolism in Clostridium acetobutylicum Revealed by 13C Metabolic Flux Analysis. Journal of Bacteriology 194:5413–5422.

34. Servinsky MD, Germane KL, Liu S, Kiel JT, Clark AM, Shankar J, Sund CJ. 2012. Arabinose is metabolized via a phosphoketolase pathway in Clostridium acetobutylicum ATCC 824. J Ind Microbiol Biotechnol 39:1859–1867.

35. Aristilde L. 2017. Metabolite labelling reveals hierarchies in Clostridium acetobutylicum that selectively channel carbons from sugar mixtures towards biofuel precursors. Microbial Biotechnology 10:162–174.

36. Baier F, Tokuriki N. 2014. Connectivity between Catalytic Landscapes of the Metallo-β-Lactamase Superfamily. Journal of Molecular Biology 426:2442–2456.

37. Dzurová L, Forneris F, Savino S, Galuszka P, Vrabka J, Frébort I. 2015. The three-dimensional structure of "Lonely Guy" from Claviceps purpurea provides insights into the phosphoribohydrolase function of Rossmann fold-containing lysine decarboxylase-like proteins. Proteins: Structure, Function, and Bioinformatics 83:1539–1546.

38. Seo H, Kim S, Sagong H-Y, Son HF, Jin KS, Kim I-K, Kim K-J. 2016. Structural basis for cytokinin production by LOG from Corynebacterium glutamicum. Sci Rep 6:31390.

39. Petrareanu G, Balasu MC, Vacaru AM, Munteanu CVA, Ionescu AE, Matei I, Szedlacsek SE. 2014. Phosphoketolases from Lactococcus lactis, Leuconostoc

mesenteroides and Pseudomonas aeruginosa: dissimilar sequences, similar substrates but distinct enzymatic characteristics. Appl Microbiol Biotechnol 98:7855–7867.

40. Wu Z, Bezwada D, Cai F, Harris RC, Ko B, Sondhi V, Pan C, Vu HS, Nguyen PT, Faubert B, Cai L, Chen H, Martin-Sandoval M, Do D, Gu W, Zhang Y, Zhang Y, Brooks B, Kelekar S, Zacharias LG, Oaxaca KC, Patricio JS, Mathews TP, Garcia-Bermudez J, Ni M, DeBerardinis RJ. 2024. Electron transport chain inhibition increases cellular dependence on purine transport and salvage. Cell Metabolism 36:1504-1520.e9.

41. Deutscher MP. 2006. Degradation of RNA in bacteria: comparison of mRNA and stable RNA. Nucleic Acids Res 34:659–666.

42. Himeoka Y, Gummesson B, Sørensen MA, Svenningsen SL, Mitarai N. 2022. Distinct Survival, Growth Lag, and rRNA Degradation Kinetics during Long-Term Starvation for Carbon or Phosphate. mSphere 7:e01006-21.

43. Grucela PK, Fuhrer T, Sauer U, Chao Y, Zhang YE. 2023. Ribose 5-phosphate: the key metabolite bridging the metabolisms of nucleotides and amino acids during stringent response in Escherichia coli? Microb Cell 10:141–144.

44. Seregina TA, Shakulov RS, Petrushanko IY, Lobanov KV, Mironov AS. 2025. Biosynthesis of Ribose-5-Phosphate—Metabolic Regulator of Escherichia coli Viability. Cells 14:1775.

45. Warfield BM, Reigan P. 2022. Multifunctional role of thymidine phosphorylase in cancer. Trends in Cancer 8:482–493.

46. Trchounian A, Trchounian K. 2019. Fermentation Revisited: How Do Microorganisms Survive Under Energy-Limited Conditions? Trends in Biochemical Sciences 44:391–400.

47. Chuang DS-W, Liao JC. 2021. Role of cyanobacterial phosphoketolase in energy regulation and glucose secretion under dark anaerobic and osmotic stress conditions. Metabolic Engineering 65:255–262.

48. Lu K-J, Chang C-W, Wang C-H, Chen FY-H, Huang IY, Huang P-H, Yang C-H, Wu H-Y, Wu W-J, Hsu K-C, Ho M-C, Tsai M-D, Liao JC. 2023. An ATP-sensitive phosphoketolase regulates carbon fixation in cyanobacteria. Nat Metab 5:1111–1126.

49. Kop LFM, Koch H, Jetten MSM, Daims H, Lücker S. 2024. Metabolic and phylogenetic diversity in the phylum Nitrospinota revealed by comparative genome analyses. ISME Commun 4:ycad017.

50. Bayer B, Saito MA, McIlvin MR, Lücker S, Moran DM, Lankiewicz TS, Dupont CL, Santoro AE. 2021. Metabolic versatility of the nitrite-oxidizing bacterium Nitrospira marina and its proteomic response to oxygen-limited conditions. ISME J 15:1025–1039.

51. Grove A. 2025. The delicate balance of bacterial purine homeostasis. Discov Bact 2:14.

52. Yang R, Guo Z, Li B. 2025. NADH reductive stress drives metabolic reprogramming. Trends in Cell Biology https://doi.org/10.1016/j.tcb.2025.07.005.

53. Yang C, Zhao Y, Wang L, Guo Z, Ma L, Yang R, Wu Y, Li X, Niu J, Chu Q, Fu Y, Li B. 2023. De novo pyrimidine biosynthetic complexes support cancer cell proliferation and ferroptosis defence. Nat Cell Biol 25:836–847.

54. Guo MS, Gross CA. 2014. Stress-Induced Remodeling of the Bacterial Proteome. Current Biology 24:R424–R434.

55. Meirelles LA, Perry EK, Bergkessel M, Newman DK. 2021. Bacterial defenses against a natural antibiotic promote collateral resilience to clinical antibiotics. PLOS Biology 19:e3001093.

56. Dar D, Thomashow LS, Weller DM, Newman DK. 2020. Global landscape of phenazine biosynthesis and biodegradation reveals species-specific colonization patterns in agricultural soils and crop microbiomes. eLife 9:e59726.

57. Perry EK, Newman DK. 2022. Prevalence and Correlates of Phenazine Resistance in Culturable Bacteria from a Dryland Wheat Field. Applied and Environmental Microbiology 88:e02320-21.

58. Gibson DG, Young L, Chuang R-Y, Venter JC, Hutchison CA, Smith HO. 2009. Enzymatic assembly of DNA molecules up to several hundred kilobases. Nat Methods 6:343–345.

59. Shanks RMQ, Caiazza NC, Hinsa SM, Toutain CM, O'Toole GA. 2006. Saccharomyces cerevisiae-Based Molecular Tool Kit for Manipulation of Genes from Gram-Negative Bacteria. Applied and Environmental Microbiology 72:5027–5036.

60. Martocello DE, Morel FMM, McRose DL. 2019. H-Aquil: a chemically defined cell culture medium for trace metal studies in Vibrios and other marine heterotrophic bacteria. Biometals 32:819–828.

61. Millard P, Delépine B, Guionnet M, Heuillet M, Bellvert F, Létisse F. 2019. IsoCor: isotope correction for high-resolution MS labeling experiments. Bioinformatics 35:4484–4487.

62. Clasquin MF, Melamud E, Rabinowitz JD. 2012. LC-MS Data Processing with MAVEN: A Metabolomic Analysis and Visualization Engine. Current Protocols in Bioinformatics 37:14.11.1-14.11.23.

63. Speth DR, Pullen N, Aroney STN, Coltman BL, Osvatic J, Woodcroft BJ, Rattei T, Wagner M. 2025. GlobDB: a comprehensive species-dereplicated microbial genome resource. Bioinformatics Advances 5:vbaf280.

64. Steinegger M, Söding J. 2017. MMseqs2 enables sensitive protein sequence searching for the analysis of massive data sets. Nat Biotechnol 35:1026–1028.

65. Shan X, Li K, Stadler P, Borbor M, Reyes G, Solórzano R, Chamorro E, Bayot B, Cordero OX. 2025. Microbiome determinants of productivity in aquaculture of whiteleg shrimp. Applied and Environmental Microbiology 91:e02420-24.

66. Katoh K, Standley DM. 2013. MAFFT Multiple Sequence Alignment Software Version 7: Improvements in Performance and Usability. Mol Biol Evol 30:772–780.

67. Price MN, Dehal PS, Arkin AP. 2010. FastTree 2 – Approximately Maximum-Likelihood Trees for Large Alignments. PLoS ONE 5:e9490.

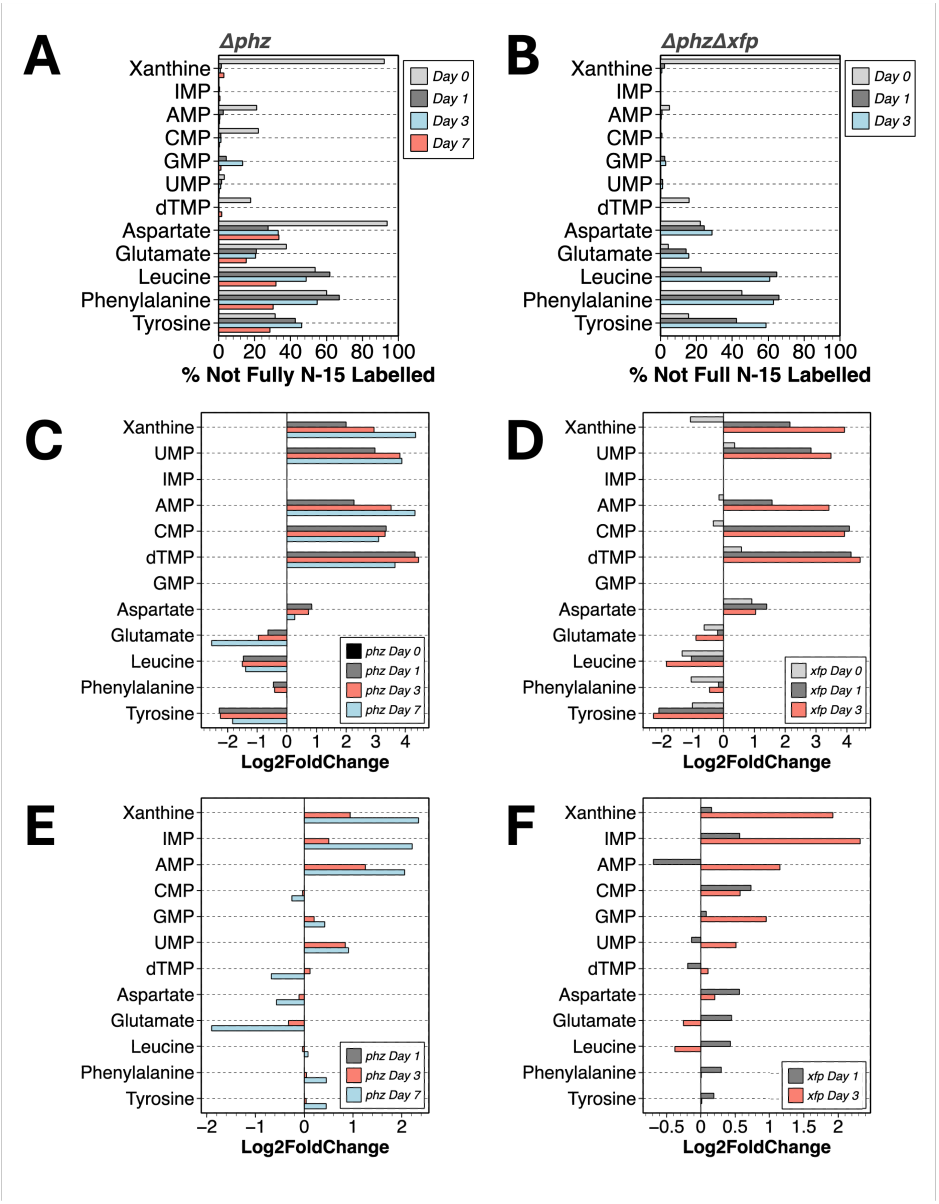

Figure S1: (A, B) Percent of metabolites lacking ^{15}N-labelling in at least 1 nitrogen atom, bars = means of 3 biological replicates. Colors denote day of anaerobic survival. A = *Δphz*, B = *ΔphzΔxfp*. (C, D, E, F) Log2-fold change of relative metabolite abundances in *Δphz* (C,E) or *ΔphzΔxfp* cells (D,F) after 0, 1, 3, or 7 days of anaerobic survival normalized to the Day 0 abundance in *Δphz* cells (C, D) or Day 1 abundance in *Δphz* cells (E, F).

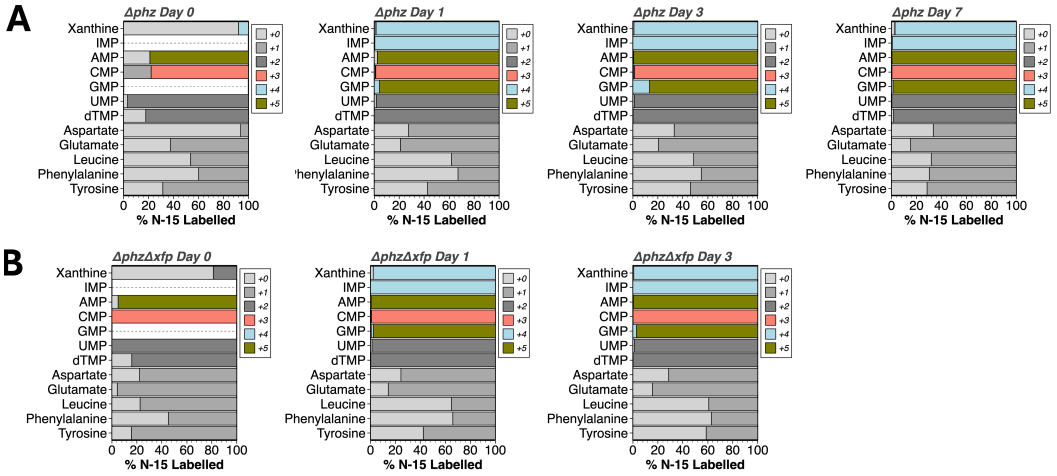

Figure S2: (A, B) Percent of metabolites labelled with ^{15}N in different amounts. Colors denote the number of N-atoms isotopically labelled. Bars represent means of 3 biological replicates. (A) *Δphz* cells (B) *ΔphzΔxfp* cells.

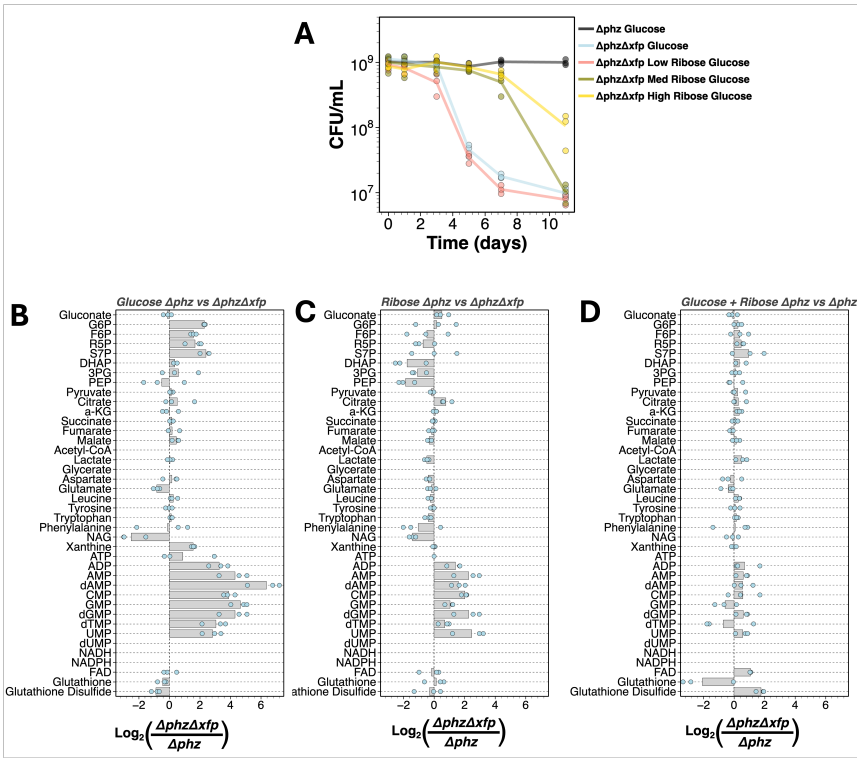

Figure S3: (A) Log-transformed CFU/mL values during anaerobic survival of *Δphz* or *ΔphzΔxfp* cells given glucose, glucose + 0.24 mM ribose (low ribose), glucose + 2.4 mM ribose (med ribose), or glucose + 24 mM ribose (high ribose). Lines = means, dots = biological replicates, n = 3. (B, C, D) Log2-fold change of metabolite abundance during anaerobic survival in *ΔphzΔxfp* cells normalized to *Δphz* cells, during survival on glucose (B), ribose (C), or glucose + ribose (D). Bars = mean *ΔphzΔxfp* levels, dots = *ΔphzΔxfp* biological replicates, n = 3. G6P = glucose-6-phosphate. F6P = fructose-6-phosphate. R5P = ribose-5-phosphate, which is in equilibrium with xylulose-5-phosphate. S7P = sedoheptulose-7-phosphate. DHAP = dihydroxyacetone phosphate, which is in equilibrium with glyceraldehyde-3-phosphate. 3PG = 3-phosphoglycerate. PEP = phosphoenolpyruvate. a-KG = alpha-ketoglutarate.

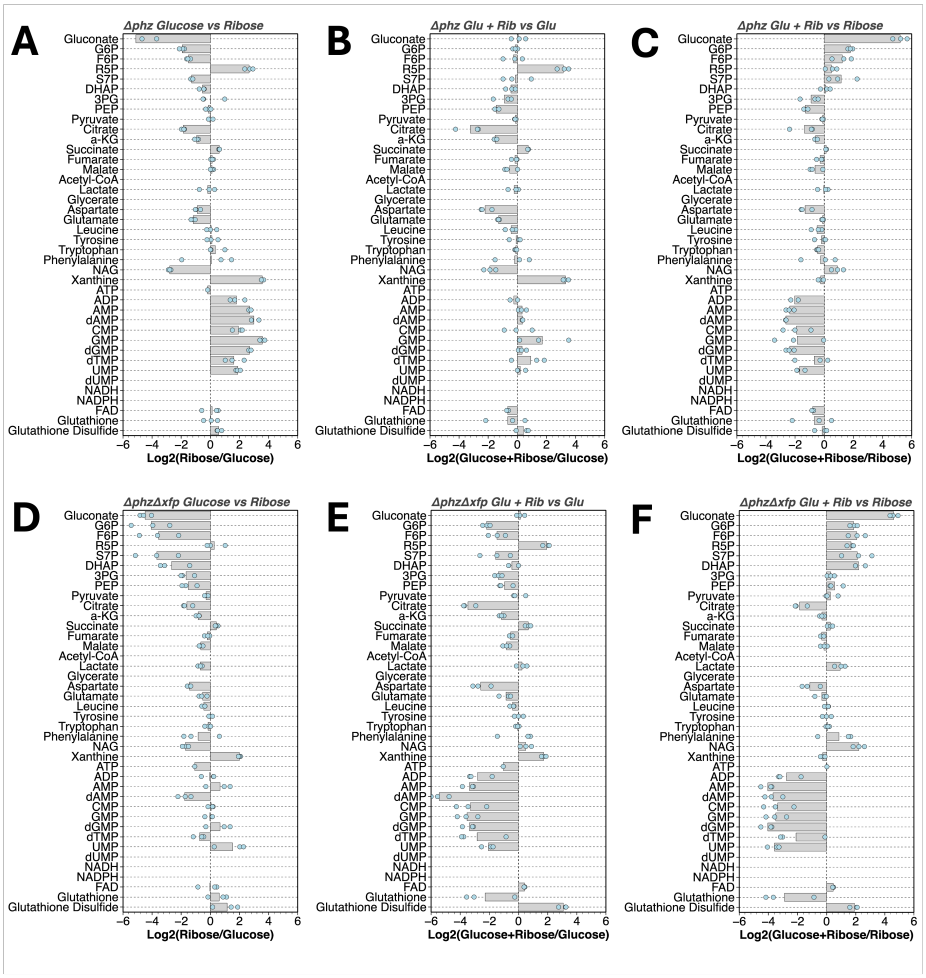

Figure S4: (A – F) Log2-fold change of metabolite abundance during anaerobic survival in *Δphz* cells (A – C) or *ΔphzΔxfp* cells (D – F). Bars and dots represent metabolite abundance during survival on ribose (A, D) or glucose + ribose (B, C, E, F) normalized to survival on glucose (A, B, D, E) or ribose (C, F). Bars = means, dots = biological replicates, n = 3. G6P = glucose-6-phosphate. F6P = fructose-6-phosphate. R5P = ribose-5-phosphate, which is in equilibrium with xylulose-5-phosphate. S7P = sedoheptulose-7-phosphate. DHAP = dihydroxyacetone phosphate, which is in equilibrium with glyceraldehyde-3-phosphate. 3PG = 3-phosphoglycerate. PEP = phosphoenolpyruvate. a-KG = alpha-ketoglutarate.

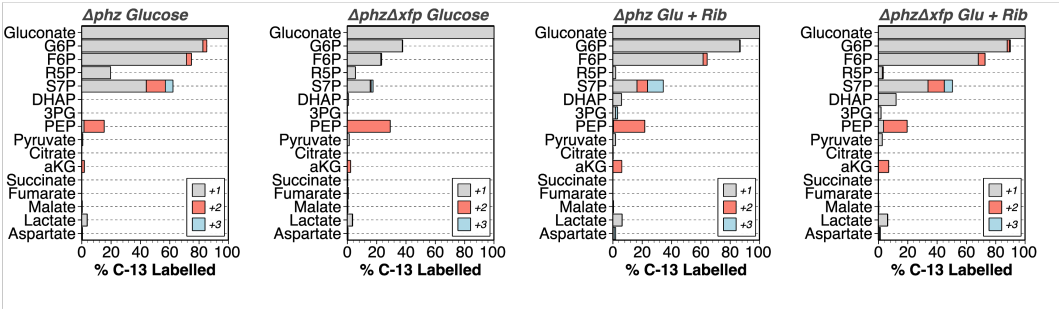

Figure S5: Percent of metabolites isotopically labelled during survival on 1-^{13}C-glucose or 1-13C-glucose + ribose. G6P = glucose-6-phosphate. F6P = fructose-6-phosphate. R5P = ribose-5-phosphate, which is in equilibrium with xylulose-5-phosphate. S7P = sedoheptulose-7-phosphate. DHAP = dihydroxyacetone phosphate, which is in equilibrium with glyceraldehyde-3-phosphate. 3PG = 3-phosphoglycerate. PEP = phosphoenolpyruvate. a-KG = alpha-ketoglutarate.

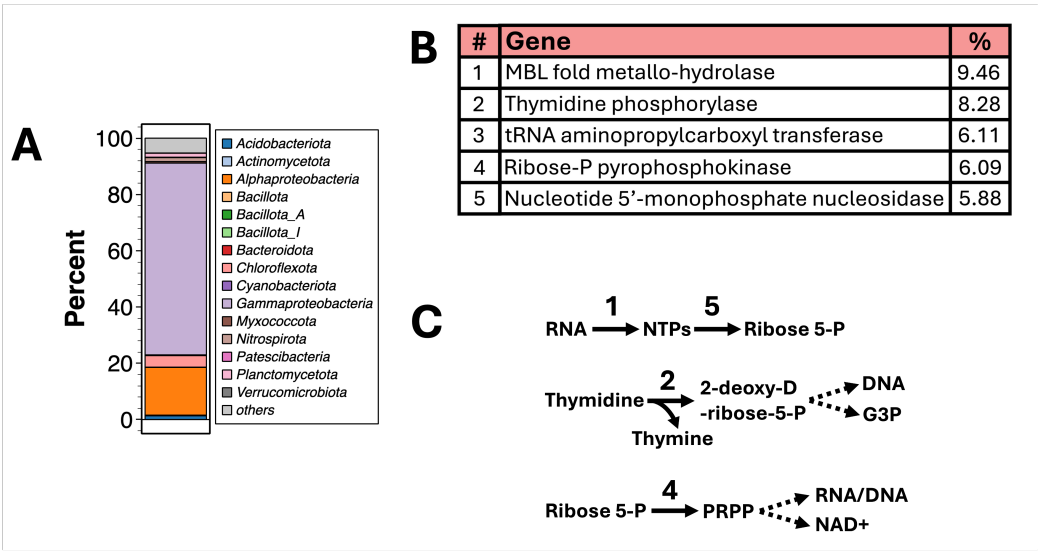

Figure S6: (A) Percent of amino acid sequences in the red portion of phylogenetic tree from FIG 4A that belong to individual bacterial taxa. (B) Table showing abundance of different gene homologs within 5 genes upstream or downstream of phosphoketolase homologs, adjusted to remove hypothetical proteins. (C) Putative functions of genes from B.

Chapter 5

CONCLUSIONS AND FUTURE DIRECTIONS

Summary

The two primary lessons I learned during this thesis are 1) by looking in new places you see new biology and 2) you don't have to go far to find these "new places". This self-education came from studying bacterial metabolism during growth arrest under the context of oxidative stress in Chapter 2, or reductive stress in Chapters 3 and 4. Despite bacteria being commonly found under growth arrest and redox stress in nature, the field of bacterial metabolism has historically been conducted under nutrient and oxidant replete conditions in heterotrophs during exponential growth. This focus on growth metabolism was essential to build our understanding of how to even conduct laboratory bacteriological experiments and domesticate bacteria. However, it has left a blind spot. We are mostly in the dark as to how the metabolic principles underlying exponential growth apply to survival under growth arrest and redox imbalance. This applies even to commonly studied model organisms, such as *Pseudomonas aeruginosa*, the species of focus within this thesis.

In Chapter 2 I show how production of phenazines by *P. aeruginosa* can suppress the bioenergetic state of cells during oxidative stress conditions, conferring protections to clinical antibiotics. Meanwhile in Chapter 3 I discover that a phosphoketolase catalyzes a new pathway for *P. aeruginosa* to catabolize glucose during anaerobic survival and reductive stress, as well as maintain survival and ribonucleotide homeostasis. I

expanded upon this discovery in Chapter 4, showing that use of phosphoketolases for non-growth anaerobic survival extends to a diverse array of other bacteria.

Key findings and speculations

Chapter 2: Under oxidative stress and carbon limitation, phenazines and toxoflavin differentially lower the membrane potential, proton pumping, and ATP levels of *P. aeruginosa* cells correlated with increasing protection to clinical antibiotics. The degree to which phenazines lowered the bioenergetic state of *P. aeruginosa* was correlated to their rate of reduction by the cell and oxidation by oxygen, reiterating the fundamental effect of electron flow on metabolism. This work hints that cells can have agency over lowering their bioenergetic state and are not solely at the whim of environmental chemical gradients. Additionally, despite historical assumptions that such bioenergetic suppression are detrimental to a cell's fitness, in the context of a world full of stressors, such bioenergetic self-poisoning could play a large role in the survival of *P. aeruginosa* communities.

Chapter 3: During anaerobic survival and reductive stress, *P. aeruginosa* metabolizes glucose to acetate via the pentose-phosphate pathway and a phosphoketolase. This contrasts with *P. aeruginosa*'s glucose catabolic pathway used during aerobic growth where glucose is entirely catabolized via the Entner-Duodoroff pathway and lower glycolysis. This discovery expands *P. aeruginosa*'s central carbon metabolic network and counters previous assumptions that production of acetate during anaerobic survival is via the Entner-Duodoroff pathway. Additionally, anaerobic survival on various carbon sources leads to dramatic accumulation of pentose-phosphate pathway metabolites and

ribonucleotides. Therefore, under reductive stress the pentose-phosphate pathway may act as a metabolite reservoir with this phosphoketolase acting as a pressure release valve.

Chapter 4: Anaerobic survival in *P. aeruginosa* triggers ribonucleotide degradation and any resynthesis of ribonucleotides is occurring via the salvage pathway. Dynamic interactions between pentose and hexose metabolite pools play a large role in mediating metabolic flux and survival in *P. aeruginosa*, hinting at mechanisms to explain the importance of phosphoketolases and ribonucleotide homeostasis in anaerobic survival of *P. aeruginosa*. Phosphoketolases similarly support anaerobic survival and glucose catabolism during reductive stress in a diversity of bacteria. Phosphoketolases may play a previously unappreciated role in mediating ribonucleotide turnover in diverse bacteria, with hints at a role for the N-terminus of *P. aeruginosa*'s phosphoketolase in regulating such a role.

Future directions

Role of the divalent cations in altering phenazine function

Chapter 2 focused on the role of oxygen and carbon availability in altering the effect of phenazines on cells. Within nature the chemical microenvironment is far more complex. For example, in seawater, magnesium is the third most abundant ion, with reported concentrations upwards of 55 mM, far above what is used in our experiments or in most bacterial growth media. Magnesium plays a large role in biology, acting to stabilize ribosomes or as an enzymatic cofactor. Additionally, magnesium, and other divalent cations, such as calcium, dramatically effect outer membrane permeability, acting as ionic bridges to link negatively charged phospholipids and lipopolysaccharides.

Furthermore, chelating divalent cations is a common method to permeabilize gram-negative bacteria for use in genetic transformation, staining for microscopy, or many other lab procedures. Therefore, the concentration and availability of divalent cations can play a major role in the results of laboratory experiments, with high concentrations known to prevent uptake of molecules such as clinical antibiotics including tobramycin. Anecdotally this appears to also be a consideration for experiments with phenazines. During my study in Chapter 2, I found that phenazines highly protected cells from tobramycin-mediated lethality in PBS-based cell suspensions. However, at one point I switched the carbon-starvation media to a MOPS-based minimal media including 1 mM $MgSO_4$ which led to dramatically less tobramycin killing and therefore, little to no phenazine-mediated protection. I later found that this magnesium was the culprit as addition of magnesium to PBS had a dose dependent effect on protecting cells from tobramycin and making phenazine-mediated protection obsolete. Additionally, during measurements of membrane potential with $DiOC_2(3)$, cells must be permeabilized with the chelator EDTA as divalent cations prevent proper uptake of this dye, making it impossible to use this method determine the effect of phenazines on membrane potential in the presence of magnesium.

Through conversations with other lab members, I also learned that the rate of reduction of phenazines by *P. aeruginosa* was lower when magnesium was present in cell suspensions. Therefore, it seems that the effect of divalent cations on permeability of the outer membrane can have substantial effects on the ability of phenazines to access and effect the inner membrane or cytosol of cells. Future studies should investigate these effects as well as the concentration and availability of divalent cations within important

environments such as *P. aeruginosa* infections in cystic fibrosis patients. These studies are crucial to understanding when and where our results on phenazine mediated bioenergetic suppression, phenazine-mediated anaerobic survival, or many other effects are relevant in nature.

Exploring the metabolism of *P. aeruginosa* under reductive stress, with an emphasis on lipid and ribonucleotide metabolisms

While my explorations in Chapters 3 and 4 uncovered new metabolic pathways and principles by which *P. aeruginosa* survives under reductive stress, this work is far from over. Future experiments should carry out more holistic metabolic flux measurements of cells surviving under oxidant-limitation as well as discover how flux through various pathways shift in response to oxidant availability. This latter goal could be done via the addition of known concentrations of phenazines or nitrate to cell suspensions. Such studies would uncover 1) what pathways are actively used during anaerobic survival and 2) the critical threshold of oxidant at which different pathways become relevant.

The resulting data and use of metabolic modeling might explain why *P. aeruginosa* is incapable of growing fermentatively. For example, tracking flux through each pathway as the concentration of available nitrate increases up until the critical concentration to support growth could elucidate whether the ability to grow anaerobically is limited by redox balance, flux through biosynthetic pathways, flux through energy conservation, or a balance of the above. Additionally, it could support our proposal in Chapter 3 of the pentose-phosphate pathway as a "metabolic reservoir" during reductive stress and the role for phosphoketolases as "pressure release valves".

Regardless of the outcome, this line of questioning would entail straightforward experiments to uncover new biology, as we lack even the fundamental measurements of *P. aeruginosa* metabolic flux through central carbon metabolism during growth through denitrification. Alternatively, such experiments may suggest an interesting idea I propose through this thesis, which is that organisms such as *P. aeruginosa* have evolved specifically to not grow fermentatively. Despite seemingly containing sufficient genes to catalyze fermentative growth, *P. aeruginosa* may evolutionarily "prefer" survival, using the anoxic cores of biofilms to act as stress tolerance "seed banks" to lie dormant until biofilm dispersal.

In a more specific direction, the metabolomic profiles from experiments in Chapters 3 and 4, as well as other publicly available datasets, such as the transposon-sequencing analysis of genetic determinates of *P. aeruginosa* anaerobic survival used in Chapter 3, contain a variety of unexplored but interesting results. While there is not room to cover all these, I believe two fruitful pathways for discovery are lipid biosynthesis and ribonucleotide salvage. Both pathways are known to support survival during growth arrest and hypoxia across the domains of life. It is unlikely that *P. aeruginosa* is an exception.

In the instance of lipids, phospholipid biosynthesis is critical for maintenance and remodeling of the cell membranes during environmental transitions and survival. Several genes involved in such processes are known to be involved in anaerobic survival of *P. aeruginosa*. For example, biosynthesis of phospholipids via the CDP-diacylglycerol pathway requires glycerol-3-phosphate, CTP, and a CoA carrier such as acetyl-CoA. Genes involved in the production of glycerol-3-phosphate from glyceraldehyde-3-

phosphate or glycerol were shown to be important for survival. Meanwhile, our results in this thesis show that *P. aeruginosa*'s phosphoketolase could be an important source for both acetyl-CoA, via its release of acetyl-P, and glyceraldehyde-3-phosphate, via its cleavage of xylulose-5-P. The large accumulation of ribonucleotides seen during anaerobic survival would provide sufficient CTP to complete such biosynthesis. Use of such a pathway would not only aid in maintenance of membrane homeostasis but also consume significant quantities of reducing equivalents helping to alleviate reductive stress.

Regarding ribonucleotide salvage, my results in Chapters 3 and 4 suggest that cells surviving anaerobically, regardless of carbon source or phosphoketolase presence, are undergoing dramatic changes to their ribonucleotide pools. Additionally, we discovered that many phosphoketolases are co-localized with ribonucleotide biosynthetic and degradative enzymes including thymidine phosphorylase. These results strikingly match those of studies exploring metabolic responses of cancer cells to hypoxia. The central carbon metabolic network of both *P. aeruginosa* and humans are highly similar while both tumors and biofilms have dynamic oxygen gradients. Therefore, it is both fascinating and seems obvious in retrospect that in both systems hypoxia trigger pentose-phosphate pathway metabolite accumulation and dramatic turnover of ribonucleotide pools.

Studies in cancer biology have shown ribonucleotide accumulation from ATP-costly futile cycling, efficient ribonucleotide salvage, or use of thymidine phosphorylase for ribonucleotide degradation to act as a nutrient source. Meanwhile, studies in bacteria frequently finding RNA degradation as a key feature during growth arrest. Across both

fields, there is far more work to be done to discover the directionality of ribonucleotide salvage during anaerobic survival, the processes which maintain or lead to dysregulation of these pools, and the consequence of such changes. Specifically, one interesting hypothesis from our work is that biosynthesis of fresh NAD+ or salvage of NADH/NAD+ could act to alleviate reductive stress, however, the pathways mediating such processes in bacteria are poorly understood. Additionally, ribonucleotides are used in a variety of processes beyond RNA. Experiments to investigate the rates of ribonuclease reductase activity, DNA/RNA consumption from internal or external sources, or use of ribonucleotides in post-translational modification and cell wall biosynthesis would be of use.

Connecting the preceding paragraphs on lipid biosynthesis to the ribonucleotide pools, it would be particularly fascinating if cells are linking RNA and ribonucleotide degradation to lipid biosynthesis. Such a strategy would minimize cellular maintenance costs by lowering ribosome, tRNA, mRNA or other macromolecule stores, generate energy through catabolism of released ribose sugars, and consume reducing equivalent through production of glycerol-3-phosphate and lipid biosynthesis. Phosphoketolases would be especially suited to aid in such a macromolecule transition via their production of essential precursors for such pathways. While not as common as ribonucleotide processing genes, we do see the occurrence of lipid biosynthesis and degrative enzymes flanking phosphoketolase homologs. Such a discovery would expand our understanding of what is means to recycle macromolecules under growth arrest.

Comparative enzymology and physiological functions of phosphoketolases

An interesting hypothesis which spawned from Chapters 3 and 4 of this thesis was that there are distinct functional groups of phosphoketolases. This is not without precedent as the phosphoketolases of organisms that rely on them for fermentative growth, such as *Bifidobacteria animalis*, are distinct to those in the cyanobacteria *Synechococcus elongatus*. The phosphoketolase of *S. elongatus* contains an N-terminal domain that binds ATP, leading to its inhibition. During growth arrest due to metabolic disruption, ATP levels lower, de-inhibiting this phosphoketolase and allowing it to drain Calvin cycle metabolites and support metabolite homeostasis. Meanwhile the phosphoketolase of *B. animalis* and other organisms do not contain this N-terminal sequence, or the putative conserved amino acid residues that confer this function.

Likewise, the phosphoketolase of *P. aeruginosa* contains an additional N-terminal sequence not found in *B. animalis* or other obligate anaerobes reliant on phosphoketolases for fermentative growth. Additionally, the phosphoketolase of *P. aeruginosa* lacks the N-terminal sequence of *S. elongatus*. Therefore, future work should carry out comparative enzymology of these different groups of phosphoketolases to determine specific functions of the *P. aeruginosa* phosphoketolase and its closely related homologs. Such studies could uncover novel regulatory mechanisms for phosphoketolase proteins which may explain the role of these enzymes in mediating ribonucleotide homeostasis.

Our results in Chapter 4 show horizontal-gene transfer of phosphoketolases from these different clades across bacterial taxa in conjugation with ribonucleotide processing genes. Such data suggests the possibility of evolutionary pressure behind an "acquired metabolism" conferred by gaining such genes. For instance, within our dataset

of phosphoketolase homologs we found *Pseudomonas putida* species with phosphoketolases more like that of *B. animalis*. Meanwhile, other *P. putida* species were found with phosphoketolases like that of *P. aeruginosa* with flanking genes related to ribonucleotide processing enzymes. It is interesting to speculate that these two strains have differential fitness under anaerobic survival depending on the carbon source or extent of ribonucleotide turnover in a manner that correlates with the identity of their phosphoketolases. Extending our brief analyses in Chapter 4 to characterize hypothetical proteins flanking these phosphoketolases, expand the strains we used for this analysis, and searching for other horizontally transferred gene islands containing phosphoketolases could help to uncover patterns in the acquisition and use of these genes.

Concluding perspective

The ideas within this final Chapter hopefully help to guide future scientists or readers to continue this work. However, the metabolic networks referenced throughout can feel quite unapproachable due to the interwoven nature of "central" carbon metabolism. Yet I wish to take these final moments together to emphasize a few things. Despite the diversity of metabolic pathways or complexity of their regulation, my discoveries came from hypotheses based on a relatively simple principle of metabolism, namely the flow of electrons from a source to a sink. This concept is nothing new, being well recognized for over a century. Additionally, these discoveries were done primarily in *P. aeruginosa,* an incredibly well studied organism. Finally, the methods used to produce the foundational phenotypes underlying each of these discoveries was quite simple: putting bacteria in situations and counting colony-forming units for survival. I don't

intend this paragraph to minimize the effort that went into generating these hypotheses/experiments or minimize the importance of these findings. Instead, I am trying to emphasize that there is still substantial room for discovery of wondrous new metabolic survival strategies in bacteria, even model organisms. Furthermore, such work can and should be accessible to scientists of all levels, requiring a bit of creativity, a stressor, a bacterium, and some petri dishes… at least at first. Meaning, the tools to explore new frontiers in bacterial metabolism are closer than they appear.

© 2026

Richard Davis Horak
ORCID: 0000-0003-0630-5481